NATIONAL AERONAUTICS AND SPACE ADMINISTRATION

Technical Report 32-1401

A Faraday Rotation Measurement of a 13-cm Signal in the Solar Corona

C. T. Stelzried

JET PROPULSION LABORATORY
CALIFORNIA INSTITUTE OF TECHNOLOGY
PASADENA, CALIFORNIA

July 15, 1970

NATIONAL AERONAUTICS AND SPACE ADMINISTRATION

Technical Report 32-1401

A Faraday Rotation Measurement of a 13-cm Signal in the Solar Corona

C. T. Stelzried

JET PROPULSION LABORATORY
CALIFORNIA INSTITUTE OF TECHNOLOGY
PASADENA, CALIFORNIA

July 15, 1970

Prepared Under Contract No. NAS 7-100
National Aeronautics and Space Administration

Preface

The work described in this report was performed by the Telecommunications Division of the Jet Propulsion Laboratory.

Acknowledgment

Mr. Gerald Levy of the Jet Propulsion Laboratory (JPL) was instrumental in the original concept of the experiment and in the final version of the polarizer measurement system. He provided support and assistance throughout the entire experiment.

Dr. Takeshi Sato of JPL was involved with the feed cone checkout, operations, and particularly with the data interpretation. Mr. Dan Bathker and Mr. Robert Cormack of JPL were in charge of the feed cone design modification. Mr. Boris Seidel of JPL contributed to the cone checkout and operations. Mr. Bruce Parham of JPL was largely responsible for the data handling equipment. Mr. Frank McCrea and Mr. William Peterschmidt of JPL were responsible for the polarizer angle readout and servo system. Mr. Harold Donnelly and Mr. James Wilcher of JPL supplied special instrumentation for the Mars station receiver error channel modifications. Dr. Charles Lawson of JPL contributed useful comments on the Faraday rotation computer program. Miss Lois Busch of JPL provided programming for the ray tracing and Faraday rotation computer programs. Mr. Alexander Abreu of JPL assisted in the derivation and provided the programming for the polarization coordinate transformation computer program. The assistance of Mrs. Beatrice McAlexander, Mrs. Carolyn Nolan, and Miss Marie Inouye of JPL is acknowledged.

Mr. Brendan Mulhall of JPL supplied the Faraday rotation data required for the earth ionospheric corrections. Mr. Dave Hubiak of JPL obtained the required *Pioneer VI* orbit data.

Drs. W. V. T. Rusch, John Ohlson, Hans Kuehl, and Don Barry of the University of Southern California (USC) were members of the Dissertion Committee and provided help with various theoretical derivations. Dr. J. Ohlson was also involved with the polarizer concept, cone checkout, operations, and data interpretation. He performed most of the system performance analysis and his help with the successful outcome of the overall project is acknowledged.

Mr. Dave Girdner of Bendix and the operational personnel at the Mars station were particularly helpful.

Dr. Kenneth Schatten of the Goddard Space Flight Center and Dr. John Wilcox of the University of California at Berkeley provided the solar magnetic field data used in the Faraday rotation calculations and provided invaluable advice on the coronal magnetic field calculations and final data interpretation.

The cooperation of Mr. Charles Hall and Mr. Robert Nunamaker of the Ames Research Center Pioneer Project Office and Mr. Alfred Siegmeth of JPL is acknowledged.

Mr. Robertson Stevens, Mr. Walter Victor, Mr. Fred Felberg, and Dr. William Pickering, all of JPL, supported the original project proposal. Dr. John Naugle of the NASA Office of Space Science and Applications gave official NASA approval to this joint JPL/USC research project carried out at JPL under NASA Contract NAS 7-100.

Contents

I. The Solar Corona 1

A. The Solar Magnetic Field 2

B. The Coronal Plasma Density 2

II. Interaction of Electromagnetic Waves With a Magnetized Plasma . . 2

A. Basic Theory of Faraday Rotation in a Magnetized Plasma . . . 3

B. Ray Paths in the Solar Corona 10

C. Faraday Rotation in the Solar Corona 12

III. Experiment Description 15

A. Description of the *Pioneer VI* Spacecraft 16

B. Vehicle Antenna and Orientation 16

C. Orbit Determination and Description 16

D. Received Signal Polarization Coordinate Transformation 19

IV. S-Band Polarimeter and Associated Instrumentation 24

A. Equipment Description 24

B. Performance Characteristics 24

C. Overall System Description and Peformance 30

V. Experimental Results 30

A. Transient Effects 33

B. Steady State 39

VI. Comparison of the Steady-State Measurements With Theoretical Models 39

A. Faraday Rotation in the Solar Corona Assuming a Modified Allen–Baumbach Electron Density and Parker Magnetic Field Model 43

B. Faraday Rotation in the Solar Corona With Measured Magnetic Field Data and Assuming a Modified Allen–Baumbach Electron Density 45

1. Magnetic field obtained from magnetograph data 45

2. Magnetic field obtained from *Explorer 33* data 45

C. Adjustment of Electron Density to Obtain Agreement Between Calculated and Measured Faraday Rotation 52

VII. Conclusions and Suggestions for Future Work 52

A. Summary of Conclusions 52

B. Suggestions for Future Work 57

Contents (contd)

Appendixes

A. Stratified Layer Ray Tracing Computer Program Listing 58

B. Integral Solution Ray Tracing Computer Program Listing 60

C. Faraday Rotation Computer Program Listing 62

D. Signal Polarization Coordinate Transformation Computer Program Listing 68

E. Special Data Manipulating Computer Programs Listings 77

References 81

Tables

1. Typical "quiet" sun values of pertinent plasma parameters in the solar corona as a function of distance from center of sun 10

2. Tabulation of the SMF feed cone antenna reflection coefficient measurements 31

3. Correlation of the Faraday rotation transients and dekametric radio bursts 38

4. Calculated values of Faraday rotation in one quadrant of a "quiet" sun using a modified Allen–Baumbach electron density and Parker magnetic field 45

5. Comparison tabulation of electron densities in the solar corona . . 56

Figures

1. Arbitrary direction of propagation (in yz plane) in relationship to applied static magnetic field $\mathbf{B}_0$ 4

2. Geometry used to calculate ray path in a radially symmetric solar corona model with uniform stratified layers 10

3. Sample computer output for stratified layer ray path program 11

4. Sample ray path output computed with identical parameters used in the stratified layer program 12

5. Geometry of magnetic field line $\mathbf{B}_0$ emanating from sun, looking down plane of ecliptic 13

6. *Pioneer VI* spacecraft in flight configuration 16

7. Projection of *Pioneer VI* orbit on plane of ecliptic relative to earth–sun line 17

Contents (contd)

Figures (contd)

8. Mars station measurements of *Pioneer VI* right ascension corrections 18
9. Coordinate system used to calculate *Pioneer VI* probe position relative to sun in plane of ecliptic 19
10. Computer tabulation of signal ray path parameters from *Pioneer VI* probe to earth relative to sun 20
11. Projection of *Pioneer VI* orbit perpendicular to plane of ecliptic relative to sun 21
12. Pictorial representation defining measured polarization angle looking along line of sight toward probe 22
13. Cartesian coordinate systems used to sequentially transform between ecliptic plane and local station coordinates 22
14. Vectors used to relate probe polarization in ecliptic plane to that measured at local station 23
15. Polarization angle relationships looking along station-to-probe line of sight 23
16. Sample computer output of signal polarization program 25
17. Interior of SMF feed cone 26
18. Simplified block diagram of SMF feed cone 27
19. S-band quarter-wave plate used in SMF feed cone polarization instrument 28
20. Block diagram of S-band receiver system 28
21. Photograph of SMF feed cone polarization tracking console . . . 29
22. Detailed block diagram of SMF feed cone 32
23. System operating noise temperature T_{op} vs time and distance from center of sun 33
24. System operating noise temperature T_{op} vs ϕ 33
25. Reflector coordinate system 33
26. Plot of three days of 200-s polarizer data standard deviation vs time 34
27. Polarimeter 200-s angular measurement error (1σ) vs time and distance from center of sun 35
28. Polarization (200-s data points) vs time for *Pioneers VI, VII,* and *VIII* observations 35
29. *Pioneer VI* polarization (10-s data points) vs time 36
30. Polarization vs time, 1000-s data (200-s data on transients) . . . 37

Contents (contd)

Figures (contd)

31. *Pioneer VI* entry and *Pioneer VII* polarization angles vs time referred to plane of ecliptic; uncorrected for ionospheric rotation 40

32. *Pioneer VI* exit and *Pioneer VII* polarization angles vs time referred to plane of ecliptic; uncorrected for ionospheric rotation 41

33. Faraday rotation due to earth's ionosphere in Goldstone–*Pioneer VI* line of sight 41

34. *Pioneer VI* polarization vs time (1000-s data with ionospheric correction) 42

35. Projection on plane of ecliptic of *Pioneer VI* spacecraft signal geometric ray path through solar corona and magnetic field emanating from sun 43

36. Geometry of a magnetic field line emanating from sun (exaggerated) 44

37. Sample computer output of Faraday rotation program using modified Allen–Baumbach electron density and Parker magnetic field models 46

38. "Measured" magnetic field of sun referred to central meridian and normalized in magnitude to solar surface as a function of time for Mount Wilson magnetograph (using 3.0 solar radii source surface) and *Explorer 33* data 47

39. Sample of computer output Faraday rotation program using modified Allen–Baumbach electron density model and measured Mount Wilson magnetic field data 48

40. Calculated signal polarization (ray offset of 6.23 solar radii) plotted as a function of ϕ 49

41. Comparison of measured signal polarization and that calculated using Mount Wilson magnetic field data with 2.5 and 3.0 solar radii source surfaces 50

42. Comparison of measured signal polarization and that calculated using *Explorer 33* magnetic field data with "quiet" sun and twice "quiet" sun electron densities 51

43. Comparison of measured signal polarization and that calculated using *Explorer 33* magnetic field data with various values of A and B 53

Abstract

The goal of this experiment was to further the scientific knowledge of the solar corona by measuring the Faraday rotation of a 2292-MHz continuous wave signal in this plasma.

The *Pioneer VI* spacecraft was launched into a circumsolar orbit on December 16, 1965, and was occulted by the sun in the last half of November, 1968. During the occultation period, the 2292-MHz S-band telemetry carrier wave underwent Faraday rotation due to the interaction of this signal with the plasma and magnetic field in the solar corona. The 210-ft-diam Goldstone Mars station antenna of the Deep Space Network located near Barstow, Calif. was used for the measurement. The antenna feed was modified for automatic polarization tracking for this experiment. This modification is described and the performance evaluated.

Three large-scale transient Faraday rotation phenomena were observed on November 4, 8, and 12. These phenomena typically lasted about 2 h and produced Faraday rotations on the order of 40 deg. Correlation with dekametric solar radio bursts was noted and the implied solar wind velocity estimated.

A steady-state Faraday rotation was observed, commencing at about 10 solar radii on the west limb of the sun. The rotation increased steadily as the ray path approached the sun. At 4 solar radii polarization had rotated over 125 deg. The signal could not be tracked closer to the sun because of the loss in receiver sensitivity caused primarily by the increased system noise temperature. The increase in system noise temperature was due to the antenna side lobes "seeing" the sun. Further loss in sensitivity was due to the spectral broadening of the signal caused by highly random motion of the excited plasma close to the sun. The rotation was of nearly equal magnitude upon exit on the east limb of the sun but of opposite sense in the outer region.

The steady-state measurement is compared with a theoretical model of the solar corona using a modified Allen–Baumbach electron density and the coronal magnetic field as derived from the Mount Wilson optical solar magnetograph and the *Explorer* 33 satellite magnetometer. Although the calculated rotation and the experimental data show general agreement with respect to the magnitude, sense, and timing of the rotation, an improved fit is obtained with an assumed equatorial electron density (in m^{-3})

$$N = 10^{14}\left(\frac{6000}{R^{10}} + \frac{0.002}{R^{2}}\right), \qquad (4 < R < 12)$$

with R in solar radii.

A Faraday Rotation Measurement of a 13-cm Signal in the Solar Corona

I. The Solar Corona

The solar corona consists of that region of the solar atmosphere that extends beyond the chromosphere. Although normally considered confined to the immediate vicinity of the sun's surface, this region actually extends into the interplanetary region and beyond (Ref. 1). For the purpose of this study, we are interested in the region from about 4 to 12 solar radii from the center of the sun. This region approximates a pure plasma, consisting largely of protons and electrons with thermal temperatures on the order of 10^6 K (Refs. 2 and 3). Although electron densities in general vary with both location and time, the static density around the "quiet" sun can be represented by an Allen–Baumbach model with radial dependence (Refs. 4–6). The "static" magnetic field postulated by Parker (Ref. 7) describes an Archimedes spiral that is essentially radial at the distances of interest. The density and structure of the corona and a current review of plasmas in space are given in Refs. 8 and 9, respectively.

Electron density measurements summarized by Hata and Saito (Ref. 10) are performed from photometric studies. The K-coronometer observations are used for routine measurements out to 10 solar radii (Ref. 11). Electron densities from 10 to 80 solar radii can also be obtained from scintillation measurements of radio sources during solar occultation (Ref. 12). The magnetic field in the solar corona has been determined from observations of solar radio bursts (Ref. 13) viewed through the solar corona. Schatten and Wilcox (Ref. 14) have calculated the magnetic field in the solar corona by a Green's Function technique from measured magnetogram data (Ref. 15). The fields are computed in the solar corona as if they originated from a "source surface." This fictitious surface is located far enough (1.6–3.0 solar radii) from the surface of the sun so that it can be assumed that transient magnetic field loops do not "break through." This technique was used (Ref. 16) to predict the coronal structure for the September 1968 solar eclipse. Ness and Wilcox (Ref. 17) obtained interplanetary magnetic field data from earth satellite instrumentation and proved this field to be essentially of solar origin.

Solar observations with a polarization radio telescope have provided interesting data by the correlation of noise temperature and polarization bursts (Ref. 18). Radar techniques provided the first probing of the solar corona with coherent continuous wave (CW) signals (Refs. 19 and 20). The first probing of the solar corona by transmission

of a CW signal through the near solar corona occurred with the *Mariner IV* spacecraft in conjunction with the Goldstone Mars station (Ref. 21). The *Mariner IV* orbit placed the spacecraft behind the sun so that the S-band circularly polarized radio signal passed within 0.6 deg of the solar disc. This experiment also provided the first operational use of the 210-ft-diam Mars station antenna with low noise masers that were required to track the spacecraft at the tremendous distance of about 2 AU. The spectral broadening of the received signal measured in this experiment caused by the differential doppler in the ray paths can be theoretically related to the solar wind.

The *Pioneer VI* spacecraft passed behind the sun during November 1968. This provided the first opportunity to observe the transmission of a linearly polarized S-band CW signal through the near solar corona. The Faraday rotation of this signal due to the solar corona was measured and the results interpreted. The measurement provided precise data on the integrated product of the electron density and the longitudinal component of the magnetic field along the ray path. This quantity combined with magnetic field data, provided electron density information in the region of the ray path.

A. The Solar Magnetic Field

The magnetic field emanating from the sun is basically radial (in a gross sense) at distances greater than about 2 solar radii from the center with a spiral effect dominating at larger distances. The Archimedes spiral of the magnetic field lines is caused by the "nozzle effect" of the solar wind emanating from the surface of the rotating sun dragging along the magnetic lines of flux. The spiral is such that its angular departure α from the radial direction is given by (see Ref. 1)

$$\tan \alpha = \frac{\omega \rho}{v} \tag{1}$$

where

ρ = distance from sun, m

ω = rotation rate of sun, rad/s

v = velocity of solar wind, m/s

An angle of 45 deg at 1 AU (1.49598×10^{11} m), with a solar sidereal period of rotation of 25.38 days, implies a solar wind velocity of 4.3×10^5 m/s. The radial and azimuthal components of the magnetic field in the Parker model are approximated respectively by (Ref. 22)

$$\left.\begin{aligned} B_R &= \frac{B_0}{R^2} \\ B_A &= \frac{B_0}{R}\frac{\omega r}{v} \end{aligned}\right\} \tag{2}$$

where

B_0 = magnetic field at surface of sun, G

R = distance from center of sun, solar radii

r = radius of sun, m

This simple Parker model does not predict the field polarity. The polarity of the magnetic field lines tend to be grouped in sectors and must be measured.

B. The Coronal Plasma Density

Photometry observations of the brightness of the K-corona during an eclipse can be used to calculate the electron density in the solar corona. The Allen–Baumbach formula for the equatorial electron density radial distribution normally given (in m^{-3}) by

$$N = 10^{14}\left(\frac{2.99}{R^{16}} + \frac{1.55}{R^6}\right) \tag{3}$$

was obtained from this type of data.

In the range of interest for this experiment ($4 < R < 12$), the R^{-16} term is negligible. In addition, as indicated by Hollweg (see Ref. 6) a term in R^{-2} is necessary to correspond to the theoretical results of Parker (Refs. 6 and 7) and to agree with the results of solar probe measurements. Thus, for this report we will use a modified form of the Allen–Baumbach equation (Ref. 6) given by

$$N = 10^{14}\left(\frac{1.55}{R^6} + \frac{0.01}{R^2}\right) \tag{4}$$

II. Interaction of Electromagnetic Waves With a Magnetized Plasma

The theory of the interaction of an electromagnetic plane wave with a magnetized plasma is presented in this section. This is required to interpret the Faraday rotation of the linearly polarized CW signal originating from the *Pioneer VI* spacecraft and propagating through the plasma of the solar corona.

A. Basic Theory of Faraday Rotation in a Magnetized Plasma

The propagation and polarization properties of a plane monochromatic wave in a magnetically biased homogeneous, lossless plasma has been well treated in the literature (Refs. 23–26). The treatment and nomenclature of Papas (Ref. 23) are closely followed in the derivation of this section. In particular, an $\exp(-i\omega t)$ time dependence is used. The plasma is regarded as a continuous medium with zero conductivity and vacuum permeability μ_0. Application of a magnetostatic field $\mathbf{B}_0$ to the plasma results in a tensor permittivity $\bar{\bar{\epsilon}}$. The tensor is derived from Maxwell's equations through the Lorentz force equation

$$m\frac{d\mathbf{v}}{dt} = e(\mathbf{E} + \mathbf{v} \times \mathbf{B}_0) \tag{5}$$

where

e = electron charge = -1.60210×10^{-19} C

m = electron mass = 9.1091×10^{-31} kg

$\mathbf{v}$ = electron velocity, m/s

$\mathbf{B}_0$ = steady magnetic field, Wb/m^2

$\mathbf{E}$ = electric field of wave, V/m

The electron velocity is related to the plasma conduction current density by

$$\mathbf{J} = Ne\mathbf{v} \tag{6}$$

where

$\mathbf{J}$ = conduction current density, A/m^2

N = electron density, m^{-3}

With the z-axis parallel to $\mathbf{B}_0$, the tensor $\bar{\bar{\epsilon}}$ is given in Cartesian coordinates by:

$$\epsilon_{xx} = \epsilon_0\left(1 - \frac{\omega_p^2}{\omega^2 - \omega_g^2}\right) = \epsilon_0\left(1 - \frac{X}{1 - Y^2}\right) = \epsilon_{yy} \tag{7a}$$

$$\epsilon_{xy} = -i\epsilon_0\frac{\omega_p^2\,\omega_g}{\omega(\omega^2 - \omega_g^2)} = -i\epsilon_0\frac{XY}{1 - Y^2} = -\epsilon_{yx} \tag{7b}$$

$$\epsilon_{zz} = \epsilon_0\left(1 - \frac{\omega_p^2}{\omega^2}\right) = \epsilon_0(1 - X) \tag{7c}$$

$$\epsilon_{xz} = \epsilon_{zx} = \epsilon_{yz} = \epsilon_{zy} = 0 \tag{7d}$$

where

ϵ_0 = free space permittivity = $\dfrac{10^7}{4\pi c^2}$ $\simeq 8.85416 \times 10^{-12}$ F/m

c = velocity of light = 2.99793×10^8 m/s

ω = signal frequency, rad/s

$\omega_p = \left(\dfrac{Ne^2}{m\epsilon_0}\right)^{1/2}$ = plasma frequency, rad/s

$\omega_g = \dfrac{eB_0}{m}$ = gyro frequency, rad/s

Note: Negative e in the case of electrons results in negative ω_g.

$$X = \left(\frac{\omega_p}{\omega}\right)^2$$

$$Y = -\left(\frac{\omega_g}{\omega}\right)$$

The foregoing neglects collisions and interaction of the signal with ions. The electric vector of a wave traveling in the k direction is given by

$$\boldsymbol{\varepsilon}(\mathbf{r},t) = Re\,\{\mathbf{E}_0 \exp[i(\mathbf{k}\cdot\mathbf{r} - \omega t)]\} \tag{8}$$

where

$\mathbf{E}_0$ = constant vector describing the wave polarization, V/m

$\mathbf{k}$ = propagation vector, rad/m

$\mathbf{r}$ = position vector, m

The steady-state form of Maxwell's equations in terms of the tensor permittivity is given by

$$\left.\begin{aligned}\nabla \times \mathbf{E} &= i\omega\mu_0\mathbf{H}\\ \nabla \times \mathbf{H} &= -i\omega\bar{\bar{\epsilon}}\mathbf{E}\end{aligned}\right\} \tag{9}$$

where

$\mathbf{H}$ = magnetic field, A/m

μ_0 = free space permeability, H/m

Manipulating the above results in the vector equation

$$k^2 \mathbf{E}_0 - \mathbf{k}(\mathbf{k} \cdot \mathbf{E}_0) = \omega^2 \mu_0 \bar{\bar{\epsilon}} \mathbf{E}_0 \tag{10}$$

Using

$$k = \frac{\omega}{v}$$

where

$$v = \text{phase velocity, m/s}$$

and orienting the Cartesian coordinate system so that $\mathbf{k}$ is in the yz plane and defining θ as the angle between $\mathbf{B}_0$ and $\mathbf{k}$ (Fig. 1) results in

$$E_{0x}\left(1 - \frac{v^2}{c^2}\frac{\epsilon_{xx}}{\epsilon_0}\right) - E_{0y}\left(\frac{v^2}{c^2}\frac{\epsilon_{xy}}{\epsilon_0}\right) + 0 = 0 \tag{11a}$$

$$E_{0x}\left(-\frac{v^2}{c^2}\frac{\epsilon_{yx}}{\epsilon_0}\right) + E_{0y}\left(\cos^2\theta - \frac{v^2}{c^2}\frac{\epsilon_{yy}}{\epsilon_0}\right) + E_{0z}(-\cos\theta \sin\theta) = 0 \tag{11b}$$

$$0 + E_{0y}(-\cos\theta\sin\theta) + E_{0z}\left(\sin^2\theta - \frac{v^2}{c^2}\frac{\epsilon_{zz}}{\epsilon_0}\right) = 0 \tag{11c}$$

from the x, y, and z components of Eq. (10). Quantities E_{0x}, E_{0y}, and E_{0z} are the Cartesian coordinates of $\mathbf{E}_0$.

Setting the determinant of the homogeneous equations equal to zero,

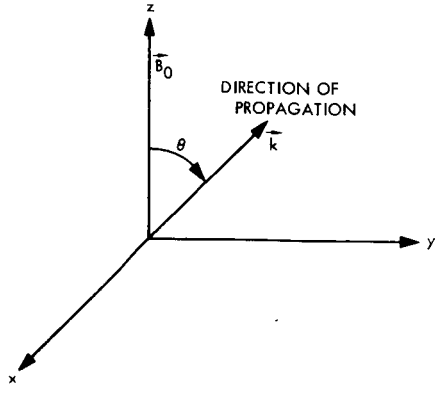

Fig. 1. Arbitrary direction of propagation (in yz plane) in relationship to applied static magnetic field $\mathbf{B}_0$

$$\begin{vmatrix} \left(1 - \frac{v^2}{c^2}\frac{\epsilon_{xx}}{\epsilon_0}\right) & \left(-\frac{v^2}{c^2}\frac{\epsilon_{xy}}{\epsilon_0}\right) & 0 \\ \left(-\frac{v^2}{c^2}\frac{\epsilon_{yx}}{\epsilon_0}\right) & \left(\cos^2\theta - \frac{v^2}{c^2}\frac{\epsilon_{yy}}{\epsilon_0}\right) & (-\sin\theta\cos\theta) \\ 0 & (-\sin\theta\cos\theta) & \left(\sin^2\theta - \frac{v^2}{c^2}\frac{\epsilon_{zz}}{\epsilon_0}\right) \end{vmatrix} = 0 \tag{12}$$

and defining

$$\left.\begin{aligned} \epsilon_1 &= \frac{\epsilon_{xx}}{\epsilon_0} - i\frac{\epsilon_{xy}}{\epsilon_0} \\ \epsilon_2 &= \frac{\epsilon_{xx}}{\epsilon_0} + i\frac{\epsilon_{xy}}{\epsilon_0} \\ \epsilon_3 &= \frac{\epsilon_{zz}}{\epsilon_0} \end{aligned}\right\} \tag{13}$$

results in the Appleton–Hartree equation

$$\tan^2\theta = \frac{-\left(\frac{1}{n^2} - \frac{1}{\epsilon_1}\right)\left(\frac{1}{n^2} - \frac{1}{\epsilon_2}\right)}{\left(\frac{1}{n^2} - \frac{1}{\epsilon_3}\right)\left[\frac{1}{n^2} - \frac{1}{2}\left(\frac{1}{\epsilon_1} + \frac{1}{\epsilon_2}\right)\right]} \tag{14}$$

where

$$n = \text{index of refraction} = \frac{c}{v}$$

The solutions for propagation parallel to $\mathbf{B}_0$ ($\theta = 0$, Fig. 1) are

$$n_1^2 = \epsilon_1 = 1 - \frac{\omega_p^2}{\omega(\omega - \omega_g)} = 1 - \frac{X}{1 - Y} \tag{15}$$

and

$$n_2^2 = \epsilon_2 = 1 - \frac{\omega_p^2}{\omega(\omega + \omega_g)} = 1 - \frac{X}{1 + Y} \tag{16}$$

The propagation constants for the two waves traveling parallel to $\mathbf{B}_0$ are

$$k_0' = \frac{\omega}{c}\left[1 - \frac{\omega_p^2}{\omega(\omega - \omega_g)}\right]^{1/2} = \frac{\omega}{c}\left(1 - \frac{X}{1 - Y}\right)^{1/2} \tag{17}$$

and

$$k_0'' = \frac{\omega}{c}\left[1 - \frac{\omega_p^2}{\omega(\omega + \omega_g)}\right]^{1/2} = \frac{\omega}{c}\left(1 - \frac{X}{1+Y}\right)^{1/2} \tag{18}$$

A similar derivation for the two waves traveling perpendicular to $\mathbf{B}_0$ ($\theta = \pi/2$, Fig. 1) results in the propagation constants

$$k'_{\pi/2} = \frac{\omega}{c}\left(1 - \frac{\omega_p^2}{\omega^2}\right) = \frac{\omega}{c}(1 - X)^{1/2} \tag{19}$$

and

$$k''_{\pi/2} = \frac{\omega}{c}\left(1 - \frac{\frac{\omega_p^2}{\omega^2}}{\frac{1 - \omega_g^2}{\omega^2 - \omega_p^2}}\right)^{1/2} = \frac{\omega}{c}\left(1 - \frac{X}{1 - \frac{Y^2}{1-X}}\right)^{1/2} \tag{20}$$

Since $k'_{\pi/2}$ is identically equal to the propagation constant of a wave in an isotropic plasma, the wave identified by a single prime is called the ordinary wave and that with a double prime the extraordinary wave.

Returning to the case for propagation parallel to $\mathbf{B}_0$ Eqs. (11) simplify to

$$\left.\begin{aligned} E_{0x}\left(1 - \frac{1}{n^2}\frac{\epsilon_{xx}}{\epsilon_0}\right) - E_{0y}\left(\frac{1}{n^2}\frac{\epsilon_{xy}}{\epsilon_0}\right) &= 0 \\ E_{0x}\left(-\frac{1}{n^2}\frac{\epsilon_{yx}}{\epsilon_0}\right) + E_{0y}\left(1 - \frac{1}{n^2}\frac{\epsilon_{yy}}{\epsilon_0}\right) &= 0 \\ E_{0z}\left(-\frac{1}{n^2}\frac{\epsilon_{zz}}{\epsilon_0}\right) &= 0 \end{aligned}\right\} \tag{21}$$

As shown by the bottom equation, E_{0z} is zero. These relations are satisfied with Eq. (15) if

$$E_{0y} = -i\,E_{0x} \tag{22}$$

while Eq. (16) requires that

$$E_{0y} = i\,E_{0x} \tag{23}$$

Consequently, the electric vectors of the two waves are

$$\mathbf{E}' = (\mathbf{a}_x - i\mathbf{a}_y)\,A \exp(ik_0' z) \tag{24}$$

and

$$\mathbf{E}'' = (\mathbf{a}_x + i\mathbf{a}_y)\,B \exp(ik_0'' z) \tag{25}$$

Eqs. (24) and (25) are, respectively, a left-hand circularly polarized wave and a right-hand circularly polarized wave. The sum is

$$\mathbf{E} = \mathbf{E}' + \mathbf{E}'' = (\mathbf{a}_x - i\mathbf{a}_y)\,A \exp(ik_0' z) + (\mathbf{a}_x + i\mathbf{a}_y)\,B \exp(ik_0'' z) \tag{26}$$

The components are

$$\frac{E_x}{E_y} = i\,\frac{1 + \left(\frac{B}{A}\right)\exp[i(k_0'' - k_0')z]}{1 - \left(\frac{B}{A}\right)\exp[i(k_0'' - k_0')z]} \tag{27}$$

For waves of equal amplitude, as required for an incident [$z = 0$ in Eq. (26)] plane wave with $\mathbf{E}$ linearly polarized in the x direction, Eq. (27) reduces to

$$\frac{E_x}{E_y} = \cot\left(\frac{k_0' - k_0''}{2}\right)z \tag{28}$$

Therefore, at any position z, the composite wave traveling parallel to $\mathbf{B}_0$ remains linearly polarized and undergoes a clockwise Faraday rotation in unit distance

$$\Omega_L = \frac{k_0' - k_0''}{2} = \frac{\omega}{2c}\left[\left(1 - \frac{X}{1+Y}\right)^{1/2} - \left(1 - \frac{X}{1+Y}\right)^{1/2}\right] = \frac{-\left(\frac{\omega}{c}\right)XY}{(1 - Y^2)(n_1 + n_2)}$$

$$= \frac{-\left(\frac{\omega}{c}\right)XY}{(1+Y)[(1-Y)(1-Y-X)]^{1/2} + (1-Y)[(1+Y)(1+Y-X)]^{1/2}} \tag{29}$$

The lower form is better suited to numerical evaluation since it does not involve the difference of nearly equal valued quantities. For $\omega_g/\omega \ll 1$ and $\omega_p/\omega \ll 1$ this simplifies to

$$\Omega_L = -\left(\frac{\omega}{2c}\right) XY \tag{30}$$

For propagation perpendicular to $\mathbf{B}_0$ ($\theta = \pi/2$, Fig. 1) substitution of Eq. (19) into Eq. (11) requires that E_{0x} and E_{0y} be identically zero. Similarly, Eq. (20) requires that E_{0z} be zero and that

$$E_{0y} = \frac{-iXY}{1 - X - Y^2} \tag{31}$$

As before, this results in

$$\mathbf{E}' = \mathbf{a}_z A \exp\left(ik'_{\pi/2} y\right) \tag{32}$$

and

$$\mathbf{E}'' = \left(\mathbf{a}_x - i\frac{XY}{1 - X - Y^2}\,\mathbf{a}_y\right) B \exp\left(ik''_{\pi/2} y\right) \tag{33}$$

The propagation constant of the wave represented by Eq. (32) is independent of $\mathbf{B}_0$. This is the ordinary wave appropriately behaving as though it were in an isotropic plasma since the $\mathbf{v} \times \mathbf{B}_0$ term in the Lorentz force equation is zero. Equation (33) represents the extraordinary wave.

As before, the sum is

$$\mathbf{E} = \mathbf{E}' + \mathbf{E}'' = \mathbf{a}_z A \exp\left(ik'_{\pi/2} y\right) + \left(\mathbf{a}_x - \frac{iXY}{1 - X - Y^2}\,\mathbf{a}_y\right) B \exp\left(ik''_{\pi/2} y\right) \tag{34}$$

With

$$\mathbf{H} = \frac{1}{\omega\mu_0}\,\mathbf{k} \times \mathbf{E} \tag{35}$$

the associated magnetic vector is

$$\mathbf{H} = \frac{1}{\omega\mu_0}\left[\mathbf{a}_x k'_{\pi/2} A \exp\left(ik'_{\pi/2} y\right) - \mathbf{a}_z k''_{\pi/2} B \exp\left(ik''_{\pi/2} y\right)\right] \tag{36}$$

Consider a wave incident on an infinite half plane propagating with $\theta = \pi/2$. Assume the $\mathbf{E}$ vector of the incident wave is aligned with $\mathbf{a}_x$ (i.e., $\mathbf{E}$ perpendicular to $\mathbf{B}_0$ which closely approximates the situation in the *Pioneer VI* experiment; see Fig. 38 for identification with the experiment)

$$\left.\begin{aligned} \mathbf{E}^{inc} &= (E_0)_\perp\,\mathbf{a}_x \exp\left(ik_0 y\right) \\ \mathbf{H}^{inc} &= \frac{-(E_0)_\perp\, k_0}{\omega\mu_0}\,\mathbf{a}_z \exp\left(ik_0 y\right) \end{aligned}\right\} \tag{37}$$

where

$(E_0)_\perp$ = component of incident electric field magnitude perpendicular to $\mathbf{B}_0$

$k_0 = \dfrac{\omega}{c}$ = magnitude of propagation vector in free space

Assume a reflected wave

$$\left.\begin{aligned} \mathbf{E}^r &= \mathbf{C} \exp\left(-ik_0 y\right) \\ \mathbf{H}^r &= \frac{k_0}{\omega\mu_0}\left(-C_z\,\mathbf{a}_x + C_x\,\mathbf{a}_z\right) \exp\left(-ik_0 y\right) \end{aligned}\right\} \tag{38}$$

Matching boundary conditions at the half plane interface ($y = 0$),

$$\left.\begin{aligned} A &= C_z = 0 \\ B &= \frac{2\,(E_0)_\perp}{\left(\dfrac{k''_{\pi/2}}{k_0} + 1\right)} \end{aligned}\right\} \tag{39}$$

so that for this case Eq. (34) becomes

$$\mathbf{E}_\perp = \frac{2(E_0)_\perp}{\left(\dfrac{k''_{\pi/2}}{k_0} + 1\right)}\left(\mathbf{a}_x - \frac{iXY}{1 - X - Y^2}\,\mathbf{a}_y\right) \exp\left(ik''_{\pi/2} y\right) \tag{40}$$

where

$\mathbf{E}_\perp$ = propagating electric field vector excited by the incident electric field vector perpendicular to $\mathbf{B}_0$, ($\theta = \pi/2$)

and

$$\mathbf{H}_{\perp} = \frac{-2(E_0)_{\perp}\,(k''_{\pi/2})}{\omega\mu_0\left(\frac{k''_{\pi/2}}{k_0}+1\right)}\,\mathbf{a}_z \exp\,(ik''_{\pi/2}y) \tag{41}$$

We, therefore, have a transverse magnetic (TM) wave with the magnetic vector parallel to $\mathbf{B}_0$. *This situation will not result in Faraday rotation.*

A similar consideration shows that for a component of the incident **E** vector parallel to $\mathbf{B}_0$ ($\theta = \pi/2$, Fig. 1)

$$\mathbf{E}_{||} = \frac{2(E_0)_{||}}{\left(\frac{k'_{\pi/2}}{k_0}+1\right)}\,\mathbf{a}_z \exp\,(ik''_{\pi/2}\,y) \tag{42}$$

and

$$\mathbf{H}_{||} = \frac{2(E_0)_{||}\,(k'_{\pi/2})}{\omega\mu_0\left(\frac{k'_{\pi/2}}{k_0}+1\right)}\,\mathbf{a}_x \exp\,(ik'_{\pi/2}\,y) \tag{43}$$

where

$\mathbf{E}_{||}$ = propagating electric field vector excited by incident electric field vector parallel to $\mathbf{B}_0$

$(E_0)_{||}$ = component of incident electric field magnitude parallel to $\mathbf{B}_0$

This is a transverse electromagnetic (TEM) wave with the magnetic field vector perpendicular to $\mathbf{B}_0$. Again, this wave will not result in Faraday rotation.

Therefore, for a wave propagating perpendicular to $\mathbf{B}_0$ ($\theta - \pi/2$, Fig. 1) but with the incident **E** vector *arbitrarily aligned* with respect to $\mathbf{B}_0$, the previous analysis indicates [using the real part of Eqs. (40) and (42)] that two transverse (the receiving system is not sensitive to a longitudinal E field component) phase coherent terms will be present.

$$\left.\begin{aligned} E_x &= \frac{2(E_0)_{\perp}}{\left(\frac{k''_{\pi/2}}{k_0}+1\right)}\cos\,(\omega t - k''_{\pi/2}y) \\ E_z &= \frac{2(E_0)^{||}}{\left(\frac{k'_{\pi/2}}{k_0}+1\right)}\cos\,(\omega t - k'_{\pi/2}y) \end{aligned}\right\} \tag{44}$$

where

E_x = x component of the transmitted wave due to $(E_0)_{\perp}$

E_z = z component of the transmitted wave due to $(E_0)_{||}$

$(E_0)_{\perp}$ = component of the incident **E** vector perpendicular to $\mathbf{B}_0$

$(E_0)_{||}$ = component of the incident **E** vector parallel to $\mathbf{B}_0$

These are recognized as parametric equations of an ellipse with an angle of rotation (Ref. 26)

$$\Omega_T = \frac{1}{2}\tan^{-1}\left[\frac{2e}{1-e^2}\cos\,(k'_{\pi/2} - k''_{\pi/2})y\right] \tag{45}$$

where

$$e = \frac{(E_0)_{||}}{(E_0)_{\perp}}\left(\frac{k''_{\pi/2}+k_0}{k'_{\pi/2}+k_0}\right)$$

The differential rotation is

$$d\Omega_T = -\frac{1}{2}\frac{\frac{2e}{1-e^2}\sin\,(k'_{\pi/2} - k''_{\pi/2})y}{1+\left[\frac{2e}{1-e^2}\cos\,(k'_{\pi/2} - k''_{\pi/2})y\right]^2} \times (k'_{\pi/2} - k''_{\pi/2})\,dy \tag{46}$$

This is the differential rotation in a plasma slab of length dy with a linearly polarized incident electric field. Without specifying the **E** field alignment with $\mathbf{B}_0$, Kraus (Ref. 27), indicates that for unit distances

$$\left.\begin{aligned} |\,\Omega_T\,| &\simeq \frac{1}{2}\,Y\,\Omega_L \\ &\simeq \frac{1}{2}\,(k'_{\pi/2} - k''_{\pi/2}) \\ &\simeq \frac{\omega}{4c} \times Y^2 \end{aligned}\right\} \tag{47}$$

The lower form of Eq. (47) requires that $X \ll 1$, $Y^2 \ll 1$. Equation (47), an upper limit (Ref. 28) to Eq. (46) has been used (see Ref. 27) to show that the Faraday rotation due to the transverse magnetic field component is negligible compared to the longitudinal component.

The Faraday rotation of a linearly polarized CW signal traversing a plasma with an arbitrary orientation with respect to the magnetic field is usually computed using the longitudinal component of the magnetic field along the propagation paths. An exact evaluation not requiring this assumption is derived in the following.

The solutions to Eq. (14) for propagation at an arbitrary angle θ with respect to $\mathbf{B}_0$ (Fig. 1) are (see Ref. 23)

$$n_{1,2}^2 = 1 - \frac{X}{1 - \frac{1}{2}\frac{Y_T^2}{1-X} \pm \left[\frac{1}{4}\frac{Y_T^4}{(1-X)^2} + Y_L^2\right]^{1/2}} \tag{48}$$

where

Y_L = Y computed with the longitudinal component of the magnetic vector $\mathbf{B}_0$

Y_T = Y computed with the transverse component of the magnetic vector $\mathbf{B}_0$

and the + and − signs are used respectively for n_1 and n_2. The propagation constants for the two waves are

$$k'_\theta = \frac{\omega}{c} n_1 \tag{49}$$

and

$$k''_\theta = \frac{\omega}{c} n_2 \tag{50}$$

where n_1 and n_2 are computed from Eq. (48). It follows from Eq. (11) that the ratios of the electric field components perpendicular to $\mathbf{k}$ are ($\mathbf{k}$ in the zy plane as in Fig. 1)

$$\rho' = \frac{E'_X}{E'_\theta} = -\frac{i}{Y_L}\left\{\frac{1}{2}\frac{Y_T^2}{1-X} - \left[\frac{1}{4}\frac{Y_T^4}{(1-X)^2} + Y_L^2\right]^{1/2}\right\} \tag{51}$$

for the ordinary wave (with propagation constant k'_θ) and

$$\rho'' = \frac{E''_X}{E''_\theta} = -\frac{i}{Y_L}\left\{\frac{1}{2}\frac{Y_T^2}{1-X} + \left[\frac{1}{4}\frac{Y_T^4}{(1-X)^2} + Y_L^2\right]^{1/2}\right\} \tag{52}$$

for the extraordinary wave (with propagation constant k''_θ). Quantity E_θ is the component of $\mathbf{E}$ in the direction of the unit vector $\mathbf{a}_\theta$ defined by

$$\frac{\mathbf{k}}{k} = \mathbf{a}_x \times \mathbf{a}_\theta \tag{53}$$

This results in

$$n_1^2 = 1 - \frac{X}{1 - iY_L\rho'} \tag{54}$$

and

$$n_2^2 = 1 - \frac{X}{1 - iY_L\rho''} \tag{55}$$

The electric vectors of the two propagating waves in the direction of $\mathbf{k}$ are

$$\mathbf{E}' = \left(\mathbf{a}_x + \frac{1}{\rho'}\mathbf{a}_\theta\right) A \exp\left(ik'_\theta \ell\right) \tag{56}$$

and

$$\mathbf{E}'' = \left(\mathbf{a}_x + \frac{1}{\rho''}\mathbf{a}_\theta\right) B \exp\left(ik''_\theta \ell\right) \tag{57}$$

where

ℓ = path length

If the total field at $\ell = 0$ is assumed to be polarized in the $\mathbf{a}_x$ direction, Eqs. (56) and (57) become

$$\mathbf{E}' = A\left(\mathbf{a}_x + \frac{1}{\rho'}\mathbf{a}_\theta\right)\exp\left(ik'_\theta \ell\right)$$

$$\mathbf{E}'' = -A\frac{\rho''}{\rho'}\left(\mathbf{a}_x + \frac{1}{\rho''}\mathbf{a}_\theta\right)\exp\left(ik''_\theta \ell\right)$$

But, if

$$\frac{Y_T^2}{2(1-X)Y_L} \ll 1$$

(which includes the condition that $Y_T = 0$), Eqs. (51) and (52) become $\rho' \simeq i$ and $\rho'' \simeq -i$, respectively, and the total field is then

$$\mathbf{E}_T = \mathbf{E}' + \mathbf{E}''$$

$$\simeq A\left[(\mathbf{a}_x - i\,\mathbf{a}_\theta)\exp\left(ik'_\theta \ell\right) + (\mathbf{a}_x + i\,\mathbf{a}_\theta)\exp\left(ik''_\theta \ell\right)\right] \tag{58}$$

Referring to Eqs. (26–29) shows that under these circumstances (i.e., the quasi-longitudinal approximation)

$$\Omega \simeq \frac{k_\theta' - k_\theta''}{2}$$

When Y_L approaches zero ($\theta \simeq \pi/2$ in Fig. 1) the situation becomes slightly more complicated. Assuming an incident linearly polarized wave

$$\mathbf{E}^{inc} = \mathbf{a}_x E_0 \exp(ik_\theta \ell)$$

on a semi-infinite slab and accounting for the reflection results in the following general solution for the constants of Eqs. (56) and (57)

$$\left.\begin{aligned} A &= \frac{2E_0\rho'}{(1+n_1)(\rho'-\rho'')} = \frac{2E_0(\rho')^2}{(1+n_1)[(\rho')^2-1]} \\ B &= \frac{-2E_0\rho''}{(1+n_2)(\rho'-\rho'')} = \frac{-2E_0}{(1+n_2)[(\rho')^2-1]} \end{aligned}\right\} \quad (59)$$

Then for $\theta = \pi/2$

$$\rho' \to 0 \qquad \frac{B}{\rho''} \to 0$$

$$A \to 0$$

$$\frac{A}{\rho'} \to 0 \qquad B \to \frac{2E_0}{(1+n_2)}$$

Inspection of Eqs. (56) and (57) with these values indicates that only a linear wave polarized in the $\mathbf{a}_x$ direction is propagated in the plasma. This results in no Faraday rotation, in agreement with previous results.

Equation (58) is recognized as the sum of a right-hand circularly polarized wave and left-hand circularly polarized wave. The Faraday rotation per unit length is therefore

$$\Omega_L = \frac{k_\theta' - k_\theta''}{2} = \frac{\omega}{2c}(n_1 - n_2)$$

$$\Omega_L = \frac{\omega}{2c}\left[\left(1 - \frac{X}{1 - i\rho' Y_L}\right)^{1/2} - \left(1 - \frac{X}{1 - i\rho'' Y_L}\right)^{1/2}\right]$$

$$\Omega_L = \frac{-\omega X Y_L}{2c} \frac{\left(Y_L^2 + \dfrac{Y_T^4}{4(1-X)^2}\right)^{1/2}}{|Y_L|\left(\dfrac{n_1+n_2}{2}\right)}$$

$$\Omega_L \simeq \frac{-\omega X Y_L}{2c} \frac{1 + \dfrac{1}{2}\left[\dfrac{Y_T^2}{2(1-X)Y_L}\right]^2}{\left(\dfrac{n_1+n_2}{2}\right)}, \qquad \left[\frac{Y_T^2}{2(1-X)Y_L}\right] \ll 1 \quad (60)$$

The lower forms which are more suitable for computation do not involve the difference of quantities of nearly equal magnitude. These reduce to the usual approximation [Eq. (30), except Y replaced by Y_L] for $Y \ll 1$, $X \ll 1$, and $(Y_T^2)/[2(1-X)Y_L] \ll 1$.

It is necessary to estimate the plasma frequency, gyro frequency, and collision frequency in the solar corona as a function of distance from the sun. This verifies the validity of the approximation used in the computation involving the *Pioneer VI* solar occultation experiment. The plasma frequency and gyro frequency (in Hz) simplify to (B_0 in G)

$$\left.\begin{aligned} f_p &= 8.97837\,(N)^{1/2} \\ f_g &= -2.799202 \times 10^6\, B_0 \end{aligned}\right\} \quad (61)$$

The approximate collision frequency is given by (Ref. 29)

$$f_c \simeq \frac{42\,N}{2\pi\, 10^6\, T^{3/2}} \simeq 6.6845 \times 10^{-15} N \quad (62)$$

where an approximate electron temperature of 10^6°K was assumed. Assuming a Parker radial field with a magnitude of 1 G at the surface of the sun and a modified Allen–Baumbach electron density for a "quiet" sun (B in G)

$$\left.\begin{aligned} B &\simeq \frac{1}{R^2} \\ N &\simeq \left(\frac{1.55}{R^6} + \frac{0.01}{R^2}\right) 10^{14} \end{aligned}\right\} \quad (63)$$

where R is in solar radii [see Eqs. (1) and (4)]. Typical "quiet" sun values as a function of R are tabulated in Table 1 for the *Pioneer VI* frequency of 2.292036×10^9 Hz. This table demonstrates the validity of the assumptions used in this investigation of the solar corona. The collision frequency is extremely low even if the density were raised by an order of magnitude. The "averaged" electron density in the solar corona is not expected to differ by more than about a factor of 2 from the modified Allen–Baumbach value, even during periods of solar activity except possibly

Table 1. Typical "quiet" sun values of pertinent plasma parameters in the solar corona as a function of distance from center of sun

Distance from sun center R, solar radii	Electron density N, 10^{11} m^{-3}	Magnetic field magnitude B, G	Plasma frequency f_p, 10^6 Hz	Gyro frequency f_g, 10^6 Hz	Collision frequency f_c, 10^{-3} Hz	Plasma frequency/ signal frequency f_p/f	Gyro frequency/ signal frequency f_g/f
3	3.237	0.1111	5.109	−0.3110	2.16	0.00223	−0.00014
6	0.3110	0.0278	1.583	−0.0778	0.208	0.00069	−0.00003
10	0.1016	0.0100	0.9048	−0.0280	—	0.00039	−0.00001
20	0.02502	0.0025	0.4491	−0.0070	—	0.00020	—

in localized regions. The low-collision frequency implies minimal signal attenuation.

B. Ray Paths in the Solar Corona

The analysis of Faraday rotation in the solar corona requires a knowledge of the ray path through the solar corona. The sophisticated techniques (Refs. 30, 31) usually required for the ionosphere are not necessary at the distances from the sun considered in this experiment. The following analysis assumes a solar corona model with radial symmetry composed of uniform stratified layers. The geometry is shown in Fig. 2. By Snell's law, when the ray goes from a stratified medium with index of refraction n_{i-1} to that with n_i

$$\sin \alpha'_{i-1} = \frac{n_{i-1}}{n_i} \sin \alpha_{i-1} \tag{64}$$

Using the law of sines

$$\left.\begin{aligned} \sin \alpha'_{i-1} &= \frac{n_{i-1}}{n_i} \sin\left(\alpha'_{i-2} + \phi_{i-1} - \phi_{i-2}\right) \\ R_i &= R_{i-1} \frac{\sin \alpha'_{i-1}}{\sin\left(\alpha'_{i-1} + \phi_i - \phi_{i-2}\right)} \end{aligned}\right\} \tag{65}$$

A ray-tracing computer program (see Appendix A) with double precision arithmetic has been written that employs these equations. The modified Allen–Baumbach[1] electron density (applicable for $R > 2$) is used to estimate the index of refraction with the equation (N in m^{-3})

$$n = \left[1 - \left(\frac{\omega_p}{\omega}\right)^2\right]^{1/2} \simeq \left[1 - \left(\frac{8.97837}{f}\right)^2\right]^{1/2} N \tag{66}$$

[1]The conclusions of this section are not affected by the "new" electron density derived in Section VI [Eq. (113)].

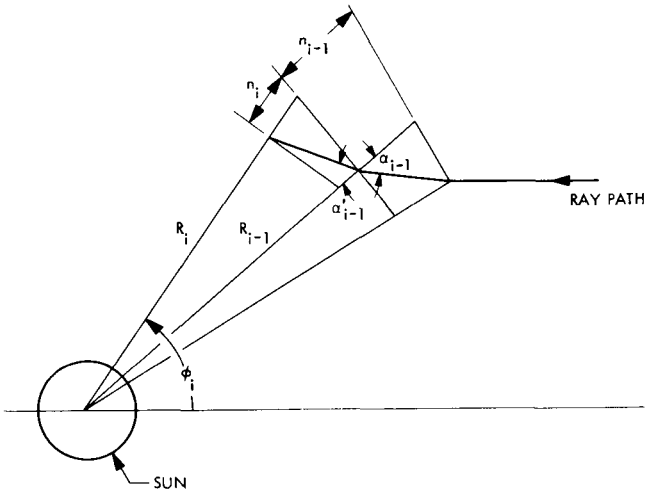

Fig. 2. Geometry used to calculate ray path in a radially symmetric solar corona model with uniform stratified layers

where

f = signal frequency, Hz

Bending of the ray is away from the sun since n is less than unity (assuming $\omega_p/\omega < 1$) in the portion of the solar corona of interest. A sample printout is shown in Fig. 3 for an initial offset A of 3 solar radii using a step size of $\Delta\phi = 1$ deg. Using smaller increments does not significantly affect the results.

Verification of the stratified layer ray-tracing computer program was obtained by an independent solution. Bracewell (Ref. 32) gives a solution for the ray (assuming spherical symmetry)

$$\phi = A \int_R^\infty \frac{d\rho}{\rho(n^2\rho^2 - A^2)^{1/2}}$$

FREQUENCY (MHZ) = 2292.036

RAY OFFSET (SOLAR R) = 3.000 (Y-A)=RHO(I)*SIN(PHI(I))-RAY OFFSET

PHI INCREMENT (DEG.) = 1.00000 RHO(I)-A = RHO(I)-RAY OFFSET

POLAR COORDINATES OF RAY PATH

I	PHI(I) (DEG)	RHO(I) (SOLAR R)	RHO'(I) (SOLAR R)	RHO(I)-RHO'(I) (SOLAR R)	ALPHA'(I) (DEG)	(Y-A)	RHO(I)-A (SOLAR R)
1	.97116	177.00000			.97116		
2	1.97116	87.21825	87.21825	.00000	1.97116	-.34694470-17	84.21825
12	11.97116	14.46345	14.46345	.69438-08	11.97116	.35732017-07	11.46345
22	21.97116	8.01839	8.01839	.43585-08	21.97116	.12699743-06	5.01839
32	31.97116	5.66580	5.66580	.40106-08	31.97117	.28835271-06	2.66580
42	41.97116	4.48594	4.48594	.47069-08	41.97118	.56329761-06	1.48594
52	51.97116	3.80855	3.80855	.60273-08	51.97120	.10385838-05	.80855
62	61.97116	3.39862	3.39862	.76132-08	61.97125	.18488637-05	.39862
72	71.97116	3.15491	3.15491	.90953-08	71.97133	.31674199-05	.15491
82	81.97116	3.02970	3.02970	.10138-07	81.97143	.51869480-05	.02970
92	91.97116	3.00178	3.00178	.10505-07	91.97154	.81018743-05	.00178
102	101.97116	3.06671	3.06671	.10118-07	101.97165	.12108586-04	.06671
112	111.97116	3.23497	3.23497	.90718-08	111.97174	.17442887-04	.23497
122	121.97116	3.53645	3.53645	.76142-08	121.97180	.24481715-04	.53645
132	131.97116	4.03512	4.03512	.60972-08	131.97184	.33969031-04	1.03512
142	141.97116	4.86975	4.86975	.49176-08	141.97186	.47558246-04	1.86975
152	151.97116	6.38427	6.38427	.45130-08	151.97186	.69442034-04	3.38427
162	161.97116	9.69356	9.69356	.56472-08	161.97187	.11331546-03	6.69356
172	171.97116	21.48084	21.48084	.12578-07	171.97186	.26130458-03	18.48084

R(N) = 212.50000

PHI(N) = 179.19039

PHI(STRAIGHT LINE) = 179.19109

Fig. 3. Sample computer output for stratified layer ray path program

The closest point of approach or "turning" point is solved from the relationship

$$n_a R_a = A$$

where

R_a = turning point radius

n_a = index of refraction at R_a

The value of ϕ at the turning point is given by

$$\phi_a = A \int_{R_a}^{\infty} \frac{d\rho}{\rho(n^2\rho^2 - A^2)^{1/2}}$$

The ray path is symmetrical about ϕ_a so that the "image" ϕ is given by

$$\phi_i = 2\phi_a - \phi$$

These equations were also programmed (see Appendix B) using a standard integration subroutine. A sample printout that indicates the close agreement is shown in Fig. 4 using the same parameters as the stratified layer program.

The difference in angle between the computed ray path and that assuming a straight line from the probe to the earth is 0.0007 deg. The difference is less at larger initial offsets. The antenna pointing error to the spacecraft is reduced by approximately one-half, or less than 0.0004 deg (since the earth–spacecraft distance is approximately twice the earth–sun distance). This indicates that the bending of the ray due to the solar corona at the distances from the sun of interest for this experiment is not significant. Furthermore, the bending of these magnitudes cannot be experimentally resolved with antenna boresight methods (see Section III). The Faraday rotation through the solar corona at distances from the sun investigated in this experiment can, therefore, be computed with sufficient accuracy along a geometric straight line ray path.

C. Faraday Rotation in the Solar Corona

The primary goal of the theoretical analysis of this report is the calculation of Faraday rotation of a CW signal traversing the solar corona. This calculation is

FREQUENCY (F),MHZ = 2292.03600 PHI(A) = 89.999645

RAY OFFSET (A),SOLAR RADII = 3.00 R(A) = .300000745117+001

R INCREMENT,SOLAR RADII = 10.000

I	R (SOLAR R)	PHI (DEG)	IMAGE PHI (DEG)
1	10.00	17.45760	162.54169
2	20.00	8.62692	171.37237
3	30.00	5.73917	174.26012
4	40.00	4.30122	175.69807
5	50.00	3.43981	176.55948
6	60.00	2.86598	177.13331
7	70.00	2.45628	177.54301
8	80.00	2.14909	177.85019
9	90.00	1.91021	178.08908
10	100.00	1.71913	178.28016
11	110.00	1.56280	178.43649
12	120.00	1.43254	178.56675
13	130.00	1.32233	178.67696
14	140.00	1.22786	178.77143
15	150.00	1.14599	178.85330
16	160.00	1.07436	178.92493
17	170.00	1.01115	178.98814
18	180.00	.95497	179.04432
19	190.00	.90471	179.09458
20	200.00	.85947	179.13982
21	210.00	.81854	179.18076
22	212.50	.80891	179.19038

Fig. 4. Sample ray path output computed with identical parameters used in the stratified layer program

traditionally made with Eq. (30) and the longitudinal component of the magnetic field. The following "exact" analysis assumes a solar corona model composed of uniform stratified sections. The term "exact" refers to the following derivation that employs a generalized coordinate system. Collisions and reflections are neglected and a straight line ray path is assumed. The assumptions regarding collisions and a straight line path have been discussed in Subsection B. The effect of reflections at S-band frequencies in the solar corona is known experimentally to be small. Goldstein (see Ref. 49) demonstrated during the *Pioneer VI* occultation that, although the received signal suffered doppler broadening, the total received power as measured by integrating the total signal spectrum was not attenuated.

The generalized coordinate system applicable to the *Pioneer VI* solar corona geometry is shown in Fig. 5. The transverse electric field in a uniform *i*th section is obtained from Eqs. (56) and (57)

$$\varepsilon(\ell,t) = Re\,\{[(R'_i\mathbf{a}_x + i\mathbf{a}_\theta)(A'_i + iB'_i)\exp(ik'_i\ell) + (\mathbf{a}_x - iR'_i\mathbf{a}_\theta)(A''_i + iB''_i)\exp(ik''_i\ell)]\exp(-i\omega t)\} \tag{67}$$

where the relation

$$\rho' = -iR' \tag{68}$$

is used. The quantities in Eq. (67) are all real and finite.

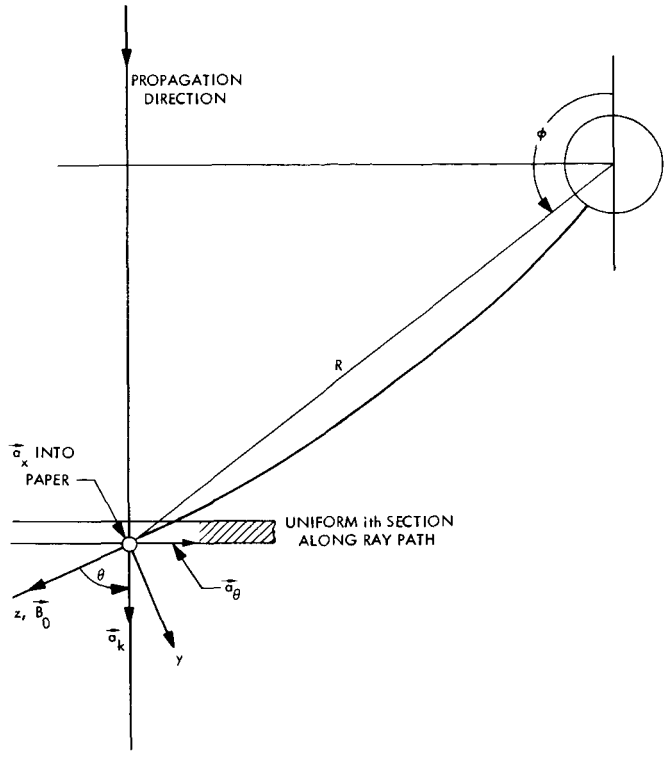

Fig. 5. Geometry of magnetic field line B_0 emanating from sun, looking down plane of ecliptic

The electric field at the output of the *i*th uniform section of thickness s is found from Eq. (67) at $\ell = s$. Expanding in sines and cosines, collecting terms and taking the real part results in

$$\varepsilon_i = \mathbf{a}_x(A_i\cos\omega t + B_i\sin\omega t) + \mathbf{a}_\theta(C_i\cos\omega t + D_i\sin\omega t) \tag{69}$$

where

$$\begin{aligned}
A_i &= R'_iA'_i\cos k'_is - R'_iB'_i\sin k'_is + A''_i\cos k''_is - B''_i\sin k''_is\\
B_i &= R'_iA'_i\sin k'_is + R'_iB'_i\cos k'_is + A''_i\sin k''_is + B''_i\cos k''_is\\
C_i &= -B'_i\cos k'_is - A'_i\sin k'_is + R'_iB''_i\cos k''_is + R'_iA''_i\sin k''_is\\
D_i &= -B'_i\sin k'_is + A'_i\cos k'_is + R'_iB''_i\sin k''_is - R'_iA''_i\cos k''_is
\end{aligned}$$

Direct computation of the coefficients as given above requires taking sines and cosines of extremely large arguments (on the order of 10^8) when dealing with propagation in the solar corona. Increased computational accuracy can be obtained by using (evaluated at *i*)

$$\begin{aligned}
A &= \cos k^-s\,[-(R'B' + B'')\sin k^+s + (R'A' + A'')\cos k^+s] + \sin k^-s\,[(R'B' - B'')\cos k^+s + (R'A' - A'')\sin k^+s]\\
B &= \cos k^-s\,[(R'A' + A'')\sin k^+s + (R'B' + B'')\cos k^+s] + \sin k^-s\,[-(R'A' - A'')\cos k^+s + (R'B' + B'')\sin k^+s]\\
C &= \cos k^-s\,[(R'A'' - A')\sin k^+s + (R'B'' - B')\cos k^+s] + \sin k^-s\,[(R'A'' + A')\cos k^+s - (R'B'' + B')\sin k^+s]\\
D &= \cos k^-s\,[(R'B'' - B')\sin k^+s - (R'A'' - A')\cos k^+s] + \sin k^-s\,[(R'B'' + B')\cos k^+s + (R'A'' - A')\sin k^+s]
\end{aligned}$$

where

$$k^{+} = \frac{k'' + k'}{2} = \frac{\omega}{c}\frac{n_2 + n_1}{2}$$

$$k^{-} = \frac{k'' - k'}{2} = -\frac{\omega}{c}\frac{X\left[Y_L^2 + \dfrac{Y_T^4}{4(1-X)^2}\right]^{1/2}}{\left[1 - Y_L^2 - \dfrac{Y_T^2}{(1-X)}\right](n_2 + n_1)}$$

Further computational accuracy can be obtained when $(Y_T^2)/[2(1-X)Y_L]$ is either very small (condition 1) or very large (condition 3). When small,

$$\left.\begin{aligned}\left[Y_L^2 + \frac{Y_T^4}{4(1-X)^2}\right]^{1/2} &\simeq Y_L\left\{1 + \frac{1}{2}\left[\frac{Y_T^2}{2(1-X)Y_L}\right]^2 - \frac{1}{8}\left[\frac{Y_T^2}{2(1-X)Y_L}\right]^4\right\}\\ R' &\simeq \frac{G}{Y_L} - 1 - \frac{1}{2}\left[\frac{Y_T^2}{2(1-X)Y_L}\right]^2 + \frac{1}{8}\left[\frac{Y_T^2}{2(1-X)Y_L}\right]^4\end{aligned}\right\} \tag{70}$$

When large,

$$\left.\begin{aligned}\left[Y_L^2 + \frac{Y_T^4}{4(1-X)^2}\right]^{1/2} &\simeq \frac{Y_T^2}{2(1-X)}\left\{1 + \frac{1}{2}\left[\frac{2(1-X)Y_L}{Y_T^2}\right]^2 - \frac{1}{8}\left[\frac{2(1-X)Y_L}{Y_T^2}\right]^4\right\}\\ R' &\simeq -\frac{1}{2}\left[\frac{2(1-X)Y_L}{Y_T^2}\right]^2 + \frac{1}{8}\left[\frac{2(1-X)Y_L}{Y_T^2}\right]^4\end{aligned}\right\} \tag{71}$$

The $\mathbf{a}_x$ and $\mathbf{a}_\theta$ components of E_i are given respectively by

$$(E_i)_x = (A_i^2 + B_i^2)^{1/2} \text{ and } (E_i)_\theta = (C_i^2 + D_i^2)^{1/2} \tag{72}$$

The incident transverse electric field from the $(i-1)$th section can be written from Eq. (69).

$$R_e\{[(\mathbf{a}_x A_{i-1} + \mathbf{a}_\theta C_{i-1}) + i(\mathbf{a}_x B_{i-1} + \mathbf{a}_\theta D_{i-1})]\exp(-i\omega t)\} \tag{73}$$

Equating with Eq. (67) at $\ell = 0$,

$$[(\mathbf{a}_x A + \mathbf{a}_\theta C) + \mathrm{i}(\mathbf{a}_x B + \mathbf{a}_\theta D)]_{i-1} = [(R'\mathbf{a}_x + i\mathbf{a}_\theta)(A' + iB') + (\mathbf{a}_x - iR'\mathbf{a}_\theta)(A'' - iB'')]_i \tag{74}$$

Then

$$\left.\begin{aligned}A_i' &= \frac{R_i' A_{i-1} + D_{i-1}}{(R_i')^2 + 1}\\ A_i'' &= \frac{-R_i' D_{i-1} + A_{i-1}}{(R_i')^2 + 1}\\ B_i' &= \frac{R_i' B_{i-1} - C_{i-1}}{(R_i')^2 + 1}\\ B_i'' &= \frac{R_i' C_{i-1} + B_{i-1}}{(R_i')^2 + 1}\end{aligned}\right\} \tag{75}$$

In the above, the tangential components of the electric field vectors were matched at the boundary to the ith section neglecting reflections.

The electric field vector given by Eq. (69) in general describes an ellipse. The tilt angle of the major (or minor) axis of the ellipse ϕ is given by

$$(\Omega_E)_i = 90\,\mathrm{deg} + \frac{1}{2}\tan^{-1}\frac{2(B_i D_i + A_i C_i)}{A_i^2 + B_i^2 - C_i^2 - D_i^2} \tag{76}$$

This gives the signal polarization angle at the output of the ith section in terms of the signal parameters at the input to the section and the plasma parameters in the section. The initial value of 90 deg represents the situation of the *Pioneer VI* signal relative to the plane of the ecliptic. The initial conditions are found by assuming an incident signal

$$\mathbf{E} = E_0 \mathbf{a}_x \exp(ik_e \ell) \tag{77}$$

Then assuming E_0 = unity, we have [from Eq. (69)]

$$A_1 = 1$$
$$B_1 = C_1 = D_1 = 0$$

The components of the signal along the major (plus sign) and minor (minus sign) axes of the ellipse are given by (Ref. 33)

$$(|E|^2_{\pm})_i = \frac{1}{2}\{A_i^2 + B_i^2 + C_i^2 + D_i^2 \pm [(A_i^2 + C_i^2 - B_i^2 - D_i^2)^2 + 4(A_iB_i + C_iD_i)^2]^{1/2}\} \tag{78}$$

This result can be used to give the polarization ellipse ratio (defined in terms of power)

$$\text{Ratio} = \frac{|E|^2_-}{|E|^2_+} \tag{79}$$

and signal power loss

$$\text{Loss} = -10 \log |E|^2_+ \tag{80}$$

The signal loss results from the fact that the receiving system is sensitive only to that component of the signal along the major axis of the ellipse.

The preceding equations have been programmed (see Section VI) on the Univac 1108 computer (see Appendix C). The program sequentially steps the solution in ϕ from the probe to the earth. The sequence of computations are (given A_1, B_1, C_1, D_1) as follows:

(1) Calculate A_2', A_2'', B_2', and B_2'' from Eq. (75).

(2) Calculate A_2, B_2, C_2, and D_2 from Eq. (69).

(3) Repeat (1) for $i = 3$ and continue.

The conditions used in Eqs. (70) and (71) are identified for each stratified layer in the computation. The layers in which these conditions are not satisfied are identified as condition 2. Under these conditions, no approximations are used in the computations.

III. Experiment Description

The *Pioneer VI* spacecraft (Refs. 34–36) was launched into a sun-orbital trajectory on December 16, 1965, from Cape Kennedy. The mission was planned for an 8-month duration. This limitation was based on the existing communication capability of the vehicle-to-earth telemetry link. The last usable signals were expected on the 85-ft antennas of the Deep Space Network (DSN) in August 1966. The completion of the 210-ft Advanced Antenna System (AAS) at the Goldstone Deep Space Communications Complex, in March 1966, the implementation of a lower noise receiver system, and the reliability of the vehicle transmitter has made it possible to track the *Pioneer VI* throughout its orbit around the sun (Refs. 36 and 37).

Initially, the linearly polarized signal from the spacecraft was received by the 85-ft ground antennas with circularly polarized feeds. The received power was reduced by a factor of 2 by the polarization mismatch, but the possibility of losing the signal entirely because of improper orientation was eliminated. The polarization loss was eliminated with instrumentation that tracked the signal polarization. This was originally developed with IF circuitry (Ref. 38). Although satisfactory for maintaining signal strength, this instrumentation which used an open loop system, did not fulfill the requirements for precise polarization tracking because of large phase shifts (20–30 deg) occurring in the masers with changing antenna elevation angle. The final system used for the Faraday rotation experiment was a remotely rotatable, RF linear feed. This closed-loop polarimeter (see Section IV) was developed and implemented so that the orientation of the polarization could be automatically tracked. This system maximized the received signal strength and yielded precise received signal polarization data.

The telemetry signal from the *Pioneer VI* spacecraft passed through increasingly dense regions of the solar corona as the earth–probe line of sight approached the sun. Since the linearly polarized high-gain antenna of the spacecraft was spin-stabilized with respect to the plane of the ecliptic, it was possible to measure rotation of the plane of polarization produced by the interaction of the microwave signal with the magnetized plasma of the propagation medium.

The polarization measurements became increasingly difficult as the sun–earth–probe (SEP) angle (i.e., elongation) decreased. The difficulty resulted from both the increase in system temperature from solar microwave radiation and the spectral broadening of the carrier produced by distortion in the solar corona. Measurements of polarization angle with the automatic tracking system began on October 26 and continued during the Goldstone view periods until November 17 when the signal-to-noise ratio deteriorated below the useful level. From November 21 (06:00 PST) through November 24 (10:00 PST), 1968, *Pioneer VI* was geometrically occulted by the photosphere. The signal was reacquired on November 29 and the experiment was continued until December 8 when the station was assigned to the *Apollo* 8 mission.

A. Description of the *Pioneer VI* Spacecraft

The *Pioneer VI* (see Ref. 36) spacecraft (Fig. 6) is cylindrical in shape and contains three booms, an antenna oblique to the spin axis (Stanford experiment) aft of the spacecraft, and a mast antenna on the cylinder axis of the spacecraft. This mast structure contains the high-gain antenna that was used for this experiment. The structure consists basically of a central equipment platform, three deployable booms, supporting rings for the solar array, the antennas, boom, and platform dampers, and necessary support equipment.

All of the spacecraft electronic equipment and most of the scientific instruments are located on the equipment platform. The platform is an aluminum panel approximately 37 in. in diameter located aft of the forward edge of the cylindrical solar array.

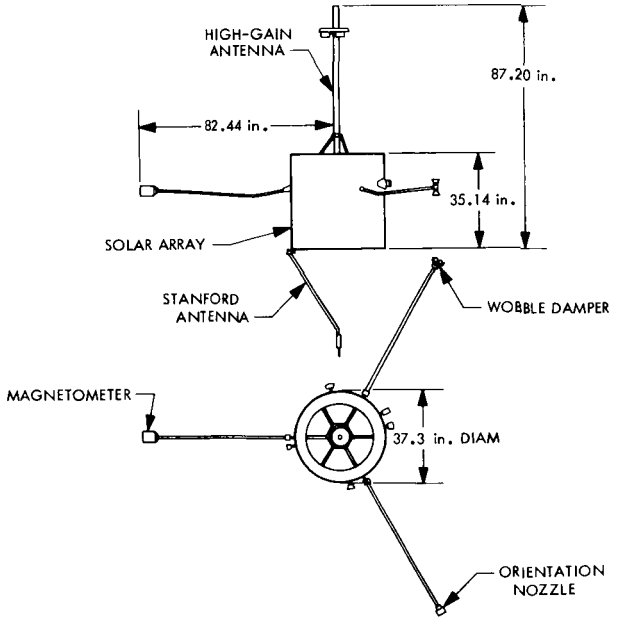

Fig. 6. *Pioneer VI* spacecraft in flight configuration

The three booms are designed to give a net moment of inertia about the principal axis such that the spacecraft is gyroscopically stable when spinning about that axis. These booms are equally spaced 120 deg apart and are hinged to the equipment platform. The wobble damper is on one of the booms.

The spacecraft is spin-stabilized at 58 rev/min with the spin axis nominally normal to the plane of the ecliptic.

B. Vehicle Antenna and Orientation

The *Pioneer VI* high-gain antenna extends approximately 52 in. above the solar array and is supported by six struts attached to the equipment platform. This antenna is a linearly polarized Franklin array with the electric field vector on the spin axis. This design with linear polarization provided the required system performance with minimum weight and minimum cost.[2] The beam of the antenna is axially symmetric with respect to the spin axis and has a width of approximately 35 deg at the half-power points. The spacecraft transmitter uses a 7.7-W traveling-wave tube excited by a solid-state driver. The transmitted frequency is 2292.036 MHz. The signal power received from *Pioneer VI* by the 210-ft antenna during the experiment was nominally approximately 4×10^{-20} W.

C. Orbit Determination and Description

The conic orbit parameters of the *Pioneer VI* spacecraft are given as follows:

Parameter	Value
Period	311.33 days
Semimajor axis	134,484,630 km
Eccentricity	0.0941610
Inclination	0.1693 deg
Longitude of ascending node	260.35 deg
Argument of perihelion	2.78 deg
Epoch of perihelion passage	02:54 GMT, May 20, 1966

[2]Dickenson, L., private communication.

Figure 7 shows an ecliptic plane projection of the spacecraft position relative to the sun–earth line.

The orbit is fairly accurately known from the pointing and doppler data of the DSN tracking stations. Right ascension and declination are computed from the JPL SPACE (Ref. 39) computer program with initial conditions obtained from PI0-602[3] with an epoch of 24:00:00.000 GMT—on January 8, 1967. The initial conditions were obtained from 200 data points (from days 239 and 249, 1967) of two-day doppler data from the Mars station. Figure 8 shows a plot of the Mars station pointing right ascenion corrections (no corrections were needed for declination since these offsets were smaller than the right ascension errors and less critical to the experiment) to the predicts. A least-squares computer fit to the data (computer program CTS 40, see Appendix E) is

$$\Delta RA = 0.0643 - 0.0003543\,T \tag{81}$$

where

ΔRA = right ascension correction, deg

T = time in 1968 decimal days

These pointing data (32 data points over a 43-day period ending on December 8, 1968) has a 1σ spread of 0.004 deg. These data are obtained by pointing the antenna off target in both directions in right ascension for equal signal degradation and algebraically determining the correction. The technique is limited by the *Pioneer VI* signal-to-noise ratio in the receiver. Three data points identified in Fig. 8 were not used in the computer fit because of the poor quality of the data, which was caused by poor signal-to-noise ratio near the sun. Refraction of the signal caused by the solar corona is not significant for these calibrations (see Section II.B). The correction to the orbit predicts was considered necessary because of the long time span between the PI0602 data used for the predicts and the occultation experiment.

These corrections are applied to the predicts of the JPL SPACE trajectory program (see footnote 4) to compute the position of the *Pioneer VI* relative to the sun in the plane of the ecliptic. A Cartesian coordinate system axis rotation (see Fig. 13a) of ϵ about the x-axis (which is aligned with the vernal equinox) is given by

[3]Reynolds, C. W., *Conditions of the Latest Pioneer VI Updated Orbit (PIO-603)*, Memorandum 312.9-156. Jet Propulsion Laboratory, Pasadena, Calif., Dec. 1967.

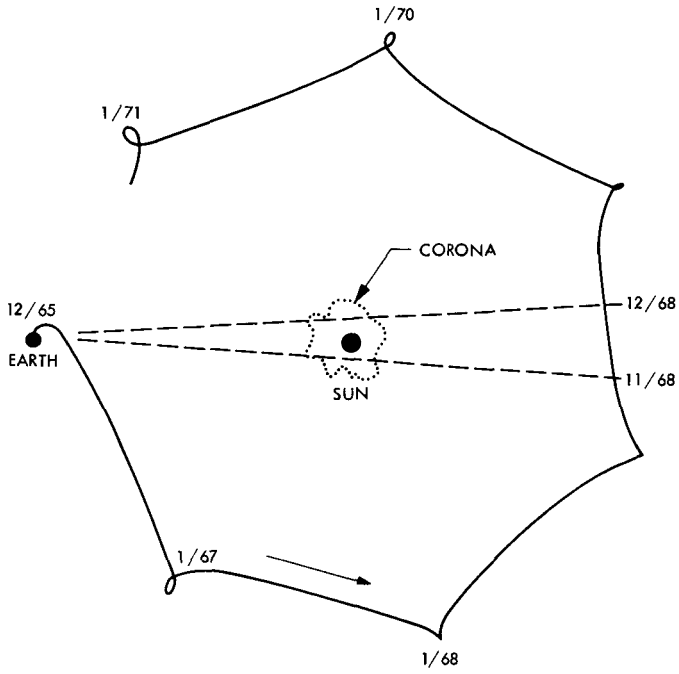

Fig. 7. Projection of Pioneer VI orbit on plane of ecliptic relative to earth–sun line

$$\left.\begin{aligned} X_\epsilon &= X_E \\ Y_\epsilon &= Y_E \cos\epsilon + Z_E \sin\epsilon \\ Z_\epsilon &= -Y_E \sin\epsilon + Z_E \cos\epsilon \end{aligned}\right\} \tag{82}$$

where

$X_\epsilon, Y_\epsilon, Z_\epsilon$ = Cartesian coordinate system in plane of the ecliptic with X_ϵ along the vernal equinox

X_E, Y_E, Z_E = Cartesian coordinate system in the earth equatorial frame with X_E along the vernal equinox

These equations transform from the earth equatorial frame to space fixed in the plane of the ecliptic. The Cartesian coordinates of the probe in the earth equatorial frame is

$$\left.\begin{aligned} X_{EP} &= R_P \cos\delta_p \cos\alpha_p \\ Y_{EP} &= R_P \cos\delta_p \sin\alpha_p \\ Z_{EP} &= R_P \sin\delta_p \end{aligned}\right\} \tag{83}$$

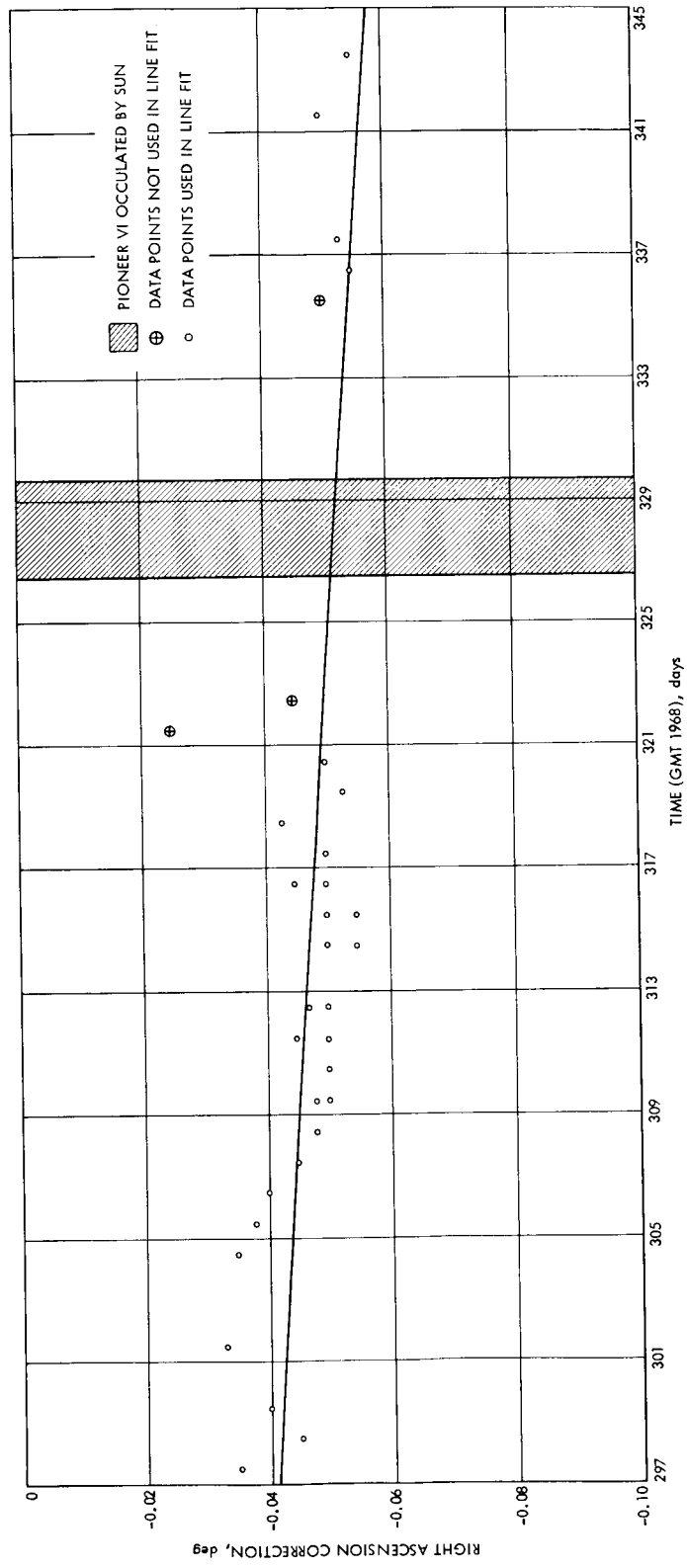

Fig. 8. Mars station measurements of *Pioneer VI* right ascension corrections

where

R_P = earth–probe distance

δ_p = probe declination (angle between the vector to the probe and the equatorial plane), deg

α_p = probe right ascension (angle between the vector to the probe and the vernal equinox), deg

Substitution into Eq. (82) yields the coordinates of the probe in the ecliptic frame:

$$\left.\begin{aligned} X_P &= R_P \cos\delta_p \cos\alpha_p \\ Y_P &= R_P(\cos\delta_p \sin\delta_p \cos\epsilon + \sin\delta_p \sin\epsilon) \\ Z_p &= R_p(-\cos\delta_p \sin\delta_p \sin\epsilon + \sin\delta_p \cos\epsilon) \end{aligned}\right\} \quad (84)$$

A similar expression is obtained for the position of the sun in this coordinate system.

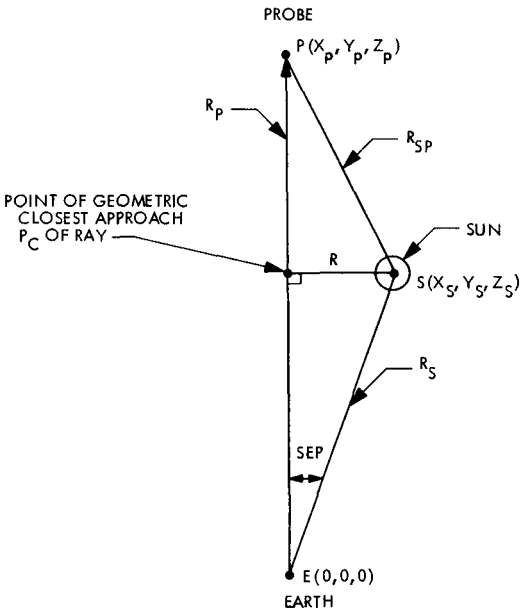

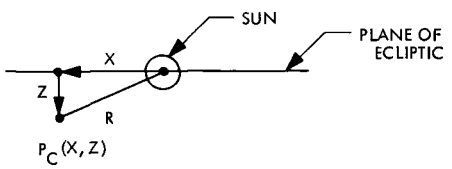

Fig. 9. Coordinate system used to calculate *Pioneer VI* probe position relative to sun in plane of ecliptic

The SEP angle (Fig. 9) found from the vector dot product of $\mathbf{R}_S$ and $\mathbf{R}_p$ is

$$\cos(\text{SEP}) = \frac{X_S X_P + Y_S Y_P + Z_S Z_P}{R_S R_P} \quad (85)$$

The additional parameters (Fig. 9) required to describe the *Pioneer VI* propagating signal path relative to the sun are

$$\left.\begin{aligned} R_{PC} &= \text{earth–}P_C\text{ (geometric point of closest approach of ray to sun) distance} = R_S \cos(\text{SEP}) \\ R &= \text{sun–}P_C\text{ distance} = R_S \sin(\text{SEP}) \\ Z &= Z_P \frac{R_{PC}}{R_P} \\ X &= (R^2 - Z^2)^{1/2} \\ R_{SP} &= \text{sun–probe distance} \\ &= [R_S^2 + R_P^2 - 2R_S R_P \cos(\text{SEP})]^{1/2} \end{aligned}\right\} \quad (86)$$

Computation with these equations (see Appendix E, program CTS 41) and the data from the JPL SPACE trajectory computer program corrected with Eq. (81) result in the parameters tabulated and plotted in Figs. 10 and 11. Time in GMT is used for these data and distance is expressed in solar radii (6.9598×10^8 m).

D. Received Signal Polarization Coordinate Transformation

The problem considered here is the determination of the signal polarization referred to the plane of the ecliptic from polarization data measured at a local station using an az–el antenna. The measured polarization angle θ_p is defined (see Ref. 27) as ccw looking toward the probe (Fig. 12) relative to the local horizon. For example, if the **E** vector of the received signal is in the plane containing the observation point, zenith, and probe, the polarization angle will be 90 deg.

The solution is found through the equations transforming the coordinate system between the plane of the ecliptic and the local station (Ref. 40). The rotation from the equatorial frame to the plane of the ecliptic, both earth centered and space fixed (Fig. 13a), is given in matrix notation [from Eq. (82)]

$$(R_\epsilon) = [M_z](R_E) \quad (87)$$

1968 DAY (GMT)	PROBE DECLINATION (deg)	PROBE RIGHT ASCENSION (deg)	R_P (SOLAR RADII)	SUN DECLINATION (deg)	SUN RIGHT ASCENSION (deg)	R_S (SOLAR RADII)	R (SOLAR RADII)	X (SOLAR RADII)	Z (SOLAR RADII)	R_{SP} (SOLAR RADII)
300.0	-.19093	3.59956	395.177	-.21628	3.67283	213.649	16.242	16.239	-.306	182.869
301.0	-.19795	3.61844	394.883	-.22221	3.68960	213.590	15.728	15.725	-.302	182.552
302.0	-.20491	3.63741	394.592	-.22811	3.70643	213.531	15.209	15.206	-.299	182.238
303.0	-.21181	3.65644	394.303	-.23394	3.72331	213.473	14.688	14.685	-.295	181.930
304.0	-.21865	3.67558	394.018	-.23970	3.74024	213.415	14.158	14.155	-.292	181.626
305.0	-.22542	3.69481	393.737	-.24541	3.75724	213.357	13.626	13.623	-.288	181.327
306.0	-.23211	3.71414	393.459	-.25103	3.77427	213.300	13.082	13.079	-.280	181.033
307.0	-.23874	3.73356	393.184	-.25659	3.79137	213.244	12.537	12.534	-.276	180.744
308.0	-.24530	3.75307	392.914	-.26211	3.80853	213.189	11.987	11.984	-.273	180.461
309.0	-.25176	3.77268	392.647	-.26754	3.82576	213.134	11.434	11.431	-.265	180.183
310.0	-.25815	3.79238	392.385	-.27288	3.84304	213.080	10.874	10.871	-.260	179.910
311.0	-.26446	3.81218	392.126	-.27817	3.86038	213.027	10.311	10.307	-.258	179.644
312.0	-.27066	3.83207	391.871	-.28337	3.87777	212.975	9.741	9.738	-.250	179.384
313.0	-.27679	3.85208	391.621	-.28848	3.89524	212.924	9.166	9.163	-.245	179.129
314.0	-.28281	3.87218	391.375	-.29352	3.91276	212.873	8.588	8.585	-.239	178.881
315.0	-.28874	3.89239	391.133	-.29848	3.93034	212.823	8.002	7.999	-.235	178.639
316.0	-.29455	3.91268	390.895	-.30337	3.94800	212.774	7.421	7.418	-.228	178.405
317.0	-.30028	3.93308	390.662	-.30815	3.96570	212.726	6.828	6.825	-.224	178.176
318.0	-.30588	3.95358	390.433	-.31286	3.98348	212.679	6.237	6.233	-.218	177.955
319.0	-.31136	3.97418	390.209	-.31747	4.00130	212.632	5.635	5.631	-.210	177.740
320.0	-.31674	3.99488	389.989	-.32199	4.01921	212.586	5.037	5.033	-.205	177.533
321.0	-.32199	4.01569	389.773	-.32641	4.03717	212.540	4.427	4.423	-.198	177.333
322.0	-.32712	4.03658	389.561	-.33073	4.05520	212.495	3.824	3.819	-.193	177.141
323.0	-.33211	4.05759	389.354	-.33498	4.07328	212.451	3.210	3.205	-.184	176.956
324.0	-.33698	4.07868	389.152	-.33910	4.09143	212.407	2.596	2.590	-.177	176.779
325.0	-.34171	4.09986	388.954	-.34313	4.10963	212.364	1.980	1.973	-.169	176.610
326.0	-.34632	4.12113	388.760	-.34705	4.12791	212.320	1.367	1.357	-.165	176.449
327.0	-.35077	4.14251	388.571	-.35088	4.14623	212.278	.751	.735	-.157	176.295
328.0	-.35508	4.16397	388.386	-.35458	4.16461	212.236	.204	.140	-.149	176.150
329.0	-.35925	4.18552	388.206	-.35819	4.18306	212.194	.548	-.529	-.143	176.013
330.0	-.36327	4.20715	388.031	-.36168	4.20156	212.153	1.165	-1.157	-.135	175.884
331.0	-.36713	4.22888	387.861	-.36507	4.22010	212.113	1.796	-1.792	-.126	175.764
332.0	-.37083	4.25067	387.695	-.36831	4.23870	212.073	2.428	-2.426	-.117	175.652
333.0	-.37439	4.27253	387.535	-.37147	4.25736	212.035	3.060	-3.058	-.113	175.549
334.0	-.37777	4.29448	387.381	-.37451	4.27605	211.997	3.700	-3.699	-.104	175.454
335.0	-.38098	4.31650	387.231	-.37741	4.29480	211.960	4.341	-4.340	-.094	175.369
336.0	-.38404	4.33859	387.087	-.38020	4.31359	211.925	4.982	-4.982	-.086	175.291
337.0	-.38693	4.36073	386.949	-.38289	4.33244	211.890	5.621	-5.621	-.080	175.223
338.0	-.38964	4.38296	386.816	-.38542	4.35133	211.857	6.268	-6.268	-.069	175.164
339.0	-.39221	4.40523	386.689	-.38786	4.37026	211.825	6.910	-6.910	-.065	175.113
340.0	-.39456	4.42756	386.568	-.39015	4.38924	211.794	7.557	-7.557	-.054	175.072
341.0	-.39676	4.44993	386.452	-.39233	4.40826	211.764	8.198	-8.198	-.047	175.039
342.0	-.39877	4.47237	386.343	-.39437	4.42730	211.736	8.848	-8.848	-.037	175.015
343.0	-.40060	4.49482	386.239	-.39629	4.44640	211.708	9.490	-9.490	-.028	175.000
344.0	-.40226	4.51733	386.141	-.39809	4.46552	211.682	10.135	-10.135	-.020	174.995
345.0	-.40372	4.53988	386.049	-.39975	4.48469	211.657	10.779	-10.779	-.011	174.998

Fig. 10. Computer tabulation of signal ray path parameters from *Pioneer VI* probe to earth relative to sun

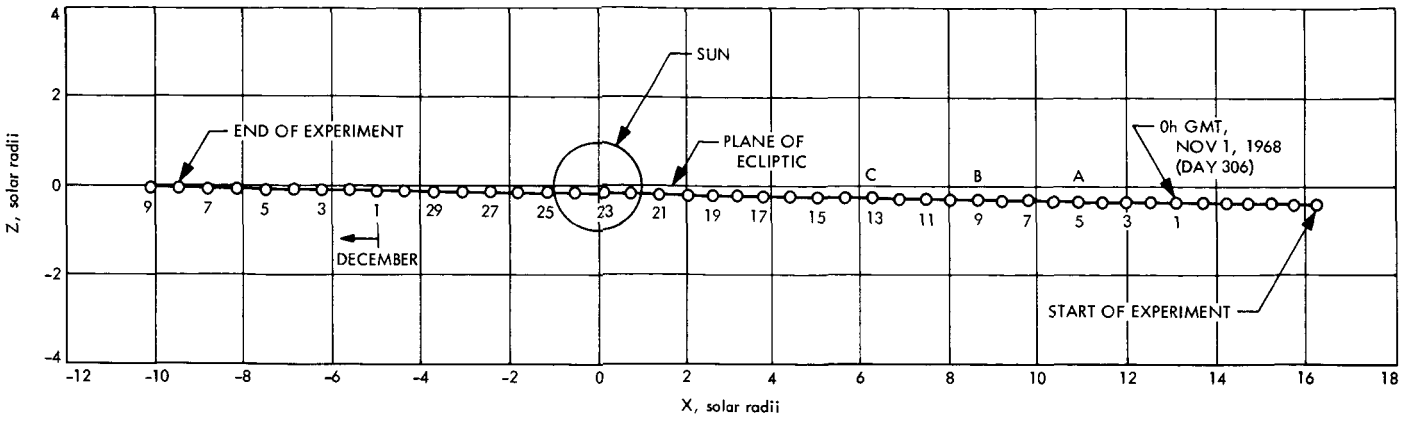

Fig. 11. Projection of *Pioneer VI* orbit perpendicular to plane of ecliptic relative to sun

where

$$[M_1] = \begin{bmatrix} 1 & 0 & 0 \\ 0 & \cos\epsilon & \sin\epsilon \\ 0 & -\sin\epsilon & \cos\epsilon \end{bmatrix}$$

$(R_E) = \begin{pmatrix} X_E \\ Y_E \\ Z_E \end{pmatrix}$ = Cartesian coordinates of probe in equatorial system, referred to vernal equinox

$(R_\epsilon) = \begin{pmatrix} X_\epsilon \\ Y_\epsilon \\ Z_\epsilon \end{pmatrix}$ = Cartesian coordinates of probe in the ecliptic plane

ϵ = angle between the equatorial plane and the plane of the ecliptic

The rotation in the equatorial frame from earth-fixed to space-fixed coordinates is accomplished with (Fig. 13b)

$$(R_E) = [M_2]\,(r) \tag{88}$$

where

$$[M_2] = \begin{bmatrix} \cos\gamma(t) & -\sin\gamma(t) & 0 \\ \sin\gamma(t) & \cos\gamma(t) & 0 \\ 0 & 0 & 1 \end{bmatrix}$$

$(r) = \begin{pmatrix} x \\ y \\ z \end{pmatrix}$ = Cartesian coordinates of probe in equatorial system referred to Greenwich longitude

$\gamma(t)$ = angle between the vernal equinox and Greenwich longitude

The transformation from the probe coordinates in terms of the station local coordinates (Fig. 13c) are given by (this rotation in longitude provides the proper coordinates for an HA-dec antenna pointing system)

$$(r) = [M_3]\,(r') \tag{89}$$

where

$$[M_3] = \begin{bmatrix} \cos\theta & -\sin\theta & 0 \\ \sin\theta & \cos\theta & 0 \\ 0 & 0 & 1 \end{bmatrix}$$

$(r') = \begin{pmatrix} x' \\ y' \\ z' \end{pmatrix}$ = local station Cartesian coordinates of probe: perpendicular earth N–S pole, east, and north

θ = station longitude (referred to Greenwich longitude)

The final rotation (Fig. 13d) in station latitude (useful for az–el antenna pointing systems such as used by the Mars station)

$$(r') = [M_4]\,(r'') \tag{90}$$

where

$$M_4 = \begin{bmatrix} \sin\phi & 0 & \cos\phi \\ 0 & 1 & 0 \\ -\cos\phi & 0 & \sin\phi \end{bmatrix}$$

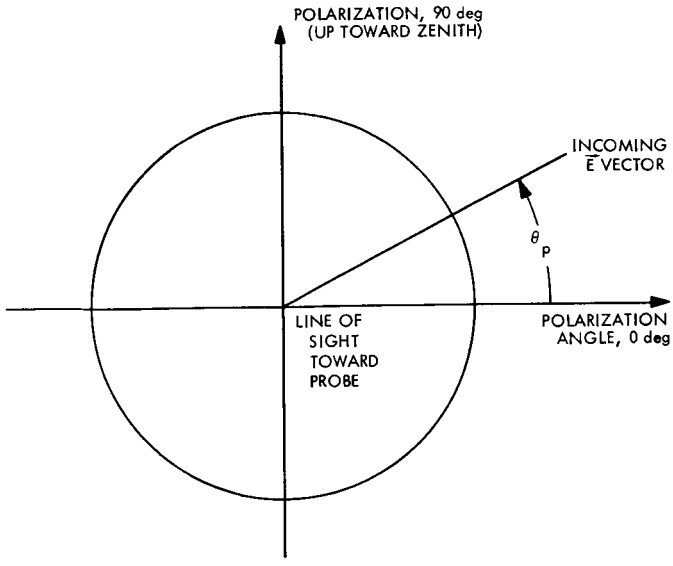

Fig. 12. Pictorial representation defining measured polarization angle looking along line of sight toward probe

$$(r'') = \begin{pmatrix} x'' \\ y'' \\ z'' \end{pmatrix} = \text{local station Cartesian coordinates of probe: in horizon, east, vertical}$$

ϕ = station latitude, deg

The probe position in station az–el coordinates (σ,γ) gives the vector from earth to probe

$$(r_p) = \begin{pmatrix} x_p'' \\ y_p'' \\ z_p'' \end{pmatrix} = \begin{pmatrix} r_p \cos\gamma \cos\sigma \\ r_p \cos\gamma \sin\sigma \\ r_p \sin\gamma \end{pmatrix} \tag{91}$$

where

r_p = station–probe distance

Defining the unit vectors (Fig. 14)

$$\mathbf{s} = \frac{\mathbf{r} \times \mathbf{r}_p}{|\mathbf{r} \times \mathbf{r}_p|}, \qquad \mathbf{u} = \frac{\mathbf{k}_\epsilon \times \mathbf{r}_p}{|\mathbf{k}_\epsilon \times \mathbf{r}_p|} \tag{92}$$

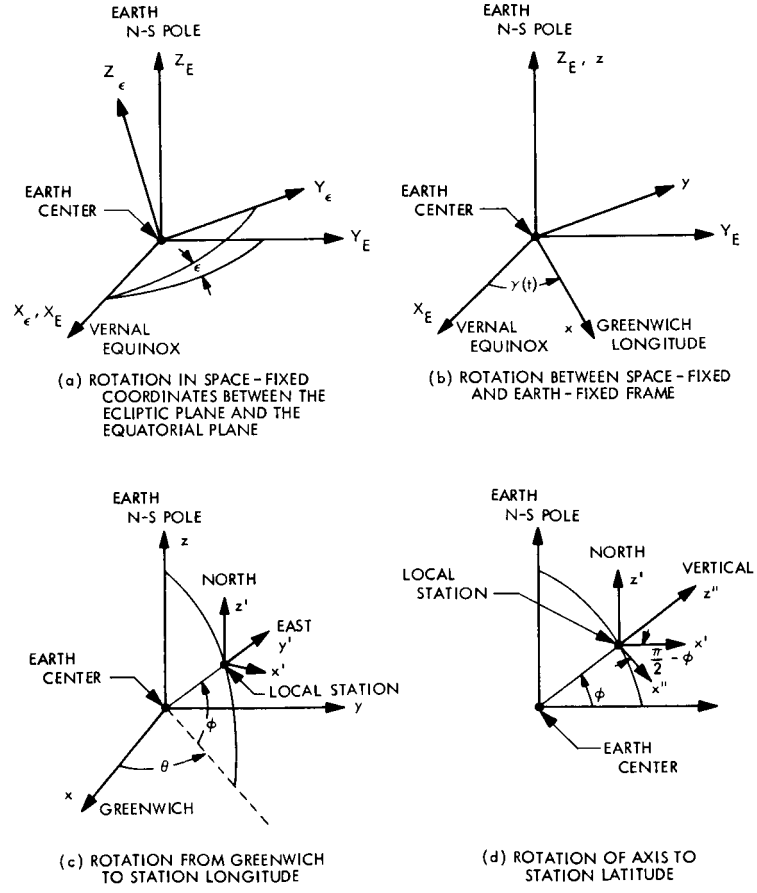

Fig. 13. Cartesian coordinate systems used to sequentially transform between ecliptic plane and local station coordinates

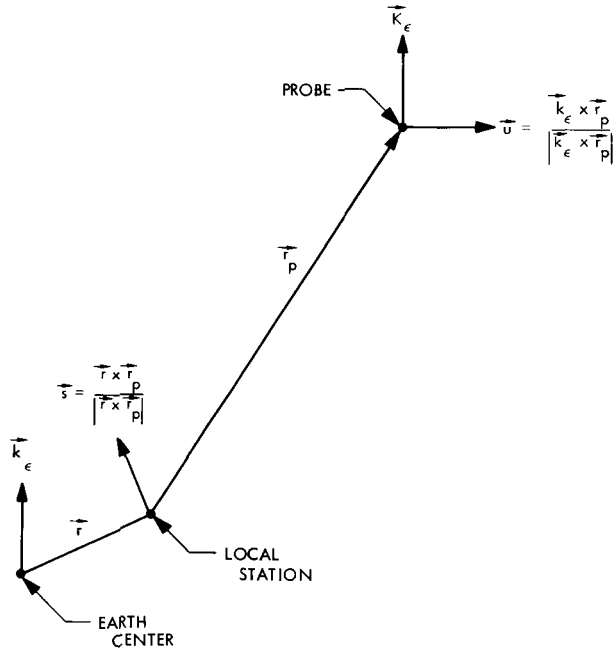

Fig. 14. Vectors used to relate probe polarization in ecliptic plane to that measured at local station

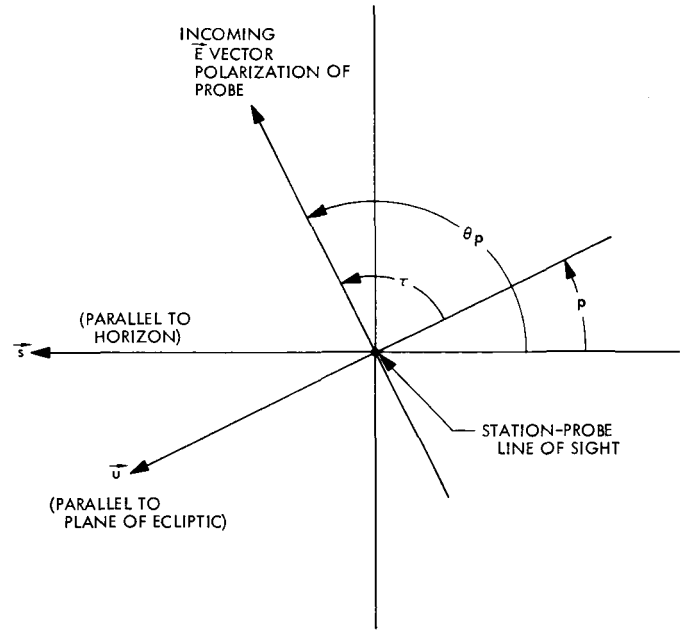

Fig. 15. Polarization angle relationships looking along station-to-probe line of sight

where

$\mathbf{r}$ = vector from earth center to local station

$\mathbf{k}_\epsilon$ = unit vector perpendicular to plane of ecliptic

The vectors $\mathbf{s}$ and $\mathbf{u}$ (Fig. 15) are both perpendicular to the station–probe line of sight. In addition, $\mathbf{s}$ is parallel to the plane of local horizon and $\mathbf{u}$ is parallel to the plane of the ecliptic.

The signal polarization (nominally perpendicular to the plane of the ecliptic[4]) referred to the plane of the local horizon is

$$\tau = \theta_p - p \tag{93}$$

where

τ = signal polarization referred to $\mathbf{u}$, deg

θ_p = signal polarization referred to $\mathbf{s}$, deg

p = the angle between the vectors $\mathbf{s}$ and $\mathbf{u}$, both perpendicular to the station to probe line of sight, deg

[4]Measurement of the signal polarization (see Section IV) presently provides the most accurate method (approximately 0.1 deg) of determining spacecraft orientation.

It is not satisfactory to obtain the angle p from the dot product of $\mathbf{s}$ and $\mathbf{u}$ since the cosine relationship loses the sign information required when p goes through zero. Define the vector

$$\mathbf{c} = \mathbf{u} \times \mathbf{s} = \mathbf{E} \, | u | \, | s | \sin p \tag{94}$$

where

$$\mathbf{E} = \text{unit vector} \frac{\mathbf{r}_p}{r_p}$$

Then since $\mathbf{u} \times \mathbf{s}$ and $\mathbf{E}$ are parallel to each other

$$\sin p = \frac{\mathbf{u} \times \mathbf{s}}{\mathbf{E}} = \frac{\mathbf{u} \times \mathbf{s}}{\frac{\mathbf{r}_p}{r_p}} \left| \begin{array}{l} x'' \text{ component} \\ \\ x'' \text{ component} \end{array} \right. \tag{95}$$

With the aid of previous transformations, we have

$$(\mathbf{k}_\epsilon) = [M_4]^{-1} [M_3]^{-1} [M_2]^{-1} [M_1]^{-1} (\mathbf{K}_\epsilon) \tag{96}$$

where

$\mathbf{k}_\epsilon, \mathbf{K}_\epsilon$ = unit vectors perpendicular to plane of ecliptic in earth-fixed coordinates (see Fig. 13d) and space-fixed coordinates (see Fig. 13a), respectively.

Then

$$\left.\begin{aligned} \mathbf{s} &= -(\mathbf{i}\sin\sigma + \mathbf{j}\cos\sigma) \\ \mathbf{u} &= \frac{\mathbf{i}\,a_x + \mathbf{j}\,a_y + \mathbf{k}\,a_y}{(a_x^2 + a_y^2 + a_z^2)^{1/2}} \\ \frac{\mathbf{r}_p}{r} &= \mathbf{i}\cos\sigma\cos\gamma + \mathbf{j}\sin\sigma\cos\gamma \\ &\quad + \mathbf{k}\sin\gamma \end{aligned}\right\} \tag{97}$$

where from Eq. (96)

$$\begin{aligned} a_x &= k_y\sin\gamma - k_z\cos\gamma\sin\sigma \\ a_y &= -k_z\cos\gamma\cos\sigma - k_x\sin\gamma \\ a_z &= k_x\cos\gamma\sin\sigma + k_y\cos\gamma\cos\sigma \\ k_x &= -[\sin\phi\cos\theta\sin\gamma(t)\sin\epsilon \\ &\quad + \sin\phi\sin\theta\cos\gamma(t)\sin\epsilon \\ &\quad + \cos\phi\cos\epsilon] \\ k_y &= \sin\theta\sin\gamma(t)\sin\epsilon - \cos\theta\cos\gamma(t)\sin\epsilon \\ k_z &= -\cos\phi\cos\theta\sin\gamma(t)\sin\epsilon \\ &\quad - \cos\phi\sin\theta\cos\gamma(t)\sin\epsilon \\ &\quad + \sin\phi\cos\epsilon \end{aligned}$$

Then

$$p = \sin^{-1}\frac{-a_z}{\cos\gamma\,(a_x^2 + a_y^2 + a_z^2)^{1/2}} \tag{98}$$

This is used with Eq. (93) to refer the measured polarization at the local station to the plane of the ecliptic. These equations have been programmed (see Appendix D) for the 7094 computer. A sample printout is shown in Fig. 16 for *Pioneer VI* data taken on November 2, 1968. The program prints every point and also averages and gives an output for blocks of 20 points every 10 s.

IV. S-Band Polarimeter and Associated Instrumentation

As indicated in Section III, a closed-loop polarimeter was developed and implemented so that the polarization of the signal received from the *Pioneer VI* spacecraft could be automatically tracked. A discussion of system description and performance follows.

A. Equipment Description

The S-band multifrequency Cassegrain feed cone (designated SMF cone) was modified (Figs. 17 and 18) to provide a polarization capability to the receiving system (Refs. 41 and 42). The cone was installed on the 210-ft antenna at the Mars station, on September 17, 1968. This cone can receive or transmit in the right- or left-circular or rotating linear polarization mode. The feed system employed a dual-mode horn followed by two rotary-joint-mounted quarter-wave plates that could be remotely oriented. The first quarter-wave plate (Fig. 19) converted the linearly polarized signal to one sense of circular polarization when the quarter-wave plate was correctly aligned with the incident signal. The second quarter-wave plate converted the circular polarization back to a linear mode, which was then incident on one of the two orthogonal output ports of the polarizer. When the upper quarter-wave plate was correctly aligned with the incoming signal, all the energy was available at the reference channel port. When the quarter-wave plate was incorrectly aligned, both senses of circular polarization were generated and some of the signal appeared at the second polarizer port for injection into the error channel of the receiver. Both ports then lead through a waveguide to separate maser preamplifiers, which were operated in their own closed-cycle cryostats at 4.2°K. The reference channel then went from the maser to the normal space communication configuration of the receiver system. The output of the error channel maser went through a receiver system normally used as a monopulse error channel. Figure 20 shows a block diagram of the overall receiver. After amplification at intermediate frequencies, the outputs of the reference and error channels were used to produce a voltage that indicated both the direction and magnitude of the misalignment of the upper quarter-wave plate. This voltage was used to drive the servoelectronics, which then caused an electric motor to rotate the upper quarter-wave plate. The upper quarter-wave plate was coupled to a digital shaft encoder which was used to generate angular data for digital recording.

The reference signal of the polarization error detector (Fig. 20) is continuously shifted in phase by twice the angular rotation of the polarizer. This is required to account for the phase shift with rotation in the RF polarizer. A photograph of the polarization tracking servosystem control panel and readout instrumentation is shown rack mounted in Fig. 21. This equipment is located in the Mars station with the receiver and associated instrumentation in the control room.

B. Performance Characteristics

Space communication low noise systems have been thoroughly investigated in the literature (Ref. 43).

DAY NUMBER 307

DEC1 -13.679 RA1 213.962 TIME 0
DEC2 -14.055 RA2 215.080 TIME 2400

DATE DAY NO.	TIME GMT	AZ DEG	EL DEG	DEC DEG	RA DEG	POL READ DEG	POL READ PRED	PRED-READ DEG	HE POL DEG	MEAS SC POL	90-MEAS POL DEG
307.66427	15.9425	126.513	21.337	-13.929	214.704	162.330	151.532	-10.798	61.532	100.798	-10.798
307.66437	15.9450	126.542	21.361	-13.929	214.705	157.400	151.512	-5.888	61.512	95.888	-5.888
307.66449	15.9478	126.574	21.388	-13.929	214.705	160.160	151.491	-8.669	61.491	98.669	-8.669
20	307.66331	96.49163	2.46727	307.66331	96.49163	2.46727					
307.66462	15.9508	126.609	21.418	-13.929	214.705	160.960	151.467	-9.493	61.467	99.493	-9.493
307.66473	15.9536	126.641	21.446	-13.929	214.705	157.630	151.445	-6.185	61.445	96.185	-6.185
307.66488	15.9572	126.683	21.481	-13.929	214.705	155.720	151.417	-4.303	61.417	94.303	-4.303
307.66500	15.9600	126.715	21.508	-13.929	214.705	161.270	151.395	-9.875	61.395	99.875	-9.875
307.66513	15.9631	126.751	21.538	-13.929	214.705	160.070	151.371	-8.699	61.371	98.699	-8.699
307.66524	15.9658	126.783	21.565	-13.929	214.705	154.820	151.349	-3.471	61.349	93.471	-3.471
307.66536	15.9686	126.815	21.592	-13.929	214.706	155.520	151.327	-4.193	61.327	94.193	-4.193
307.66546	15.9711	126.844	21.617	-13.929	214.706	159.100	151.307	-7.793	61.307	97.793	-7.793
307.66558	15.9739	126.876	21.644	-13.929	214.706	160.900	151.285	-9.615	61.285	99.615	-9.615
307.66570	15.9769	126.912	21.674	-13.929	214.706	160.320	151.261	-9.059	61.261	99.059	-9.059
307.66582	15.9797	126.944	21.701	-13.929	214.706	155.720	151.239	-4.481	61.239	94.481	-4.481
307.66586	15.9806	126.954	21.709	-13.929	214.706	153.830	151.232	-2.598	61.232	92.598	-2.598
307.66597	15.9833	126.986	21.736	-13.929	214.706	156.070	151.210	-4.860	61.210	94.860	-4.860
307.66608	15.9861	127.019	21.763	-13.929	214.706	159.920	151.188	-8.732	61.188	98.732	-8.732
307.66620	15.9889	127.051	21.790	-13.929	214.707	158.800	151.166	-7.634	61.166	97.634	-7.634
307.66646	15.9950	127.122	21.850	-13.929	214.707	158.570	151.118	-7.452	61.118	97.452	-7.452
307.66657	15.9978	127.154	21.877	-13.929	214.707	157.930	151.096	-6.834	61.096	96.834	-6.834
307.66670	16.0008	127.190	21.906	-13.929	214.707	157.300	151.071	-6.229	61.071	96.229	-6.229
307.66682	16.0036	127.223	21.933	-13.930	214.707	155.860	151.049	-4.811	61.049	94.811	-4.811
307.66692	16.0061	127.252	21.958	-13.930	214.707	158.130	151.029	-7.101	61.029	97.101	-7.101
20	307.66574	96.67086	2.17387	307.66574	96.67086	2.17387					
307.66703	16.0089	127.284	21.985	-13.930	214.707	158.930	151.007	-7.923	61.007	97.923	-7.923
307.66716	16.0119	127.320	22.014	-13.930	214.708	156.400	150.983	-5.417	60.983	95.417	-5.417
307.66728	16.0147	127.352	22.041	-13.930	214.708	157.020	150.960	-6.060	60.960	96.060	-6.060
307.66743	16.0183	127.395	22.076	-13.930	214.708	158.800	150.931	-7.869	60.931	97.869	-7.869
307.66755	16.0211	127.427	22.103	-13.930	214.708	158.520	150.909	-7.611	60.909	97.611	-7.611
307.66767	16.0242	127.463	22.133	-13.930	214.708	156.730	150.884	-5.846	60.884	95.846	-5.846
307.66779	16.0269	127.496	22.160	-13.930	214.708	160.530	150.862	-9.668	60.862	99.668	-9.668
307.66789	16.0294	127.525	22.184	-13.930	214.708	158.620	150.842	-7.778	60.842	97.778	-7.778
307.66801	16.0322	127.558	22.211	-13.930	214.709	156.600	150.820	-5.780	60.820	95.780	-5.780
307.66812	16.0350	127.590	22.238	-13.930	214.709	158.030	150.797	-7.233	60.797	97.233	-7.233
307.66825	16.0381	127.626	22.267	-13.930	214.709	155.830	150.773	-5.057	60.773	95.057	-5.057
307.66837	16.0408	127.659	22.294	-13.930	214.709	155.920	150.750	-5.170	60.750	95.170	-5.170
307.66840	16.0417	127.669	22.302	-13.930	214.709	158.800	150.743	-8.057	60.743	98.057	-8.057
307.66852	16.0444	127.701	22.329	-13.930	214.709	160.160	150.721	-9.439	60.721	99.439	-9.439
307.66863	16.0472	127.734	22.356	-13.930	214.709	154.760	150.698	-4.062	60.698	94.062	-4.062
307.66875	16.0500	127.767	22.383	-13.930	214.709	153.720	150.676	-3.044	60.676	93.044	-3.044
307.66900	16.0561	127.839	22.441	-13.930	214.710	158.520	150.626	-7.894	60.626	97.894	-7.894
307.66912	16.0589	127.872	22.468	-13.930	214.710	158.030	150.604	-7.426	60.604	97.426	-7.426
307.66925	16.0619	127.908	22.498	-13.930	214.710	154.320	150.579	-3.741	60.579	93.741	-3.741
307.66936	16.0647	127.941	22.524	-13.930	214.710	155.900	150.556	-5.344	60.556	95.344	-5.344
20	307.66816	96.52090	1.79152	307.66816	96.52090	1.79152					
307.66946	16.0672	127.970	22.548	-13.931	214.710	158.920	150.536	-8.384	60.536	98.384	-8.384
307.66958	16.0700	128.003	22.575	-13.931	214.710	155.470	150.513	-4.957	60.513	94.957	-4.957
307.66971	16.0731	128.039	22.605	-13.931	214.710	155.130	150.488	-4.642	60.488	94.642	-4.642
307.66982	16.0758	128.072	22.631	-13.931	214.711	160.430	150.466	-9.964	60.466	99.964	-9.964

Fig. 16. Sample computer output of signal polarization program

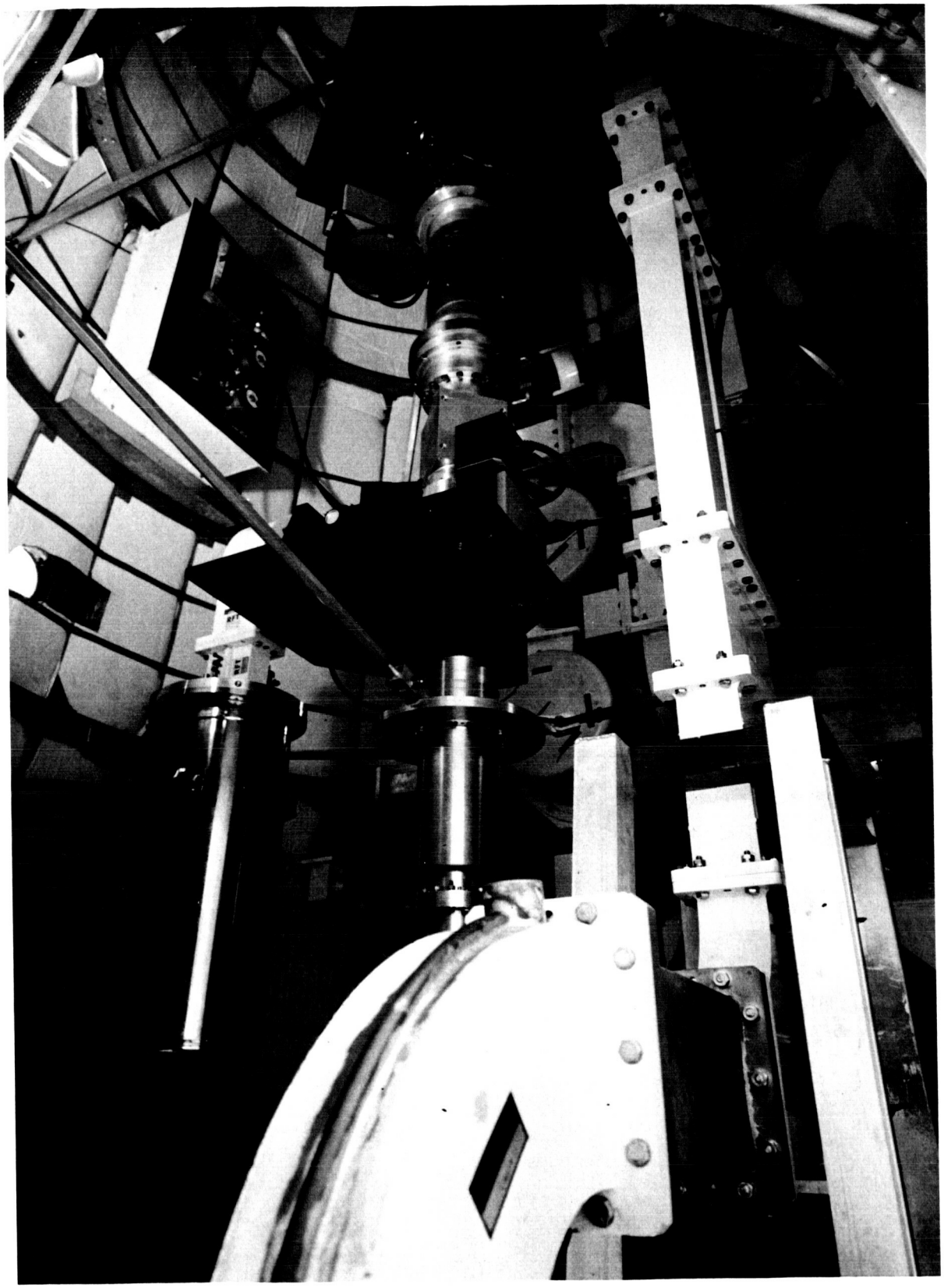

Fig. 17. Interior of SMF feed cone

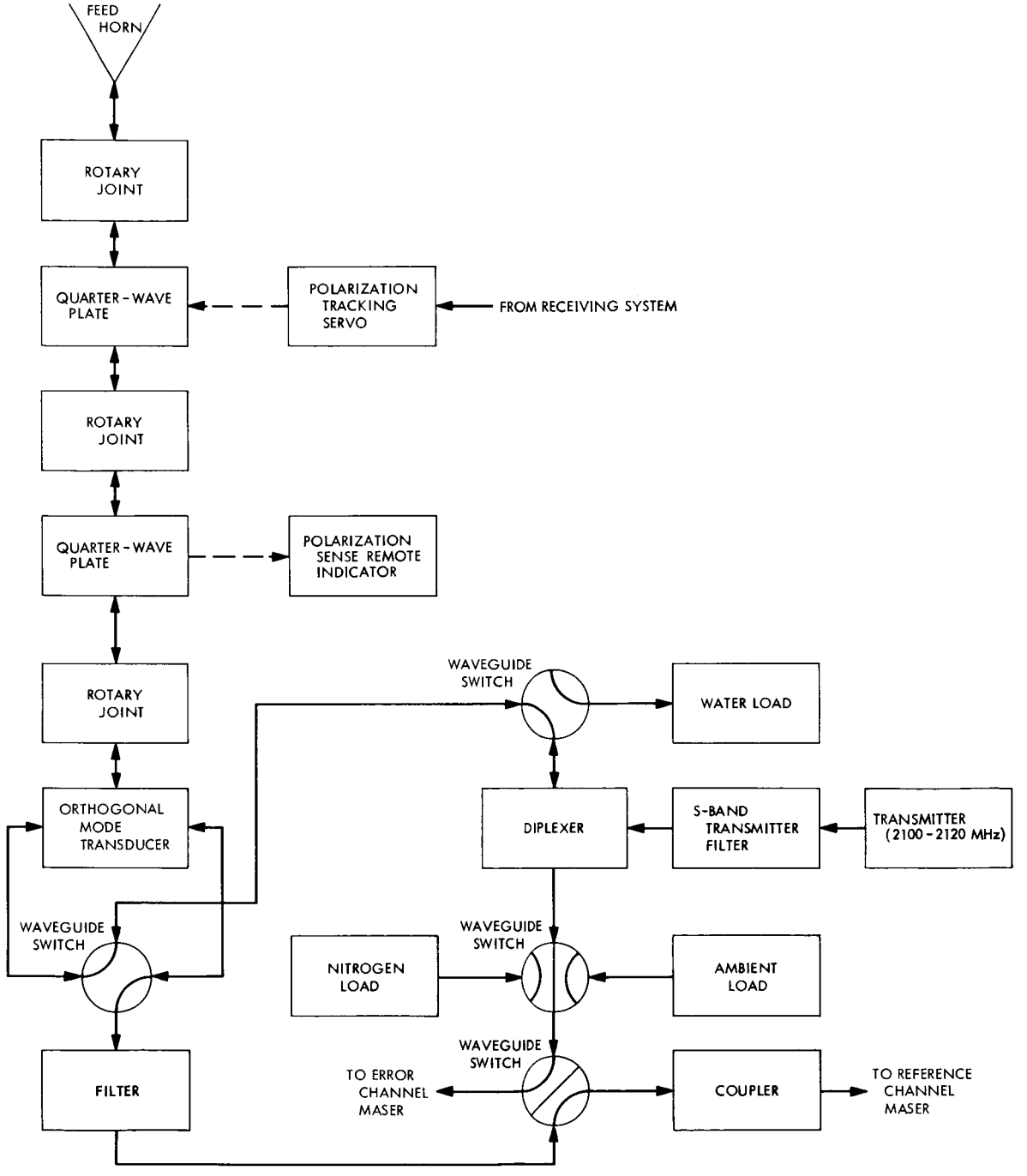

Fig. 18. Simplified block diagram of SMF feed cone

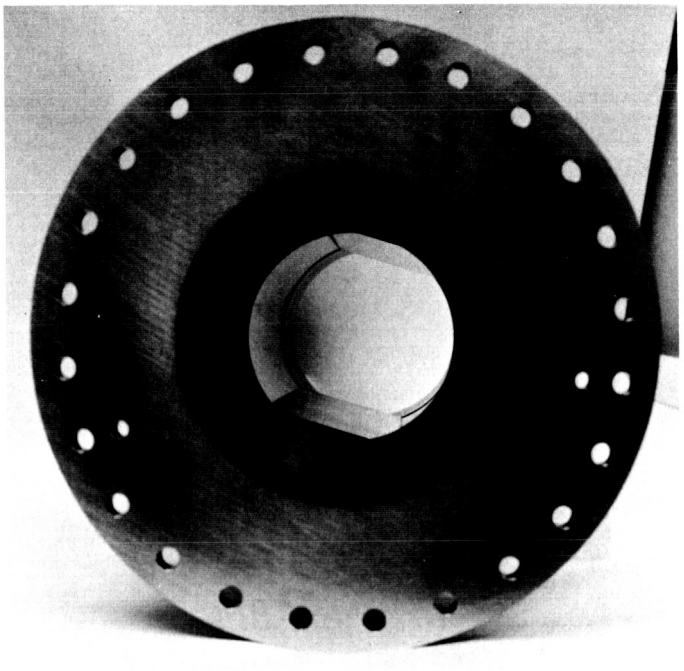

Fig. 19. S-band quarter-wave plate used in SMF feed cone polarization instrument

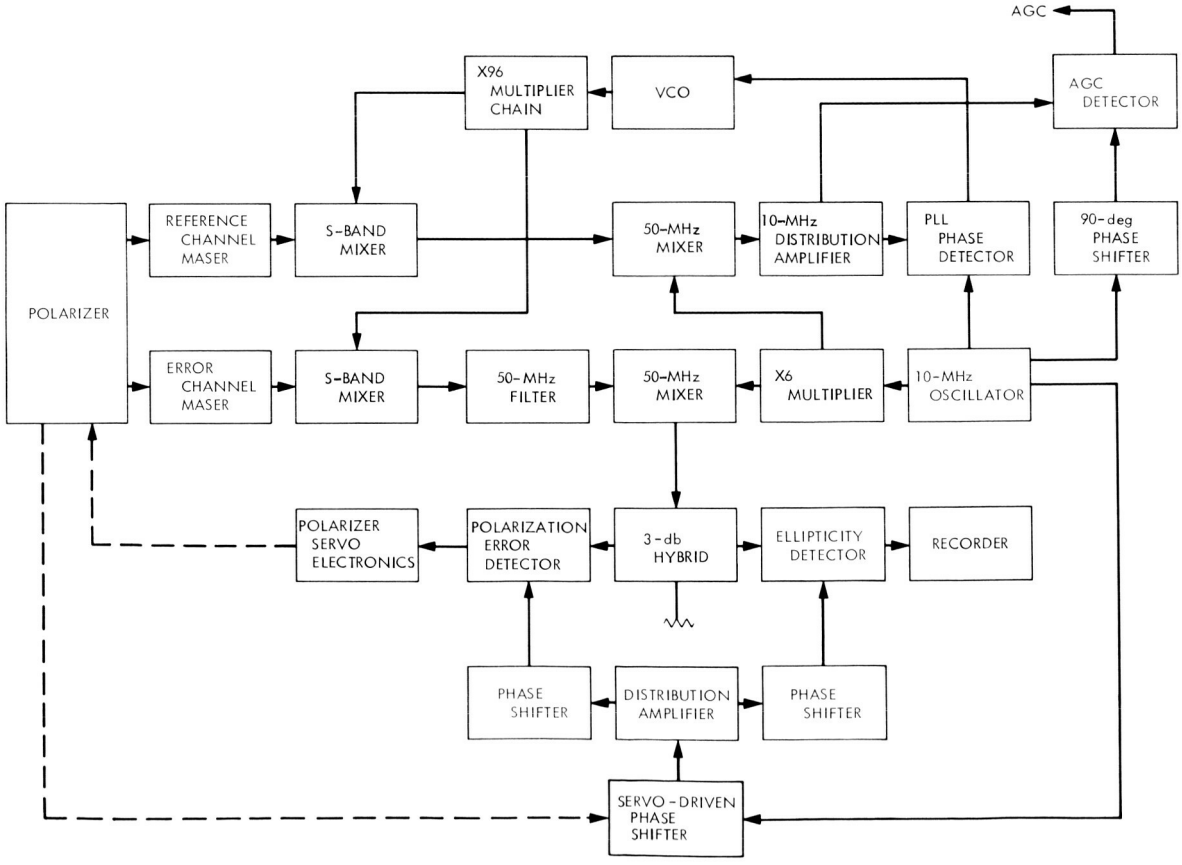

Fig. 20. Block diagram of S-band receiver system

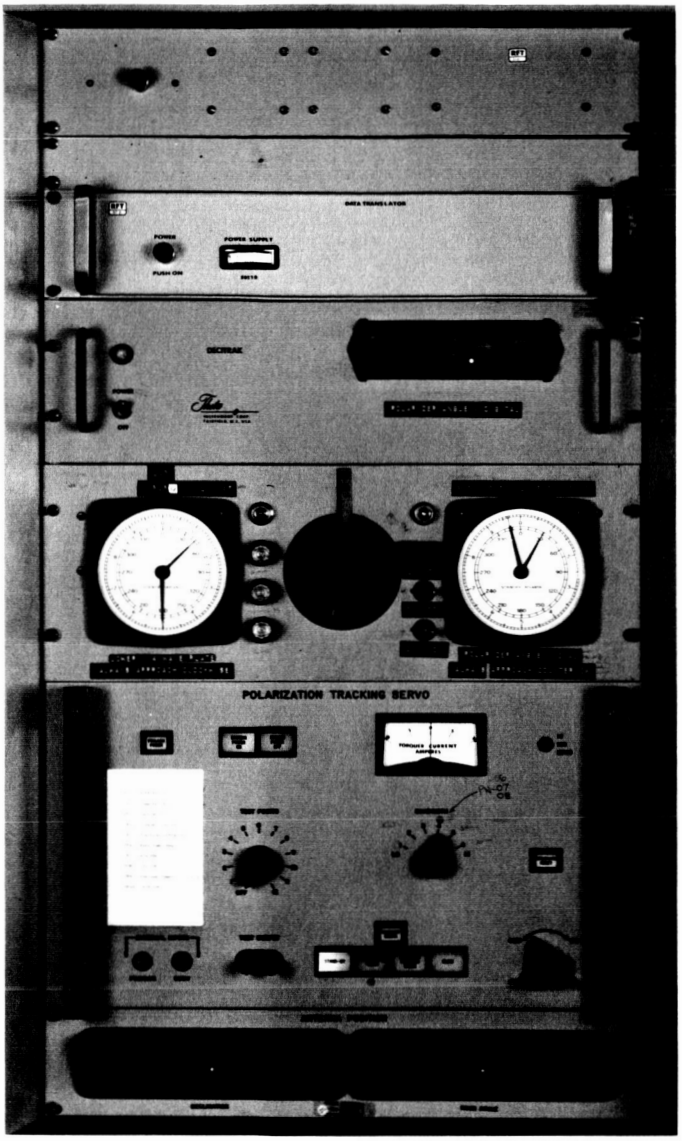

Fig. 21. Photograph of SMF feed cone polarization tracking console

The sensitivity of a low-noise receiving system is usually evaluated in terms of its operating noise temperature T_{op}. With a received signal power P_S, the signal-to-noise ratio is then

$$\frac{P_S}{P_N} = \frac{P_S}{k\,T_{\text{op}}\,B} \tag{99}$$

where

k = Boltzmann's constant = 1.38054×10^{-23} J/K

B = overall bandwidth defined to the point of use, Hz

The received power is a function of incident power density P_{si} and antenna gain or effective collecting area.

$$P_S = \eta\, A\, P_{\text{si}}$$

where

A = antenna area, m^2

η = antenna efficiency

The incident power is, again, a function of spacecraft antenna gain and transmitter power and space loss. The receiver and transmission line components contribute to the system operating noise temperature and are usually evaluated separately for both temperature contributions and match performance.

Parameters of interest in the polarimeter hardware are loss, ellipticity, null depth, and match performance. The overall performance of the system operating as a polarimeter is given in terms of angle resolution. This has been adequately treated in detail[5] and shows that for the closed-loop system used for this experiment

$$\sigma_\theta^2 = \frac{k\,(T_{\text{op}})_E\,Q}{\tau P_S} \exp\left[\left(\frac{kT_{\text{op}}B_T}{P_S}\right)^{0.622}\right] \tag{100}$$

where

σ_θ = standard deviation of polarization angle measurements, deg

$(T_{\text{op}})_E$ = operating noise temperature of error channel, K

T_{op} = operating noise temperature of reference channel

B_T = bandwidth, Hz

Q = constant obtained from servosystem damping $\simeq 0.6338$

τ = effective system time constant, s

For this system [$B_T \simeq 12$ Hz, $P_S \simeq -165$ dBmW, $(T_{\text{op}})_E \simeq T_{\text{op}} + 8$], the approximate relation

$$\sigma_\theta \simeq \left(\frac{T_{\text{op}}}{\tau}\right)^{1/2} \tag{101}$$

[5]Ohlson, J. E., and Stelzried, C. T., "A Tracking Polarimeter for Measuring Solar and Ionospheric Faraday Rotation of Signals from Deep Space Probes," article in preparation, Jet Propulsion Laboratory, Pasadena, Calif., 1969.

is useful. The operating noise temperature is not constant but increases in this experiment as the spacecraft approaches the sun because of the noise contribution of the sun in the sidelobes of the antenna beam (Ref. 44).

C. Overall System Description and Performance

Considerable RF testing was performed on the SMF cone. Table 2 summarizes the reflection coefficient measurements of the antenna feed system. The measurement reference points are defined in the detailed block diagram in Fig. 22.

The reference maser noise temperature (see Ref. 42) was calibrated with waveguide input helium cooled (see Fig. 17) and ambient terminations by Y-factor techniques. This resulted in a calibrated maser noise temperature of 4.5 K. The total system operating noise temperature of the cone on the ground was measured to be 18.5 K. The total operating system noise temperature was increased with the cone on the antenna to 22.5 K. Both of these measurements were made with the antenna pointed toward the zenith and using the reference maser. The calibration on the antenna consisted of averaging 52 measurements using the ambient load Y-factor technique. The standard deviation of the measurements was 0.6 K. The operating noise temperature was also continuously monitored with a chart recorder during the experiment. It was found that the contribution of the sun not only increased as the probe approached the sun (Fig. 23) but was also a function of the time of day.[6] The minimum and maximum values are indicated on the graph. The variation is caused by the absence of axially symmetric antenna sidelobes. Figure 24 indicates this variation with ϕ (defined in Fig. 25).

The overall angular measurement performance of the polarimeter servo system was determined by evaluating three days of averaged data. The computer program provides punched cards, each of which represents an average of 20 data points each taken every 10 s. These points were further averaged in groups of five. The standard deviation of these averages is plotted and averaged in Fig. 26. There is undoubtedly some Faraday rotation of the signal due to the solar corona during these three days. However, the effect is small (see Fig. 33) and an upper limit is established. The average standard deviation for the 200-s data for the three days is 0.36 deg. This is in reasonable agreement with 0.5 deg calculated from Eq. (101) using $T_{op} = 50\,K$ and $\tau = 200\,s$. The standard deviations of the actual polarization angle measurement during the experiment and that predicted from Eq. (101) with the polarimeter operating in the near corona are shown in Fig. 27. The experimental performance is determined from a daily average of 200-s data. The agreement is quite good over the operating range of the experiment.

Although signal attenuation is not significant in this region of the solar corona, there is considerable spectral broadening of the signal (see Ref. 21). This results in an effective attenuation since the total energy is not totally contained within the narrow band of the locked loop of the receiver. It is expected that the measured performance of the polarimeter should be degraded slightly from that predicted for the following reasons:

(1) Perturbations in the spectral broadening of the signal in the near region of the solar corona cause difficulties with the polarimeter tracking loop.

(2) The receiving system is continually dropping lock during this period.

(3) Because the signal-to-noise ratio is less than 5 dB in this region, the assumption in the analysis of a linearized error signal is no longer valid, the "theoretical" formula based on a "high" signal-to-noise ratio assumption gives an optimistic result.

Performance data are not available closer than about 4 solar radii because the receiver was not able to lock up on the signal in this region.

V. Experimental Results

The experiment (Ref. 45) consisted basically of continuous measurement of the received signal polarization before and after *Pioneer VI* was occulted by the sun. This was accomplished by digitally recording time and the position of the microwave feed quarter-wave plate every 10 s. These angle data were then converted to the plane of the ecliptic with the signal polarization coordinate transformation computer program (see Appendix D). A nominal 30-s time constant was used in the servo loop in the initial stages of the experiment.

The data for October 26–29 are shown in Fig. 28. Polarization angles are presented as a function of time for observations of *Pioneers VI, VII,* and *VIII* during the period October 26–29. Each point is an average of 20 samples for 200-s averaging. The most conspicuous feature of this graph is the diurnal variation due to the earth ionosphere. The ranges of *Pioneers VI, VII,* and *VIII*

[6] Bathker, D. A., et al., "A Multipurpose Feed System for Deep Space Applications," article in preparation, Jet Propulsion Laboratory, Pasadena, Calif., 1969.

Table 2. Tabulation of the SMF feed cone antenna reflection coefficient measurements

Antenna line configuration	Input-to-output path[a]	Antenna polarization			Maximum/minimum voltage reflection coefficients
		Receive mode[b]	Lower plate angle, deg	Upper plate indicated[c] angle, deg	
Maser 2 Normal receive path (reference channel)	Part 1 to feedhorn output via switches 2 and 1, and lower orthomode transducer	RCP	0	270	0.0172 ±0.0008
		LCP	0	0	0.0172 ±0.0008
		LP	45	25.0	0.0359 ±0.0015
				110.8	0.0562 ±0.0021
				209.2	0.0359 ±0.0015
				299.4	0.0562 ±0.0021
			315	71.4	0.0363 ±0.0015
				169.4	0.0575 ±0.0021
				254.2	0.0355 ±0.0015
				336.8	0.0569 ±0.0021
Maser 1 Orthogonal polarization path	Part 1 to feedhorn output via switches 2 and 1, and upper orthomode transducer	CP	0	270	0.0367 ±0.0015
		CP	0	0	0.0394 ±0.0016
		LP	45	49.6	0.0822 ±0.0028
				136.7	0.0110 ±0.0006
				234.2	0.0851 ±0.0029
				315.0	0.0111 ±0.0006
			315	42.3	0.0822 ±0.0028
				132.5	0.0112 ±0.0006
				224.2	0.0822 ±0.0028
				315.0	0.0111 ±0.0006
Maser 2 Orthogonal polarization path	Part 6 to feedhorn output via switches 2 and 4, diplexer, switches 3 and 1, and lower orthomode transducer	CP	0	270	0.0462 ±0.0018
		CP	0	0	0.0432 ±0.0017
		LP	45	43.7	0.0014 ±0.0002
				143.0	0.0891 ±0.0030
				233.0	0.0015 ±0.0002
				315.0	0.0891 ±0.0030
			315	49.6	0.0015 ±0.0002
				136.6	0.0902 ±0.0030
				229.8	0.0015 ±0.0002
				318.3	0.0891 ±0.0030
Maser 2 Normal receive path (error channel)	Part 6 to feedhorn output via switches 2 and 4, diplexer, switches 3 and 1, and upper orthomode transducer	CP	0	270	0.0617 ±0.0022
		CP	0	0	0.0638 ±0.0023
		LP	45	37.1	0.1023 ±0.0033
				132.2	0.0126 ±0.0007
			315	66.4	0.1000 ±0.0032
				330.6	0.0126 ±0.0007

[a]Path is shown in detail in Fig. 22.

[b]RCP = right-circular polarization; LCP = left-circular polarization; LP = linear polarization; CP = circular polarization.

[c]Indicated upper plate angle is −45 deg with respect to the actual angle of the upper plate.

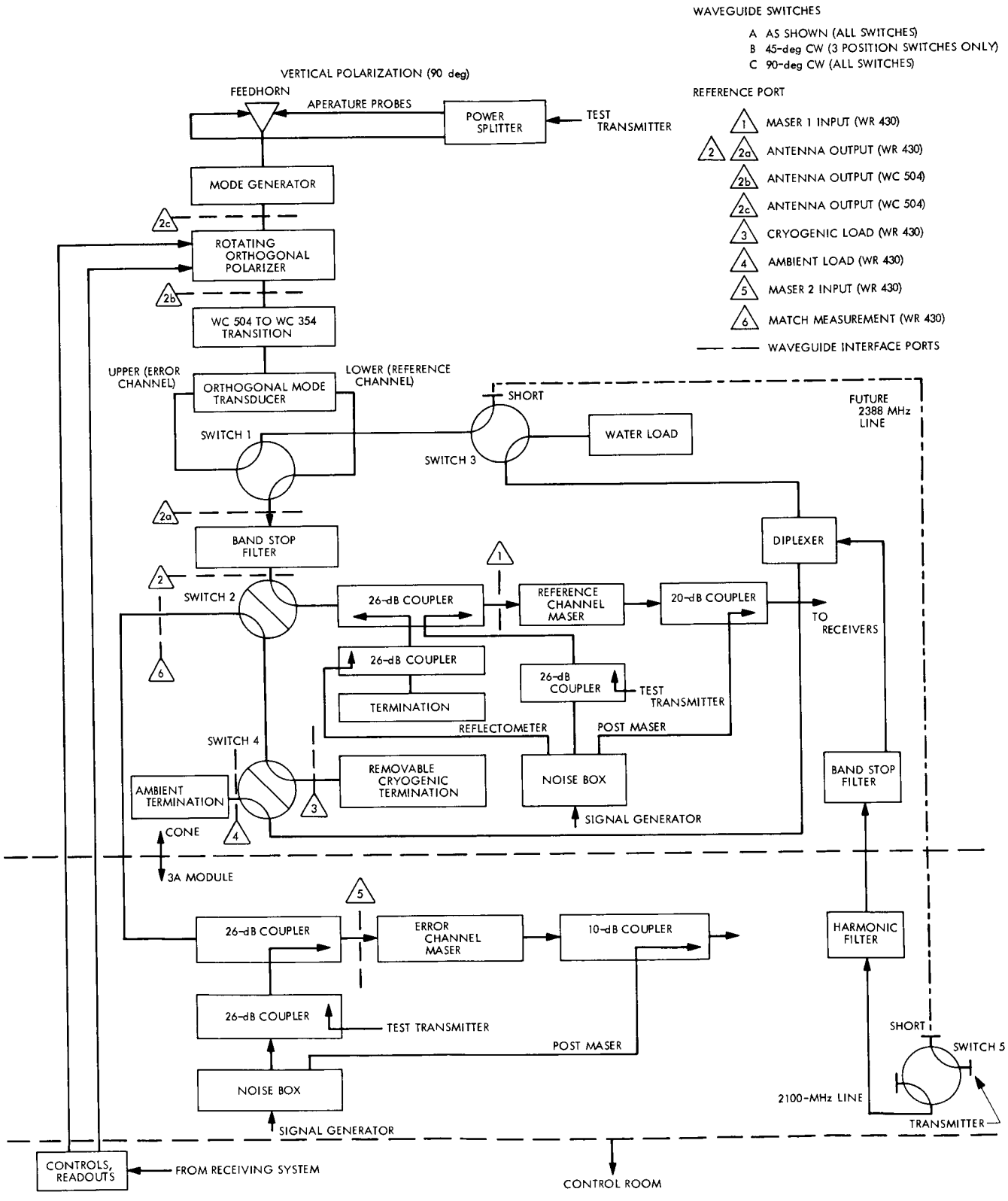

Fig. 22. Detailed block diagram of SMF feed cone

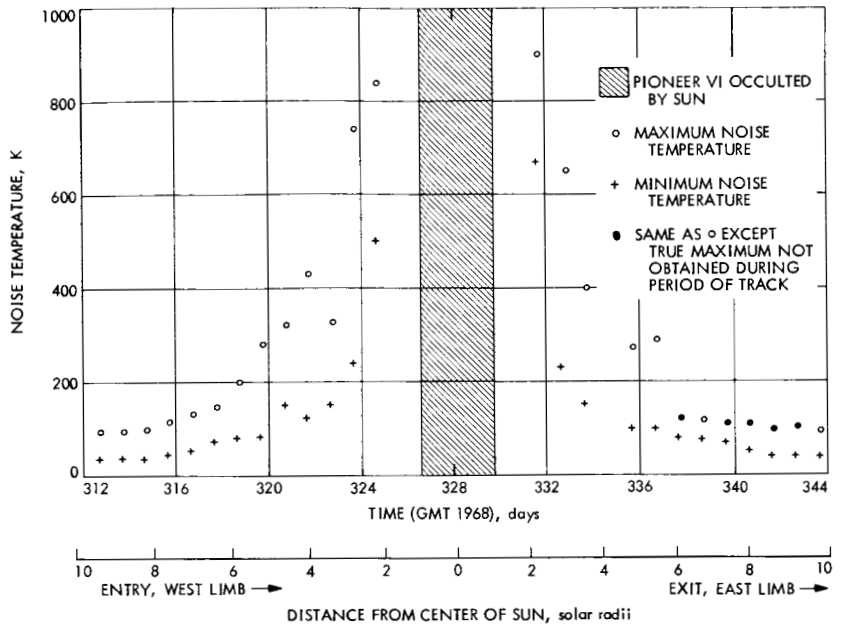

Fig. 23. System operating noise temperature T_{op} vs time and distance from center of sun

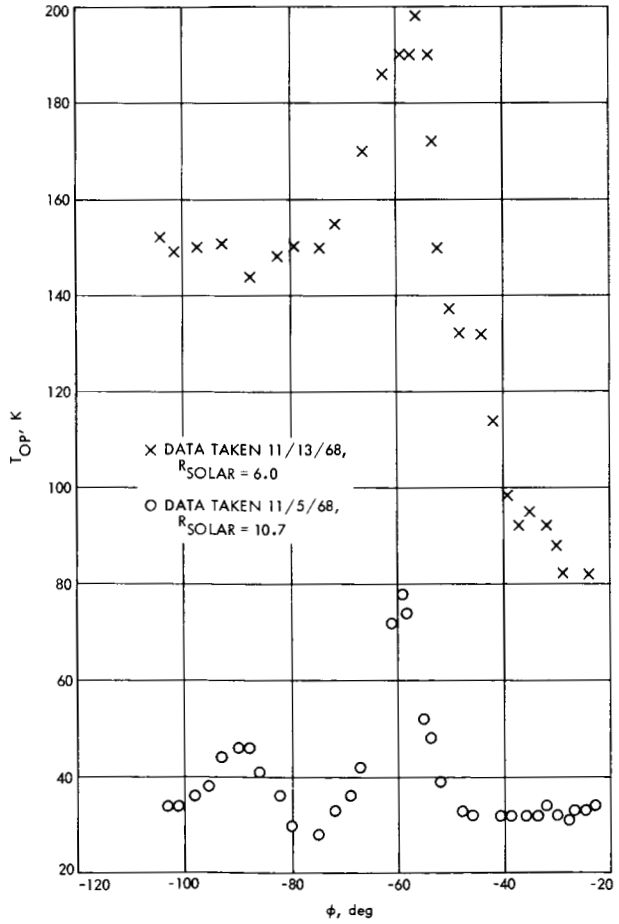

Fig. 24. System operating noise temperature T_{op} vs ϕ

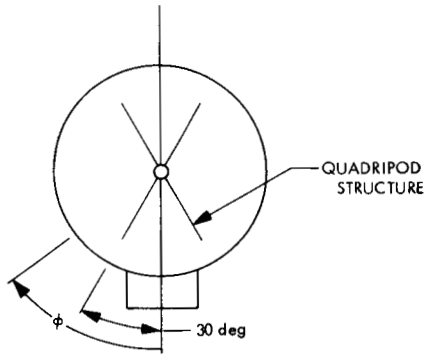

Fig. 25. Reflector coordinate system

were approximately 1.9, 1.2, and 0.4 AU, respectively. The relative scatter of measurements can be seen to increase with increasing range from the earth and, therefore, reduced the signal-to-noise ratio. In the case of *Pioneer VI*, the line of sight of the spacecraft was approximately 15 solar radii from the center of the sun so that there was also a slight increase in system noise temperature due to microwave thermal radiation in the antenna sidelobes (see Section IV).

A. Transient Effects

Figure 29a shows a plot of polarization angle vs time for November 4. Every 10-s measurement point is shown; a 30-s servo time constant was used at this time. It can be seen (see Fig. 11) that the phenomenon labeled A occurred

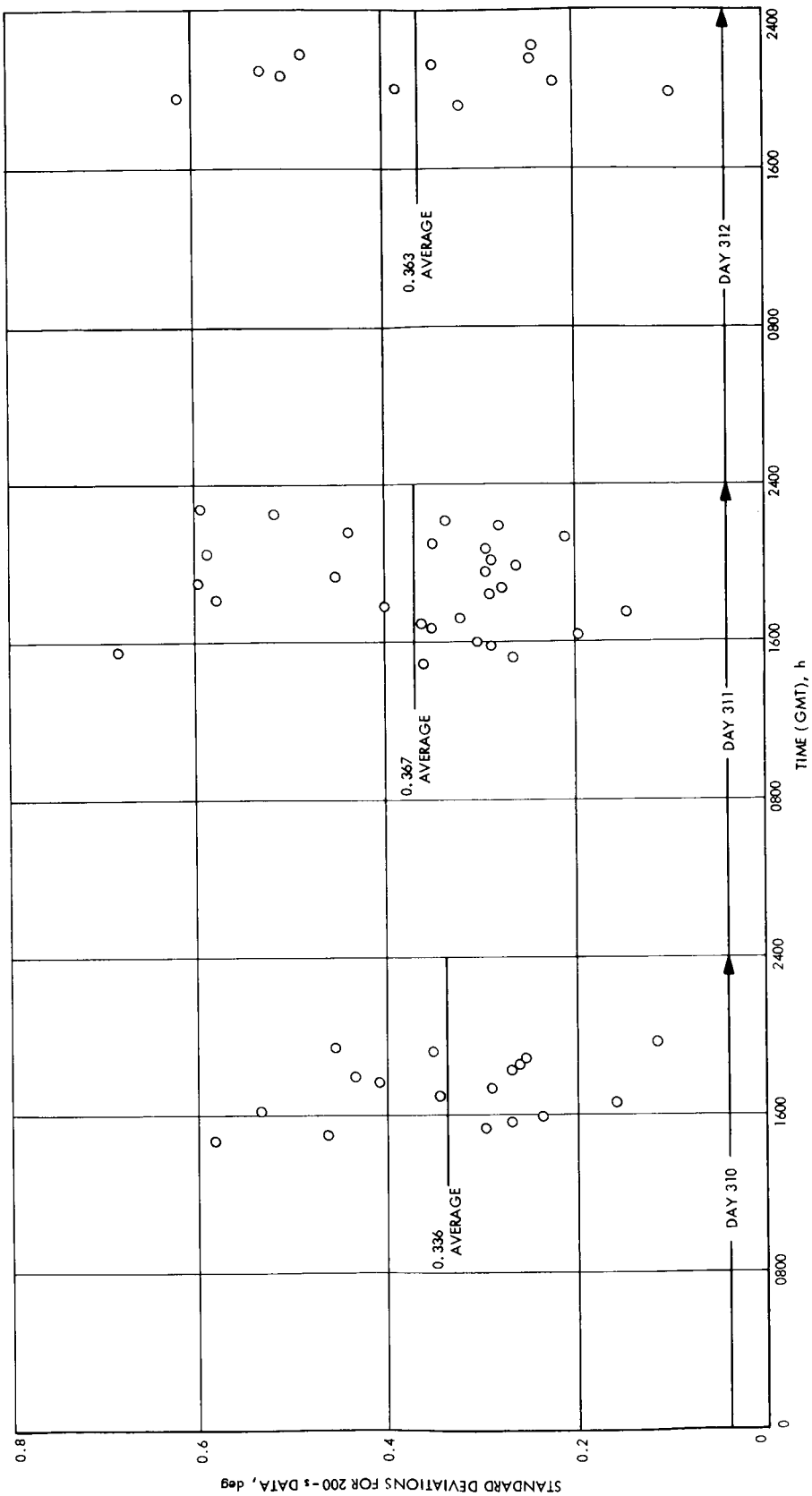

Fig. 26. Plot of three days of 200-s polarizer data standard deviation vs time

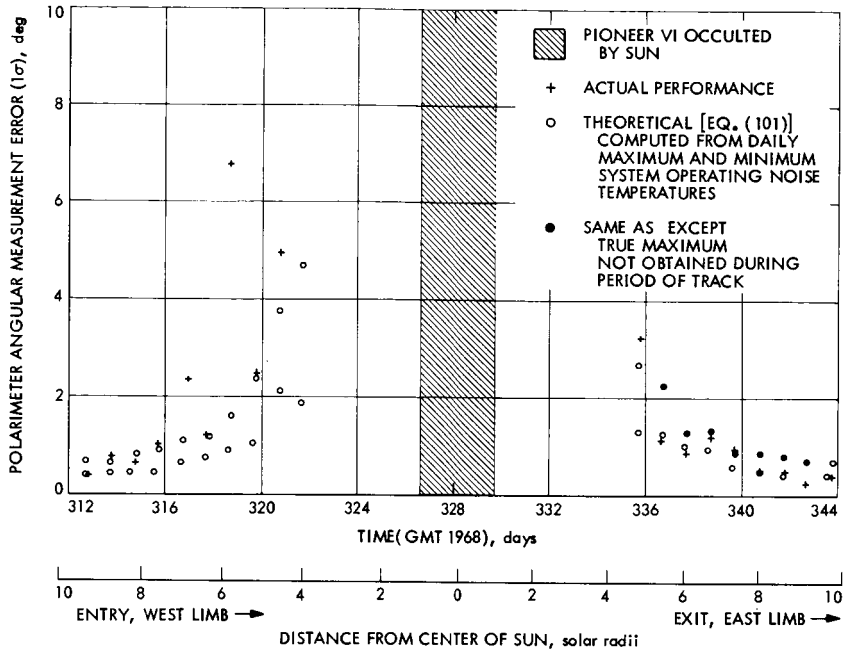

Fig. 27. Polarimeter 200-s angular measurement error (1σ) vs time and distance from center of sun

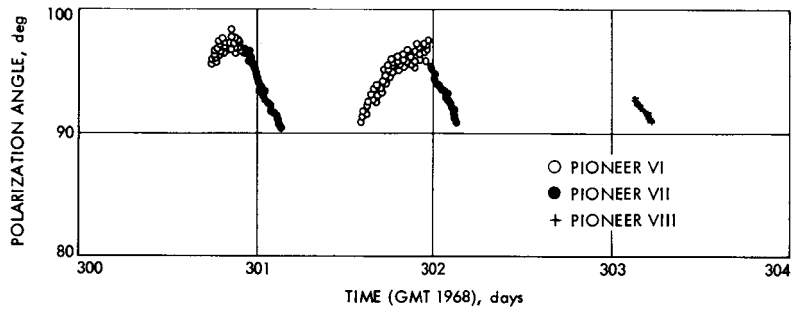

Fig. 28. Polarization (200-s data points) vs time for *Pioneers VI, VII,* and *VIII* observations

at a distance of 10.9 solar radii from the center of the sun. The next polarization transient was observed November 8 and is shown in Fig. 29b. The servo time constant had been increased to 300 s. This transient (labeled B in Fig. 11) occurred 8.6 solar radii from the solar center. The last observed polarization transient shown in Fig. 29c occurred November 12. Unfortunately, there was a loss of data during 45 min of the early part of this transient because of operational problems. This transient (labeled C in Fig. 11) occurred at a distance of 6.2 solar radii. The three events are shown in one graph in Fig. 30 using 200-s data for the events and 1000-s data for the remainder of the data.

It can be seen that in the first two events, the base line is approximately 97 deg. The positive direction of the base line above 90 deg is due primarily to the longitudinal components of the magnetic field of the earth interacting with the electrons in the earth's ionosphere. An increase in polarization angle is caused by an increase in the electron content of the ionosphere; a decrease in electrons could not reduce the angle below 90 deg. Either there had to be a change in the sign of the particles in the ionosphere or a large concentration of electrons in a region where the magnetic field's longitudinal component is opposed to the direction of the earth's field in order to produce the phenomena observed. The logical conclusion

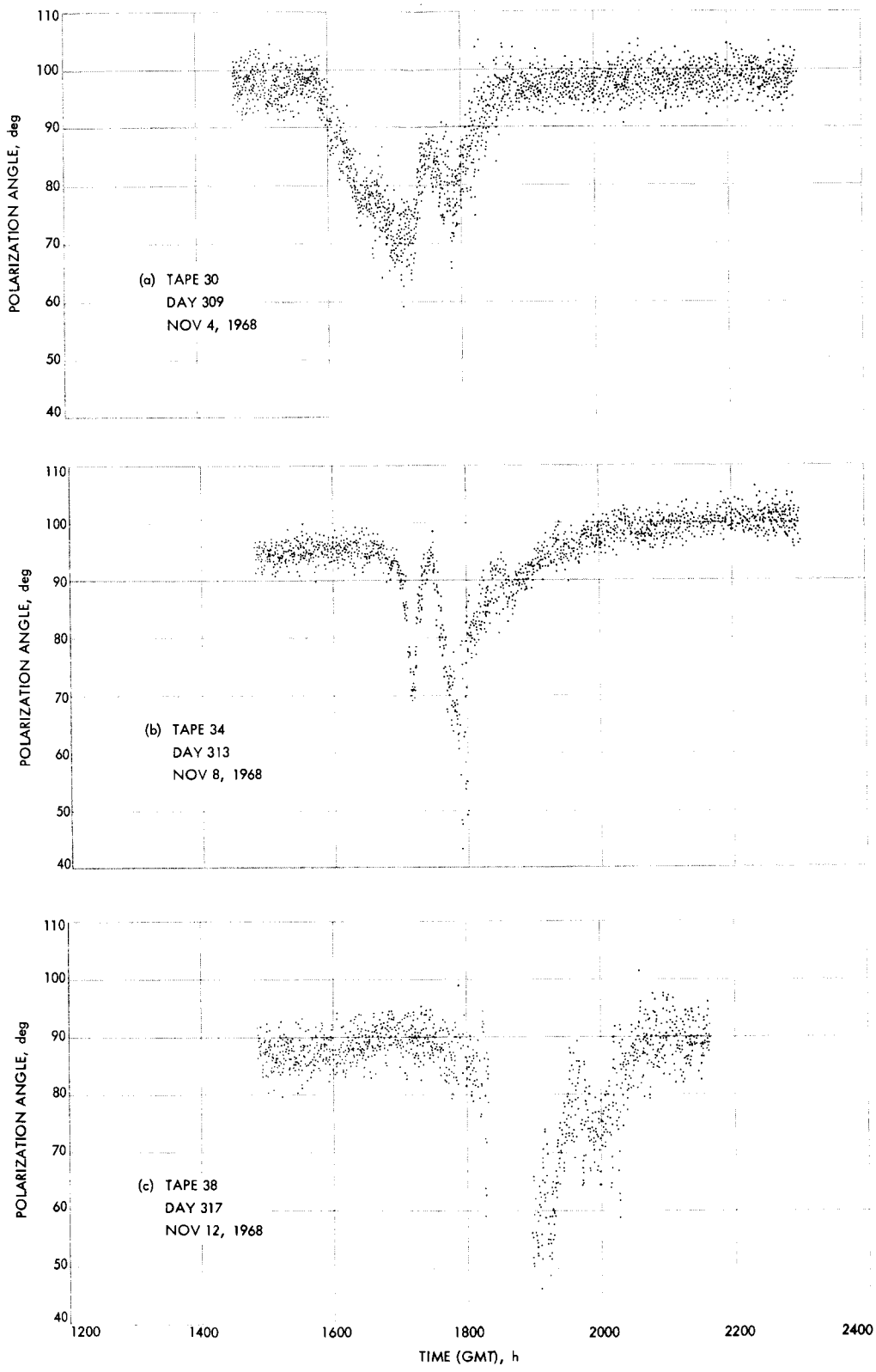

Fig. 29. *Pioneer VI* polarization (10-s data points) vs time

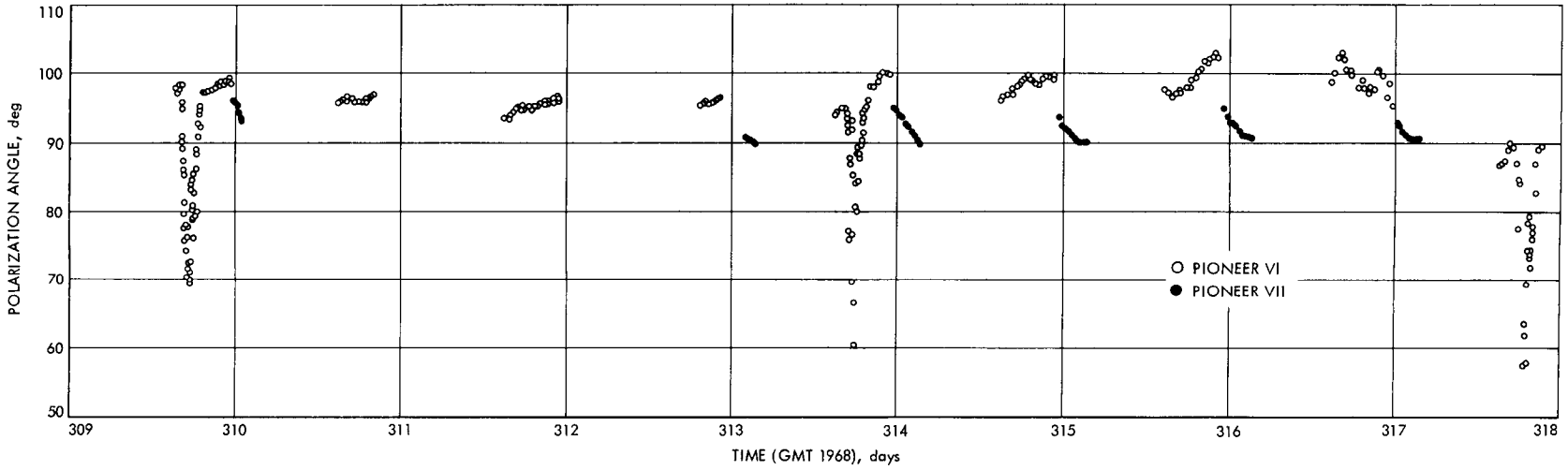

Fig. 30. Polarization vs time, 1000-s data (200-s data on transients)

is that the phenomena were produced by plasma near the sun.

The base line was at approximately 87 deg in the third event. This was caused by an increase in the steady-state plasma density and magnetic field as the line of sight approached the sun (see Subsection B of this section). Study of the events indicates a "fine structure" at least once during each event. This is especially marked for the event on November 8 where the rotation has returned to almost "normal" for a short period at about 17:30 GMT. Goldstein (Ref. 46) used the same antenna to measure spectral broadening at the same time these polarization measurements were made. Six marked and several minor enhanced spectral broadening effects were observed and reported during this experiment. There was marked enhanced spectral broadening of the signal simultaneously with *all* three of the Faraday rotation transients.

Apparently, the spectrogram technique is more sensitive than the Faraday rotation measurement for detecting these transient effects. Enhancement of spectral broadening is consistent with increased plasma density and turbulence of the coronal portion of the line of sight. The simultaneous measurement of spectral broadening of the signal virtually rules out instrumentation problems.

Two possible explanations of the observed transient polarization effects[7] are: (1) a moving plasma concentration that is ejected by the sun, or (2) a quasi-stationary structure that is probed by the line of sight. If it is assumed that fairly stationary objects are observed, then one dimension of these objects can be determined by the time it took to sweep through them. Since the durations of the events were approximately 2 h and the velocity of the line of sight relative to the plane containing the sun was approximately one-half solar radius per day, the dimensions required of these objects would be of the order of 0.04 solar radius.

If a high-velocity concentration of plasma ejected from the sun were observed, a correlation with surface effects would be expected. On the three days that these transients were observed, active areas were seen near the west limb where the observations were made. These areas were observed (Ref. 47) by several different radio frequency mapping surveys. The events were not well correlated with reported (Ref. 48) optical flares. However, in each case it appears that dekametric noise-burst events preceded these transient Faraday rotation phenomena. On November 8, the only dekametric events which were reported prior to the Faraday rotation transient occurred between 16:31 and 16:32 GMT and were classified as intensities 1 and 3. On both November 4 and 12, there were many bursts. All dekametric bursts (all were type III) that occurred within 11 h before the Faraday rotation transient, together with the reported intensity (where available), are shown in Table 3. Furthermore, the velocity that the plasma clouds must have had if they were produced by the same mechanism that produced the dekametric noise bursts can be calculated (Table 3).

Unfortunately, the origins of these dekametric noise bursts on the photosphere were not indicated. Because only three transients were observed during a period of high solar activity, the significance of the correlation with noise bursts is not well established.

Because prominences rarely extend beyond three solar radii (see Ref. 1), a search for a correlation between prominences and the Faraday rotation transients was not made. However, since the cause of the transients is presently unknown, the correlation with prominences should be investigated.

An intriguing question is raised by the fact that the three transient Faraday rotation effects all occur four days apart at the same time (to within one hour). It has been

Table 3. Correlation of the Faraday rotation transients and dekametric radio bursts

Date (Nov 1968)	Distance from solar center, solar radii	Time, GMT		Burst intensity[a]	Calculated velocity, 10^3 km/s
		Faraday rotation transient	Dekametric noise burst		
4	10.9	17:00	12:44	—	0.45
			13.05	—	0.49
			14:57	2	0.93
			15:02	2	0.97
			15:22	2	1.17
8	8.6	17:30	16:31	3	1.49
12	6.2	19:00	16:43	3	0.44
			16:47	2	0.43
			17:26	3	0.64
			17:46	1	0.82

[a]Intensity scale: 1–3.

[7]These transient effects have now been investigated in more detail: Schatten, K., "Flare Identification Associated With Coronal Disturbances," *Science*, Vol. 168, p. 395, April 17, 1970.

assumed that this is coincidental. The probability of these events occurring within the same time span is increased by narrowing the observing window. The daily observation runs were nominally of about 8-h duration during this period. Further, the observation times of the six enhanced spectral broadening measurements of the signal did not maintain this pattern.

It is shown in Subsection B of this section that the steady-state effect changes sign between "entry" and "exit." An interesting question is what happens to the sign of the transient effects. Since no transients were observed on the exit, this will have to await future experiments.

B. Steady State

The received signal polarization angles of *Pioneers VI* and *VII* were recorded on magnetic tape at 10-s intervals. The computer program provides a punched card output that is obtained by averaging 20 data points in both time and polarization angle to provide 200-s data points. These have been further averaged in groups of five (computer program CTS 46, see Appendix E) to provide the 1000-s data points. Data points that were inconsistent with the majority of the data were culled before the final averaging. The culled data, which amounted to possibly 0.1% of the total, were concentrated at the beginning and end of the tracking periods and included most of the data near occultation.

The 1000-s data are plotted in Fig. 31 (*Pioneer VI* entry to sun on west limb) and Fig. 32 (*Pioneer VI* exit from sun on east limb) for the period November 3–December 8, 1968 as a function of day of the year, GMT. The peak-to-peak measurement scatter increases near the sun to about 20 deg on days 321 and 334 (the last day on entry and first day on exit, respectively, of usable nonambiguous data). The system operating noise temperature varied between about 150 and 400 K on these days. The polarization angle instrumentation has a 180-deg ambiguity so that the measurements become meaningless when the uncertainty approaches this magnitude.

Figures 31 and 32 are uncorrected for the earth's ionospheric Faraday rotation. Data for this correction were obtained from Faraday rotation measurements through the earth's ionosphere between the *Applications Technology Satellite 1* (*ATS-1*) and the Goldstone Venus station. The *ATS-1*, which is in a geostationary orbit over the Pacific Ocean at 151°W lon, transmits a linearly polarized signal. The received signal polarization is continuously measured, digitized, and recorded. The result is transformed through a suitable model of the earth's magnetic field and electron density distribution to an equivalent Faraday rotation in the Goldstone–*Pioneer VI* line of sight (Ref. 49).

Typically, the rotation due to the earth's ionosphere at 2.3 GHz is less than 1 deg at night rising to about 4–7 deg at midday. Figure 33 shows a sample translation for day 309. These data are of particular interest since a polarization transient "event" (Fig. 29) occurred at about 17:00 GMT on this same day. Fig. 34 shows several days of *Pioneer VI* polarization data (compare with Fig. 30) with a correction (CTS 43 computer program, see Appendix E) made for the earth's ionosphere. The correction does not bring the measurements to 90 deg, probably because of: (1) inaccuracy of correction, (2) the small effect of the solar corona, and (3) orientation of the spacecraft not exactly perpendicular to the plane of the ecliptic.

The polarization system has the capability of detecting ellipticity in the received signal (see Fig. 20). No detectable ellipticity (instrumentation resolution of power axial ratio was ≈ 0.1) was observed. The records were inspected closely during the time of the transient effects. As shown in Section VI (see Fig. 38), the expected ellipticity ratio is on the order of 10^{-10} for a signal passing within 6 solar radii of the sun.

VI. Comparison of the Steady-State Measurements With Theoretical Models

The Parker magnetic field model and the modified Allen–Baumbach electron density model for the sun have been described in Section I. These static models assume a homogeneous and radially symmetric solar corona. The actual magnetic fields and electron densities are certainly not homogeneous and vary considerably as a function of time in both magnitude and distribution.

The derivations and computations for the Faraday rotation through the solar corona for these various static models as a function of signal-ray-path offset from the sun are presented in this section.

These static models are useful primarily for providing order of magnitude estimates of the Faraday rotation through the solar corona. Comparisons of the measured Faraday rotation data with computed Faraday rotation are presented by the use of measured magnetic field data and the modified Allen–Baumbach electron density model.

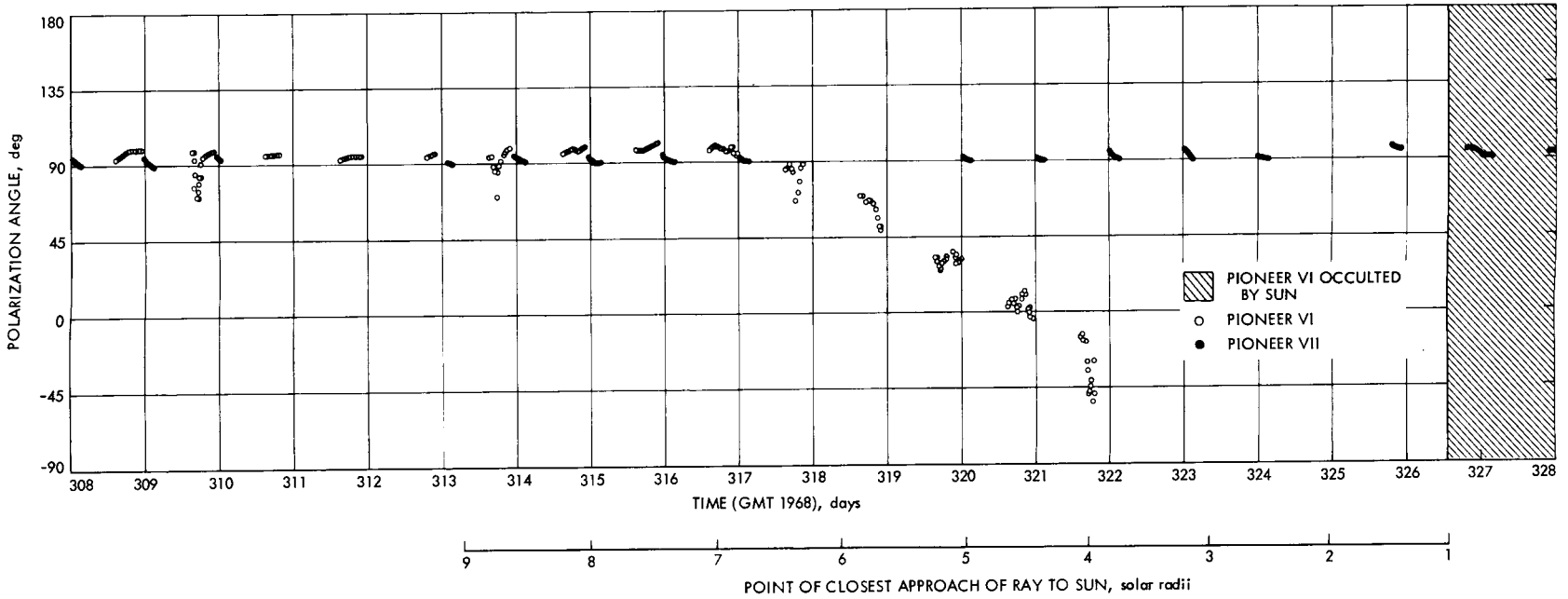

Fig. 31. *Pioneer VI* entry and *Pioneer VII* polarization angles vs time referred to plane of ecliptic; uncorrected for ionospheric rotation

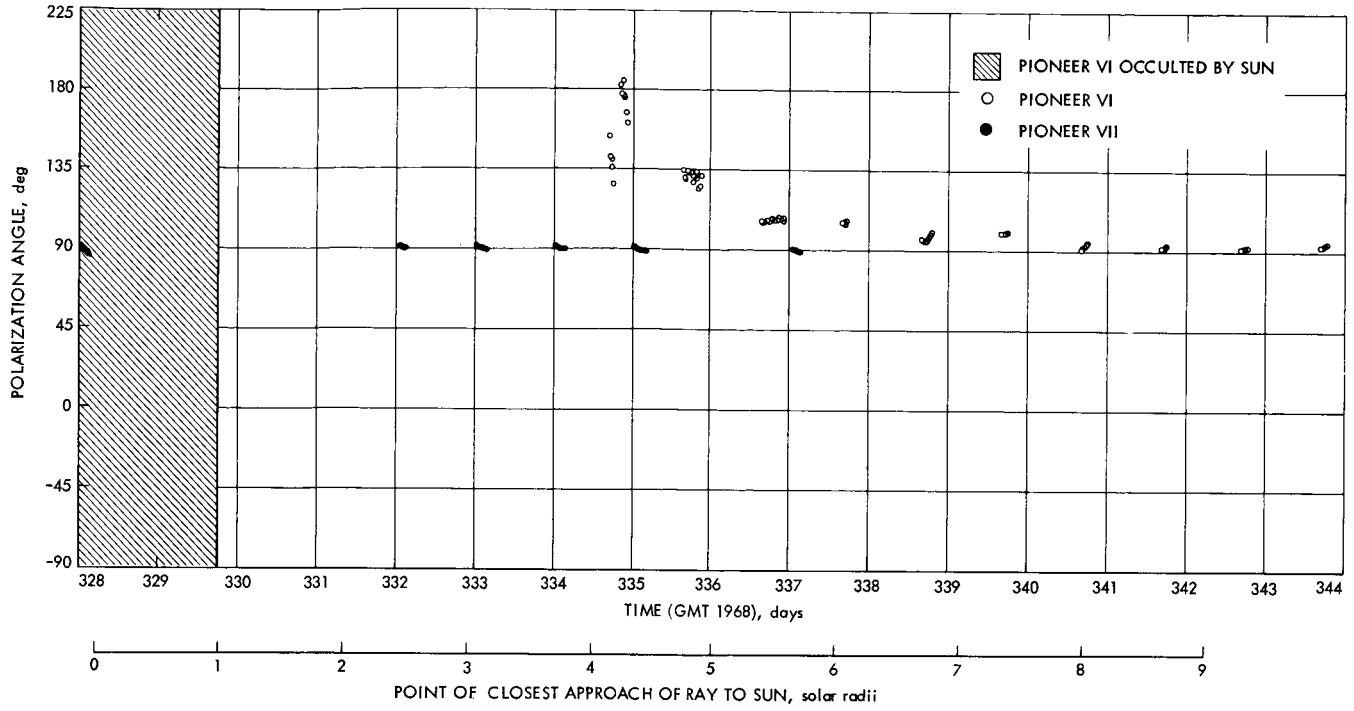

Fig. 32. *Pioneer VI* exit and *Pioneer VII* polarization angles vs time referred to plane of ecliptic; uncorrected for ionospheric rotation

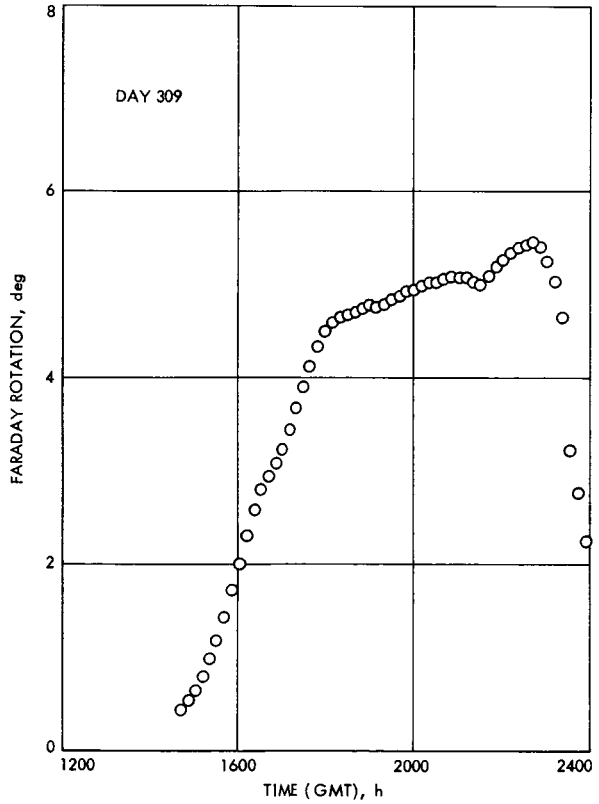

Fig. 33. Faraday rotation due to earth's ionosphere in Goldstone–*Pioneer VI* line of sight

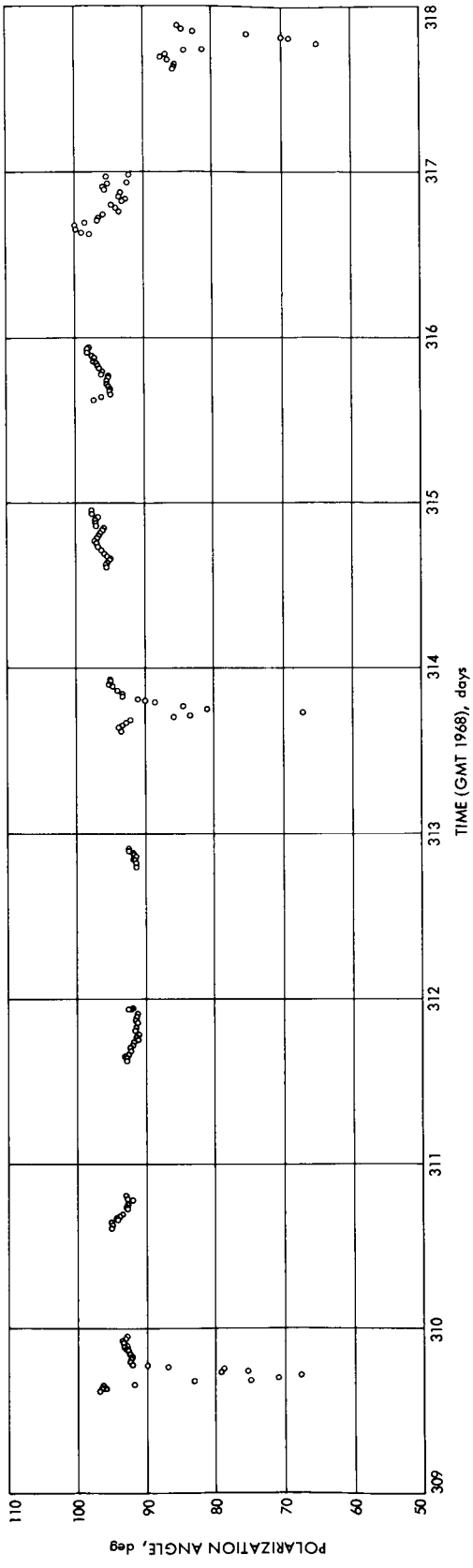

Fig. 34. *Pioneer VI* polarization vs time (1000-s data with ionospheric correction)

A. Faraday Rotation in the Solar Corona Assuming a Modified Allen–Baumbach Electron Density and Parker Magnetic Field Model

The differential Faraday rotation of a linearly polarized signal in a plasma due to the longitudinal component ($\theta = 0$ deg, Fig. 1) of the magnetic field is [see Eq. (30)]

$$d\Omega_L\,(\text{deg}) = -\frac{180}{cf^2} f_p^2(s)\, f_g(s)\, ds = \frac{QL}{f^2} N(s)\, B_L(s)\, ds \tag{102}$$

where

f = signal frequency, Hz

$f_p \simeq 8.97837\,(\text{N})^{1/2}$

$f_g = = 2.799202 \times 10^6\, B_L$, Hz

N = electron density, m^{-3}

B_L = longitudinal component of magnetic field, G

c = velocity of propagation in a vacuum, 2.997925×10^8 m/s

$Q = 135.4816$

L = unit scaling factor for ds ($L = 1$ if ds in meters, $\simeq 6.9598 \times 10^8$ if ds in solar radii)

The total Faraday rotation of the signal due to the longitudinal component of $\mathbf{B}_0$ is given by integrating along the path (Fig. 35) shown so that

$$\Omega_L = \frac{QL}{f^2} \int N(s)\, B_L\,(s)\, ds \tag{103}$$

For the modified Allen–Baumbach electron density [see Eq. (4)] and Parker magnetic field [see Eq. (2)], we have a Faraday rotation (due to the longitudinal magnetic field component along the propagation path),

$$\Omega_L = \frac{QL\,10^{14}}{f^2}\left[\int\left(\frac{1.55}{R^6} + \frac{0.01}{R^2}\right)\frac{PB_0}{R^2}\, d\phi + \int\left(\frac{1.55}{R^6} + \frac{0.01}{R^2}\right)\frac{PB_0}{R}\,\frac{\omega}{v}\sin\phi\, d\phi\right]$$

$$= \Omega_{LR} + \Omega_{LA} \tag{104}$$

where

Ω_L = total Faraday rotation, deg

P = magnetic field polarity = ± 1

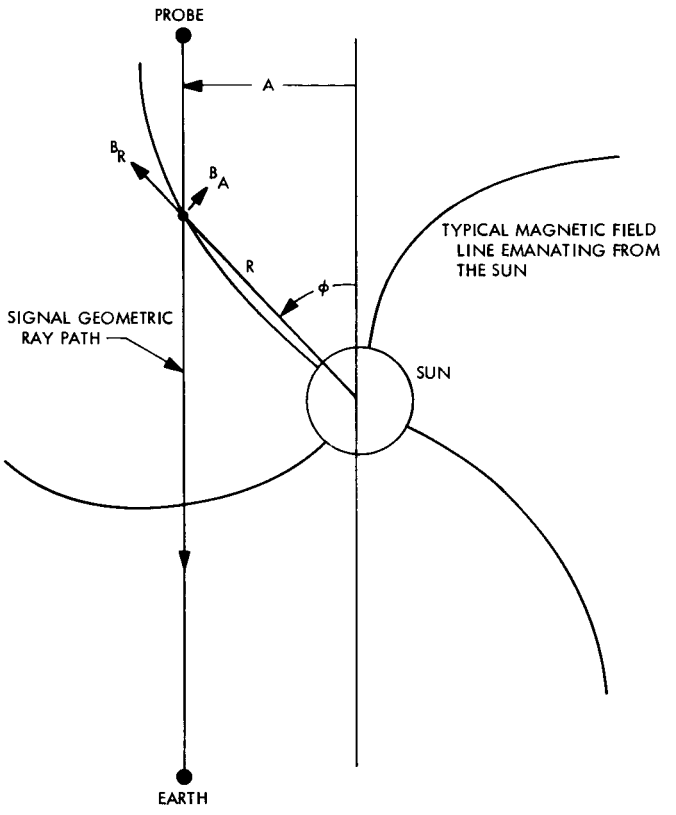

Fig. 35. Projection on plane of ecliptic of *Pioneer VI* spacecraft signal geometric ray path through solar corona and magnetic field emanating from sun

Ω_{LR} = Faraday rotation contributed by radial component of magnetic field from sun, deg

Ω_{LA} = Faraday rotation contributed by azimuthal component of magnetic field from sun, deg

If the field has the same polarity over the total path length ($\phi = 0$ to π), the cosine term forces Ω_{LR} to zero and we only have a contribution from the azimuthal component. Conversely, if the field changes polarity at $\phi = \pi/2$, the sine term forces Ω_{LA} to zero and we only have a contribution from the radial component. The range of magnitudes of the two components can be investigated by integrating over a quadrant ($\phi = 0$ to $\pi/2$) and solving for the two terms separately (in degrees)

$$\Omega_{LR}\,\frac{\pi}{2} = \frac{QL10^{14}}{f^2}\int_0^{\pi/2}\left(\frac{1.55\sin^6\phi}{A^6} + \frac{0.01\sin^2\phi}{A^2}\right) \times \frac{B_0\sin^2\phi\cos\phi}{A^2}\,\frac{A d\phi}{\sin^2\phi}$$

$$= \frac{397440}{A^7} + \frac{5983.0}{A^3} \tag{105}$$

$$\Omega_{LA}\frac{\pi}{2} = \frac{QL10^{14}}{f^2}\int_0^{\pi/2}\left(\frac{1.55\sin^6\phi}{A^6} + \frac{0.01\sin^2\phi}{A^2}\right) \times \frac{B_0\sin^2\phi}{A}\frac{\omega}{v}\frac{Ad\phi}{\sin^2\phi}$$

$$= \frac{5599.2}{A^6} + \frac{57.798}{A^2} \tag{106}$$

where A (the ray path offset in solar radii) and ϕ are defined in Fig. 35 and values of 2.292036×10^9, 1×10^5, and 4.3×10^5 m/s were assumed for f, B_0, and v, respectively. Equations (105) and (106) have been calculated for representative values of A and tabulated in Table 4. This table is useful to visualize the magnitudes of the Faraday rotation in a large sector (quadrant) due to the "quiet" sun static field model. If the field were all of the same polarity, the total Faraday rotation (ϕ from 0 to π) would be $2\Omega_{LA}(\pi/2)$. If the polarity changed at $\phi = \pi/2$, then the total Faraday rotation would be $2\Omega_{LR}(\pi/2)$. Obviously nothing can be said from this model about the relative magnitude or sign between exit and entry. Similarly, for propagation transverse to the magnetic field ($\theta = \pi/2$, see Fig. 1), we have an upper limit estimate [Eq. (47) where Fig. 36 identifies the nomenclature and axis orientation used in Section II]

$$|d\Omega_T\ (\text{deg})| = \frac{90}{cf^3} f_p^2(s)\, f_g^2(s)\, ds = \frac{Q_T L}{f^3} N(s)\, B_T^2(s)\, ds \tag{107}$$

where

$$Q_T = 1.896205 \times 10^8$$

So that

$$|\Omega_T| = \frac{Q_T L}{f}\int N(s)\, B_T^2(s)\, ds \tag{108}$$

and for the modified Allen–Baumbach electron density [see Eq. (3)] and radial magnetic field [see Eq. (2) with $B_0 = 1$ G], we have (in degrees) for a quadrant

$$\Omega_{TR}\left(\frac{\pi}{2}\right) = \frac{Q_T L\, 10^{14}}{f^3}\int_0^{\pi/2}\left(\frac{1.55}{R^6} + \frac{0.01}{R^2}\right) \times \left(\frac{B_0\sin\phi}{R^2}\right)\frac{Ad\phi}{\sin^2\phi}$$

$$= \frac{656.68}{A^9} + \frac{5.380}{A^5} \tag{109}$$

This is also tabulated in Table 4 for comparison with the $\theta = 0$ deg case. This contribution is not significant for this experiment. The Faraday rotation has been computed with the aforementioned data (modified Allen–Baumbach electron density and Parker magnetic field) using the "exact" Faraday rotation computer program (see Section II-C and Appendix C). A sample printout is shown in Fig. 37 for Ω_E with conditions identical to the above except ϕ_1 and ϕ_N (initial and final values of ϕ) are chosen so that the probe and earth are 177.0 and 212.0 solar radii, respectively, from the sun. An initial value of 90 deg is assumed for Ω_E to represent the situation with the *Pioneer VI* probe relative to the plane of the ecliptic. The computed values are in good agreement with Table 4 for $A = 3$. The "exact" computation differs very little from that calculated using the longitudinal component of the magnetic field for the plasma parameters of the solar corona ($A > 3$). Further, the propagation loss due to signal ellipticity is negligible for this experiment.

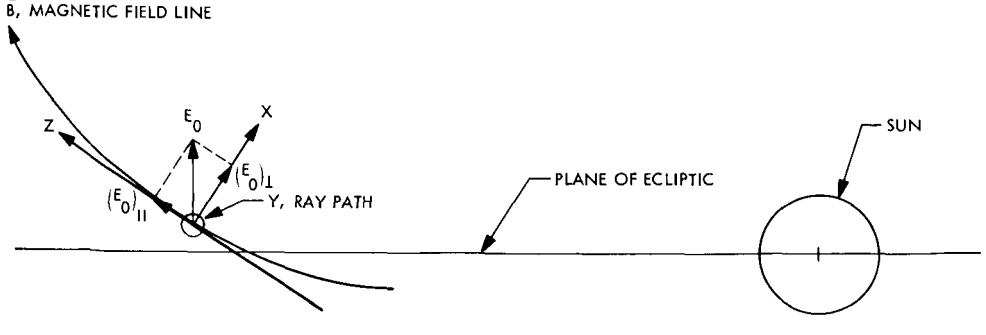

Fig. 36. Geometry of a magnetic field line emanating from sun (exaggerated)

Table 4. Calculated values of Faraday rotation in one quadrant of a "quiet" sun using a modified Allen–Baumbach electron density and Parker magnetic field

Path of closest approach of ray A, solar radii	Longitudinal component of magnetic field (θ = 0 deg), deg		Transverse component of magnetic field (θ = 90 deg), deg
	Radial field from sun Ω_{LR}	Azimuth field from sun Ω_{LA}	radial field from sun Ω_{TR}
3	403.3	10.2	0.055
4	117.7	3.6	0.008
5	53.0	1.9	0.002
6	29.1	1.2	0.001
7	17.9	0.9	—
8	11.9	0.7	—
9	8.3	0.5	—
10	6.0	0.4	—

B. Faraday Rotation in the Solar Corona With Measured Magnetic Field Data and Assuming a Modified Allen–Baumbach Electron Density

1. Magnetic field obtained from magnetograph data. Schatten (Ref. 14) has computed and supplied digitized coronal magnetic field data computed from the Mount Wilson magnetograph observations. The magnetic tapes used for this computation were supplied by Dr. Robert Howard of the Mount Wilson and Palomar Observatories. This computation refers the magnetic field to the central meridian of the sun normalized in magnitude to the surface as a function of time. These data are shown plotted (using 3.0 R_0 source surface) in Fig. 38. The entry and exit data overlap because these data are required approximately 14 days before and after the first and last Faraday rotation computations. Since the magnetic fields change slowly, the longitudinal component of the radial field at a particular time T, radius R, and angle ϕ (as defined in Fig. 5) can be computed from[8]

$$B_R(T,R,\phi) = \frac{-B_{cm}(t)\cos\phi}{R^2} \qquad (110)$$

where

$B_{cm}(t)$ = magnetic field at the central meridian of the sun at time t, G

[8]Schatten, K. H., private communication.

$$t = T \pm 27.2753\left(\frac{1}{2} - \frac{\phi}{360}\right)$$

and time is computed in decimal days. The synodic period of rotation of the sun is used to conform with the solar Mount Wilson magnetograph data. Since the sun rotates counterclockwise (looking down on the plane of the ecliptic), the + and − signs are used for exit and entry data, respectively. The above equations are incorporated into the Faraday rotation computer program (see Appendix C).

A sample computer output from the Faraday rotation program is shown in Fig. 39 using 0.5-deg steps in ϕ for day 318 (ray offset of 6.23 solar radii) computed from the Mount Wilson magnetograph magnetic field data assuming a 3.0 solar radii source surface. This indicates a total Faraday rotation of −33.5 deg (resulting in a predicted polarization angle measurement of −56.5 deg). The computation was also made using 0.2-deg steps in ϕ without any appreciable difference. The Faraday rotation of −33.5 deg is composed of +2.7 deg rotation due to the azimuthal component and −36.2 deg due to the radial component of the magnetic field. Figure 40 shows the signal polarization (referred to the plane of the ecliptic) for these data (day 318) plotted as a function of ϕ.

Figure 41 shows the signal polarization data computed for the period of the experiment using a source surface (see Ref. 14) of 2.5 and 3.0 solar radii as a function of ray path offset in solar radii. (Positive offset refers to the entry on the west limb.) Although the choice of source surface radius has an effect, it is not critical. Also shown are the averaged measured data (same as Figs. 31 and 32 except corrected for the effects of the earth's ionosphere and transient "events"). Both the measured and computed polarizations tend to "decrease" upon entry and exit. The agreement seems a little better on entry than exit. The two polarization measurements nearest the sun (near 4 solar radii) are plotted showing a possible 180-deg ambiguity, which cannot be resolved by the instrumentation.

2. Magnetic field obtained from Explorer 33 data. Interplanetary magnetic field data in the vicinity of the earth were made available from observations with the Ames Research Center magnetometer on *Explorer* 33, for which C. P. Sonnett is the principal investigator; D. S. Colburn and J. M. Wilcox supplied the data (Ref. 50). Again, since the magnetic field changes slowly,

DAY = 323.000000 A = 3.000000 R(1) = 177.000000

DPHI = .50000 L = .69598+09 RN = 212.000000

I	PHI(I)	R(I)	N(I)	BT(I)	BL(I)	DO(I)	O(I)	EX(I)	ET(I)	OE(I)	ERR(I)	LOSS(I)	RATIO	YL
1	.971	177.000	3.192+07	0.000	3.192-05		9.00+01			9.0000+01				
2	1.471	116.851	4.632+07	9.872-07	4.631-05	2.3-03	9.00+01	1.0+00	4.0-05	9.0002+01	-3.3-10	3.8-17	-4.3-19	1
12	6.471	26.619	1.301+09	1.409-04	1.293-03	6.7-02	9.03+01	1.0+00	5.4-03	9.0312+01	-4.3-08	4.2-16	-8.7-19	1
22	11.471	15.085	4.215+09	8.180-04	4.123-03	2.2-01	9.17+01	1.0+00	3.0-02	9.1737+01	-2.1-07	8.5-16	0.0	1
32	16.471	10.581	8.767+09	2.421-03	8.321-03	4.4-01	9.51+01	1.0+00	8.8-02	9.5065+01	-5.1-07	1.4-15	4.3-18	1
42	21.471	8.196	1.503+10	5.268-03	1.357-02	7.3-01	1.01+02	9.8-01	1.9-01	1.0101+02	-8.0-07	8.7-15	8.0-16	1
52	26.471	6.730	2.327+10	9.582-03	1.946-02	1.1+00	1.10+02	9.4-01	3.5-01	1.1024+02	-7.2-07	3.9-13	4.4-14	1
62	31.471	5.746	3.397+10	1.547-02	2.553-02	1.5+00	1.23+02	8.3-01	5.5-01	1.2343+02	3.7-07	9.3-12	1.1-12	1
72	36.471	5.047	4.784+10	2.292-02	3.130-02	2.0+00	1.41+02	6.3-01	7.8-01	1.4128+02	3.6-06	1.1-10	1.2-11	1
82	41.471	4.530	6.565+10	3.179-02	3.629-02	2.6+00	1.64+02	2.7-01	9.6-01	1.6448+02	1.1-05	5.4-10	6.2-11	1
92	46.471	4.138	8.804+10	4.182-02	4.007-02	3.2+00	1.94+02	2.3-01	9.7-01	1.9356+02	2.4-05	5.3-10	6.1-11	1
102	51.471	3.835	1.152+11	5.264-02	4.229-02	3.8+00	2.29+02	7.5-01	6.6-01	2.2863+02	4.7-05	8.2-10	9.5-11	1
112	56.471	3.599	1.469+11	6.380-02	4.268-02	4.3+00	2.69+02	1.0+00	1.5-02	2.6915+02	8.3-05	8.0-09	9.2-10	1
122	61.471	3.415	1.817+11	7.481-02	4.109-02	4.6+00	3.14+02	7.2-01	6.9-01	3.1366+02	1.3-04	2.5-10	2.9-11	1
132	66.471	3.272	2.179+11	8.515-02	3.752-02	4.6+00	3.60+02	4.9-03	1.0+00	3.5972+02	2.0-04	2.7-08	3.1-09	1
142	71.471	3.164	2.527+11	9.429-02	3.206-02	4.2+00	4.04+02	7.0-01	7.2-01	4.0404+02	2.7-04	2.5-09	2.9-10	1
152	76.471	3.086	2.832+11	1.018-01	2.496-02	3.5+00	4.43+02	9.9-01	1.2-01	4.4284+02	3.5-04	1.2-07	1.4-08	1
162	81.471	3.034	3.066+11	1.072-01	1.656-02	2.4+00	4.72+02	9.2-01	3.8-01	4.7239+02	4.2-04	4.1-08	4.8-09	1
172	86.471	3.006	3.205+11	1.104-01	7.291-03	1.1+00	4.90+02	7.7-01	6.4-01	4.8961+02	4.6-04	8.7-08	1.0-08	2
182	91.471	3.001	3.234+11	1.110-01	2.367-03	3.6-01	4.94+02	7.2-01	6.9-01	4.9391+02	4.7-04	7.7-07	8.9-08	2
192	96.471	3.019	3.150+11	1.092-01	1.190-02	1.8+00	5.05+02	5.7-01	8.2-01	5.0543+02	4.9-04	2.1-06	2.4-07	1
202	101.471	3.061	2.963+11	1.049-01	2.080-02	3.0+00	5.30+02	1.7-01	9.9-01	5.3022+02	5.6-04	3.3-06	3.8-07	1
212	106.471	3.128	2.691+11	9.836-02	2.862-02	3.9+00	5.66+02	4.3-01	9.0-01	5.6564+02	6.4-04	3.0-06	3.4-07	1
222	111.471	3.224	2.361+11	9.000-02	3.495-02	4.5+00	6.08+02	9.3-01	3.7-01	6.0816+02	7.1-04	1.9-06	2.2-07	1
232	116.471	3.351	2.002+11	8.022-02	3.951-02	4.6+00	6.54+02	9.1-01	4.1-01	6.5393+02	7.8-04	1.9-06	2.2-07	1
242	121.471	3.517	1.644+11	6.949-02	4.212-02	4.4+00	6.99+02	3.5-01	9.4-01	6.9943+02	8.4-04	2.4-06	2.8-07	1
252	126.471	3.731	1.309+11	5.834-02	4.273-02	4.0+00	7.42+02	3.7-01	9.3-01	7.4182+02	8.8-04	2.4-06	2.8-07	1
262	131.471	4.004	1.014+11	4.728-02	4.142-02	3.5+00	7.79+02	8.6-01	5.1-01	7.7926+02	9.1-04	2.2-06	2.6-07	1
272	136.471	4.356	7.650+10	3.680-02	3.840-02	2.9+00	8.11+02	1.0+00	1.4-02	8.1082+02	9.3-04	2.2-06	2.5-07	1
282	141.471	4.816	5.641+10	2.730-02	3.398-02	2.3+00	8.36+02	9.0-01	4.4-01	8.3639+02	9.3-04	2.2-06	2.5-07	1
292	146.471	5.431	4.062+10	1.909-02	2.855-02	1.8+00	8.56+02	6.9-01	7.2-01	8.5637+02	9.4-04	2.2-06	2.6-07	1
302	151.471	6.281	2.840+10	1.240-02	2.257-02	1.3+00	8.71+02	4.8-01	8.8-01	8.7139+02	9.4-04	2.2-06	2.6-07	1
312	156.471	7.515	1.897+10	7.282-03	1.653-02	9.1-01	8.82+02	3.1-01	9.5-01	8.8216+02	9.4-04	2.2-06	2.6-07	1
322	161.471	9.440	1.175+10	3.705-03	1.090-02	5.8-01	8.89+02	1.8-01	9.8-01	8.8938+02	9.4-04	2.2-06	2.6-07	1
332	166.471	12.824	6.338+09	1.500-03	6.118-03	3.2-01	8.94+02	1.1-01	9.9-01	8.9370+02	9.4-04	2.2-06	2.6-07	1
342	171.471	20.228	2.587+09	3.944-04	2.554-03	1.3-01	8.96+02	7.3-02	1.0+00	8.9582+02	9.4-04	2.2-06	2.6-07	1
352	176.471	48.740	4.784+08	3.153-05	4.774-04	2.5-02	8.96+02	6.1-02	1.0+00	8.9649+02	9.4-04	2.2-06	2.6-07	1
358	179.189	212.000	2.784+07	5.153-07	2.783-05	1.4-03	8.97+02	6.0-02	1.0+00	8.9654+02	9.4-04	2.2-06	2.6-07	1

OMEGA = 8.965357+02 DEG. OMEGA(E) = 8.965366+02 DEG. ERROR = 9.401638-04 DEG. LOSS = 2.241840-06 DB

A = -4.562697-02 B = 3.959618-02 C = -7.593619-01 D = 6.478579-01

EX = 6.041257-02 ETHETA = 9.981735-01

Fig. 37. Sample computer output of Faraday rotation program using modified Allen–Baumbach electron density and Parker magnetic field models

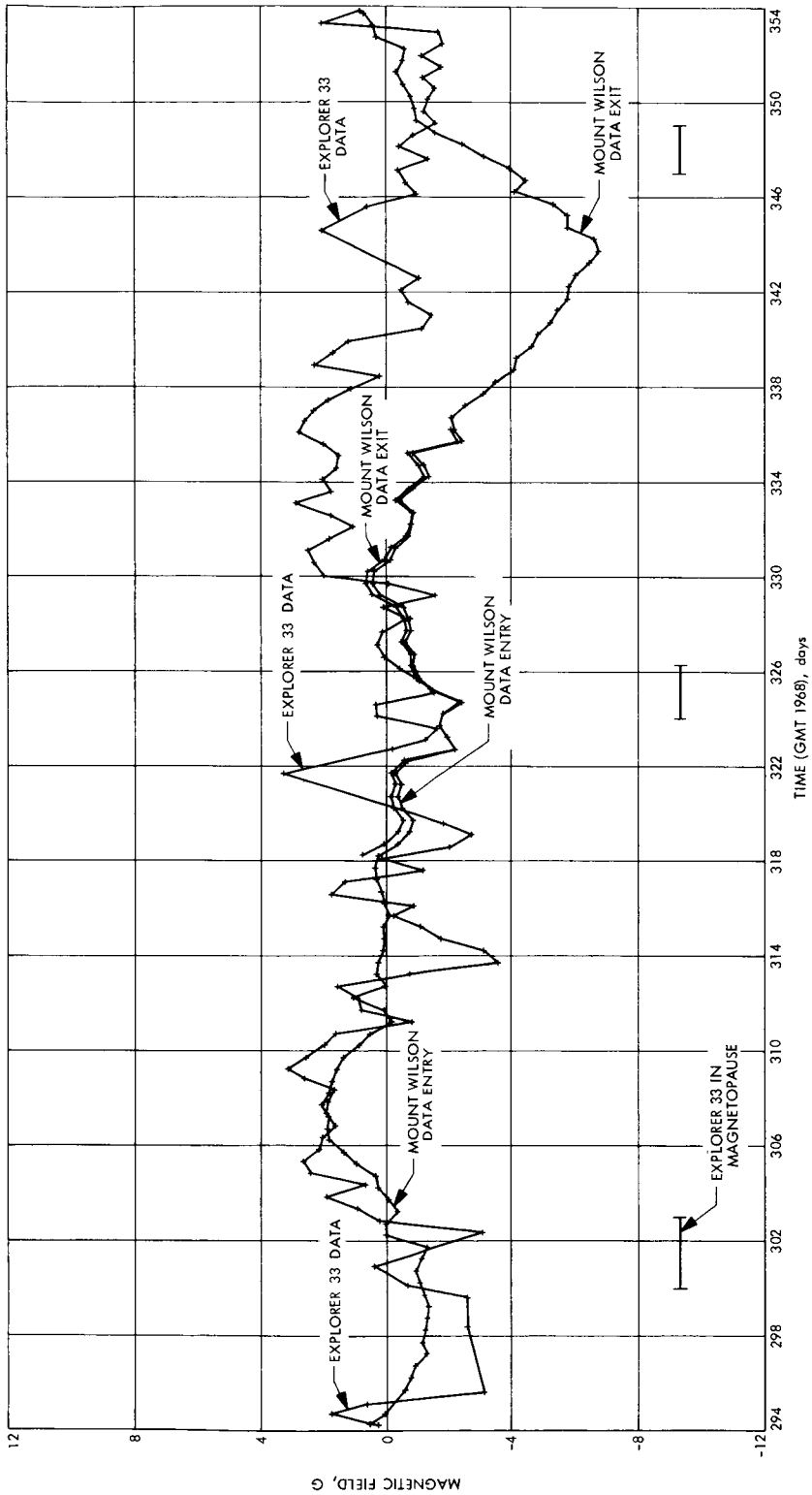

Fig. 38. "Measured" magnetic field of sun referred to central meridian and normalized in magnitude to solar surface as a function of time for Mount Wilson magnetograph (using 3.0 solar radii source surface) and *Explorer* 33 data

DAY = 318.000000 A = 6.233700 R(1) = 177.955400

DPHI = .50000 L = .69598+09 RN = 212.679200

I	PHI(I)	R(I)	N(I)	BT(I)	BL(I)	DO(I)	O(I)	EX(I)	ET(I)	OE(I)	ERR(I)	LOSS(I)	RATIO	YL
1	2.007	177.955	3.158+07	8.552-06	-9.733-06		9.00+01			9.0000+01				
2	2.507	142.486	3.895+07	9.795-06	-1.215-05	-3.0-04	9.00+01	1.0+00	5.3-06	9.0000+01	4.3-11	3.0-17	0.0	1
12	7.507	47.711	4.097+08	8.200-05	-2.233-04	-5.6-03	9.00+01	1.0+00	4.0-04	8.9977+01	3.2-09	3.6-16	-8.7-19	1
22	12.507	28.784	1.159+09	4.072-04	-1.118-03	-2.8-02	8.98+01	1.0+00	3.3-03	8.9814+01	2.5-08	7.3-16	-4.3-19	1
32	17.507	20.722	2.266+09	1.164-03	-2.765-03	-7.0-02	8.93+01	1.0+00	1.2-02	8.9324+01	8.8-08	1.1-15	-4.3-19	1
42	22.507	16.284	3.699+09	2.721-03	-5.428-03	-1.4-01	8.83+01	1.0+00	3.0-02	8.8282+01	2.1-07	1.4-15	0.0	1
52	27.507	13.497	5.421+09	5.093-03	-8.519-03	-2.1-01	8.65+01	1.0+00	6.2-02	8.6465+01	4.1-07	1.8-15	2.3-17	1
62	32.507	11.600	7.391+09	7.991-03	-1.126-02	-2.9-01	8.39+01	9.9-01	1.1-01	8.3922+01	6.4-07	7.7-15	6.5-16	1
72	37.507	10.238	9.561+09	1.124-02	-1.340-02	-3.4-01	8.08+01	9.9-01	1.6-01	8.0754+01	8.8-07	8.1-14	9.0-15	1
82	42.507	9.226	1.188+10	1.628-02	-1.644-02	-4.2-01	7.69+01	9.7-01	2.3-01	7.6920+01	1.1-06	7.8-13	8.9-14	1
92	47.507	8.454	1.429+10	2.073-02	-1.769-02	-4.6-01	7.24+01	9.5-01	3.0-01	7.2393+01	1.3-06	5.8-12	6.7-13	1
102	52.507	7.857	1.674+10	2.351-02	-1.686-02	-4.4-01	6.79+01	9.3-01	3.8-01	6.7913+01	1.4-06	2.5-11	2.9-12	1
112	57.507	7.391	1.914+10	2.691-02	-1.603-02	-4.2-01	6.36+01	9.0-01	4.4-01	6.3584+01	1.4-06	8.1-11	9.3-12	1
122	62.507	7.027	2.143+10	2.935-02	-1.423-02	-3.8-01	5.96+01	8.6-01	5.1-01	5.9570+01	1.3-06	2.1-10	2.5-11	1
132	67.507	6.747	2.351+10	3.041-02	-1.164-02	-3.1-01	5.61+01	8.3-01	5.6-01	5.6108+01	1.2-06	4.6-10	5.3-11	1
142	72.507	6.536	2.532+10	2.864-02	-8.215-03	-2.2-01	5.34+01	8.0-01	6.0-01	5.3419+01	1.1-06	8.3-10	9.5-11	1
152	77.507	6.385	2.676+10	2.114-02	-4.125-03	-1.1-01	5.18+01	7.9-01	6.2-01	5.1810+01	1.0-06	1.1-09	1.3-10	1
162	82.507	6.287	2.777+10	1.502-02	-1.597-03	-4.4-02	5.11+01	7.8-01	6.3-01	5.1084+01	9.6-07	1.3-09	1.5-10	1
172	87.507	6.240	2.830+10	4.957-03	-9.379-05	-2.6-03	5.09+01	7.8-01	6.3-01	5.0898+01	9.5-07	1.4-09	1.6-10	1
182	92.507	6.240	2.832+10	-2.799-03	-1.915-04	-5.3-03	5.09+01	7.8-01	6.3-01	5.0873+01	9.5-07	1.4-09	1.6-10	1
192	97.507	6.288	2.784+10	1.570-03	2.466-04	6.8-03	5.09+01	7.8-01	6.3-01	5.0870+01	9.5-07	1.4-09	1.6-10	1
202	102.507	6.385	2.687+10	1.851-02	4.598-03	1.3-01	5.15+01	7.8-01	6.2-01	5.1522+01	9.9-07	1.5-09	1.7-10	1
212	107.507	6.536	2.547+10	1.216-02	4.185-03	1.1-01	5.31+01	8.0-01	6.0-01	5.3055+01	1.1-06	1.8-09	2.0-10	1
222	112.507	6.748	2.370+10	1.991-03	8.886-04	2.4-02	5.35+01	8.0-01	6.0-01	5.3487+01	1.1-06	1.8-09	2.0-10	1
232	117.507	7.028	2.164+10	5.563-03	3.099-03	8.3-02	5.40+01	8.1-01	5.9-01	5.4046+01	1.1-06	1.8-09	2.1-10	1
242	122.507	7.392	1.937+10	3.993-03	2.715-03	7.2-02	5.48+01	8.2-01	5.8-01	5.4817+01	1.1-06	1.8-09	2.1-10	1
252	127.507	7.858	1.697+10	2.214-03	1.815-03	4.7-02	5.54+01	8.2-01	5.7-01	5.5419+01	1.1-06	1.8-09	2.1-10	1
262	132.507	8.456	1.453+10	1.007-03	9.891-04	2.6-02	5.57+01	8.3-01	5.6-01	5.5749+01	1.1-06	1.8-09	2.1-10	1
272	137.507	9.228	1.211+10	5.885-04	6.939-04	1.8-02	5.60+01	8.3-01	5.6-01	5.5960+01	1.1-06	1.8-09	2.1-10	1
282	142.507	10.242	9.780+09	5.256-04	7.496-04	1.9-02	5.61+01	8.3-01	5.6-01	5.6147+01	1.1-06	1.8-09	2.1-10	1
292	147.507	11.604	7.593+09	3.908-05	6.857-05	1.7-03	5.63+01	8.3-01	5.6-01	5.6265+01	1.1-06	1.8-09	2.1-10	1
302	152.507	13.504	5.602+09	-5.687-05	-1.266-04	-3.2-03	5.62+01	8.3-01	5.6-01	5.6213+01	1.1-06	1.8-09	2.1-10	1
312	157.507	16.295	3.854+09	9.090-05	2.723-04	6.9-03	5.62+01	8.3-01	5.6-01	5.6243+01	1.1-06	1.8-09	2.1-10	1
322	162.507	20.739	2.391+09	7.532-05	3.449-04	8.7-03	5.63+01	8.3-01	5.5-01	5.6326+01	1.1-06	1.8-09	2.1-10	1
332	167.507	28.818	1.251+09	2.838-05	3.077-04	7.7-03	5.64+01	8.3-01	5.5-01	5.6409+01	1.1-06	1.8-09	2.1-10	1
342	172.507	47.805	4.661+08	-1.203-05	1.568-04	3.9-03	5.65+01	8.3-01	5.5-01	5.6467+01	1.1-06	1.8-09	2.1-10	1
352	177.507	143.338	5.794+07	-1.205-05	2.209-05	5.5-04	5.65+01	8.3-01	5.5-01	5.6486+01	1.1-06	1.8-09	2.1-10	1
354	178.320	212.679	2.604+07	-8.113-06	9.549-06	2.4-04	5.65+01	8.3-01	5.5-01	5.6487+01	1.1-06	1.8-09	2.1-10	1

OMEGA = 5.648687+01 DEG. OMEGA(E) = 5.648687+01 DEG. ERROR = 1.059636-06 DEG. LOSS = 1.808825-09 DB

A = 3.084800-01 B = 7.745932-01 C = -2.042641-01 D = -5.129538-01

EX = 8.337593-01 ETHETA = 5.521281-01

Fig. 39. Sample computer output of Faraday rotation program using modified Allen–Baumbach electron density model and measured Mount Wilson magnetic field data

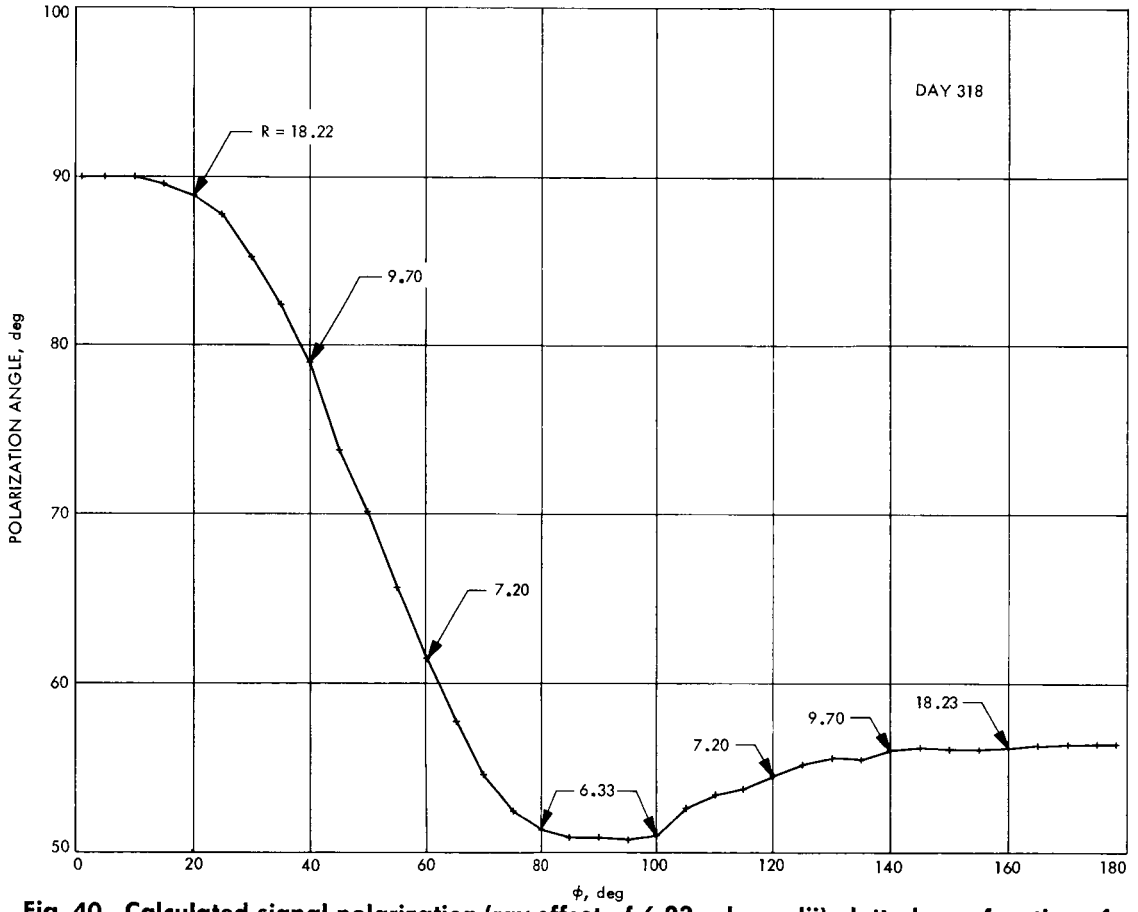

Fig. 40. Calculated signal polarization (ray offset of 6.23 solar radii) plotted as a function of ϕ

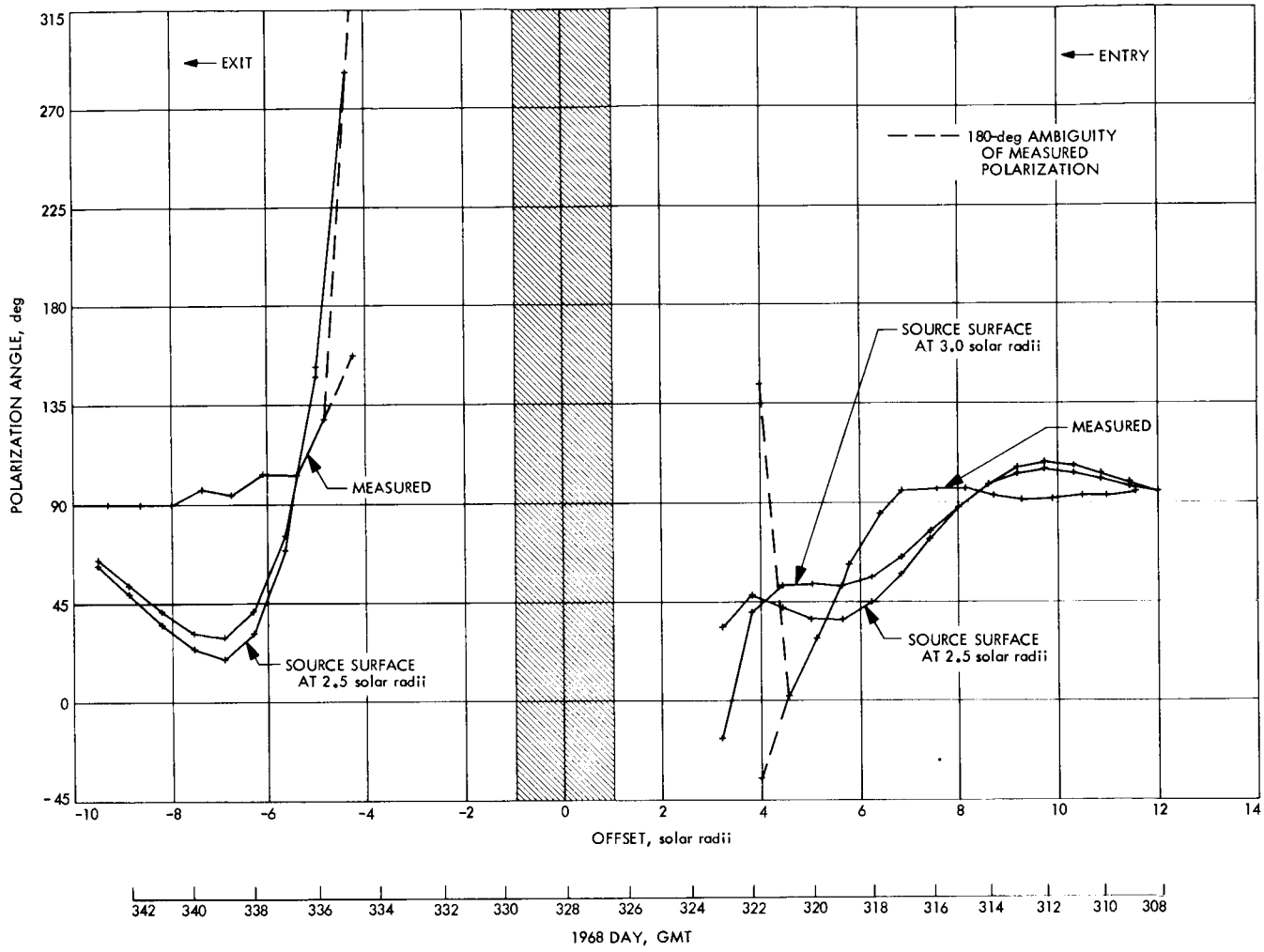

Fig. 41. Comparison of measured signal polarization and that calculated using Mount Wilson magnetic field data with 2.5 and 3.0 solar radii source surfaces

the magnetic field at the central meridian of the sun is calculated from

$$B_{cm}(t) = -B \cos\theta \cos\phi \, R_N^2 \qquad (111)$$

where

B = magnetic field intensity measured by *Explorer* 33 in the vicinity of earth, G (positive B defined as "toward" sun)

R_N = sun-earth distance

θ = angle with respect to solar equatorial plane (+90 deg means a field directed north)

ϕ = azimuthal angle in solar equatorial coordinates (0.0 deg from the earth toward sun)

In the above it is assumed that the magnetic field lines are "frozen" in the solar wind plasma, which takes about 5 days to travel from the sun to the earth. This requires that $B_{cm}(t)$ be calculated using data for B delayed by 5 days.

The *Explorer* 33 data (excluding that data contaminated when the earth satellite was situated in the magnetopause) were transformed (Appendix E, CTS 44) by Eqs. (110) and (111) and used with the Faraday rotation program. These data are shown plotted in Fig. 40 for comparison with the Mount Wilson data. It appears that the fields computed from the Mount Wilson magnetograph data tend to be "smeared out" from the appearance of that computed from the *Explorer* 33 data. The output from the Faraday rotation program is shown in Fig. 42. Comparison with the experimental data appears to be slightly better than Fig. 41, especially upon exit near

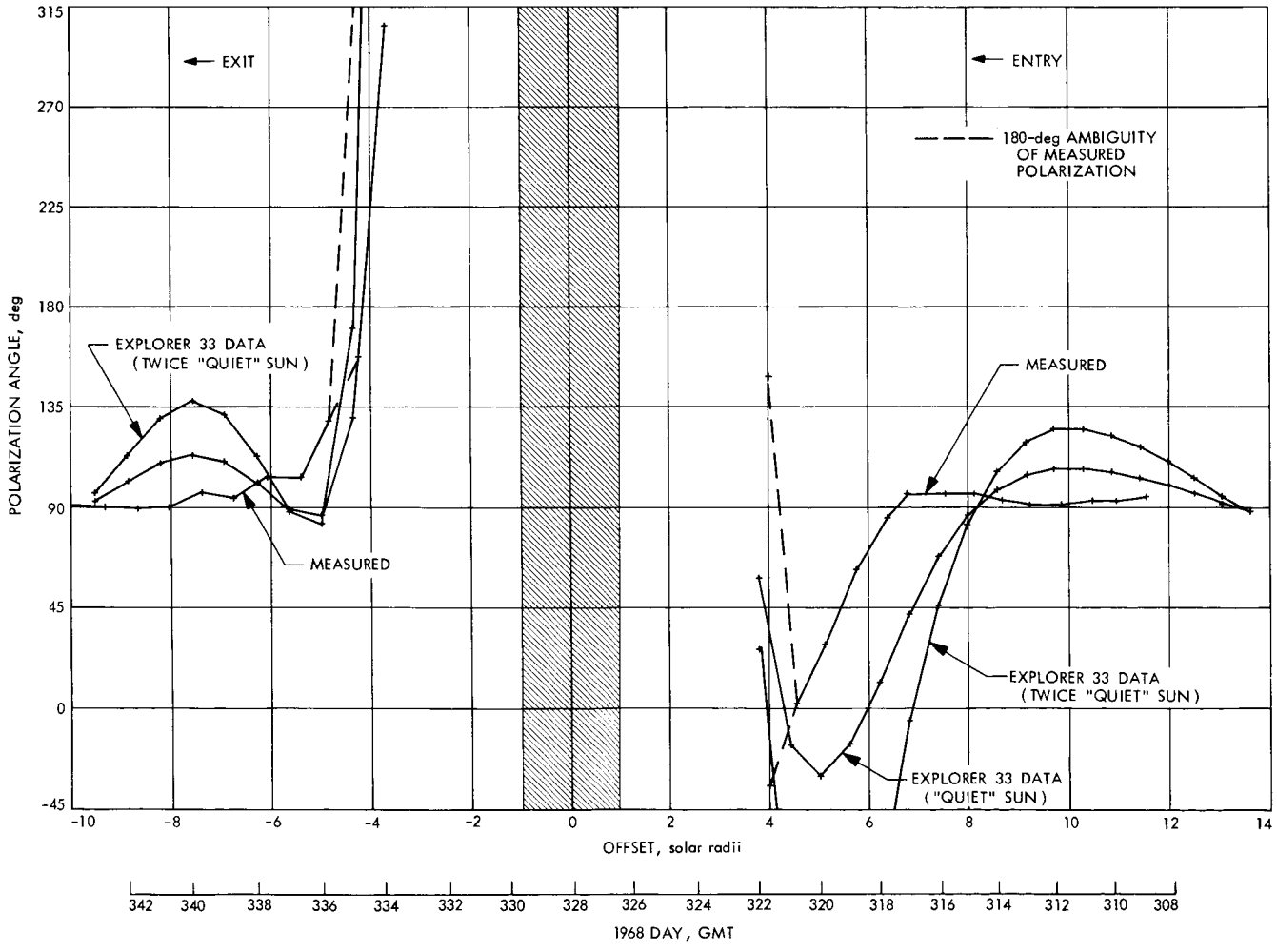

Fig. 42. Comparison of measured signal polarization and that calculated using *Explorer* 33 magnetic field data with "quiet" sun and twice "quiet" sun electron densities

−7 solar radii. There was considerable solar activity during the time of the exit. This might contribute significantly greater errors (see footnote 7) in the magnetic fields as calculated from the Mount Wilson magnetograph data using the source surface technique (Ref. 14) than those calculated using the *Explorer* 33 magnetometer data.

C. Adjustment of Electron Density to Obtain Agreement Between Calculated and Measured Faraday Rotation

The electron density is usually assumed to be about doubled (Ref. 8) during the active portion of the solar cycle (appropriate to the time of this experiment) relative to the quiet part of the cycle. The assumed electron density was doubled and the *Explorer* 33 magnetometer data were rerun to investigate this effect (Fig. 42). This simple idea is apparently not adequate for these data since this curve deviates even more from the measured data.

Assume an equatorial electron density

$$N = 10^{14}\left(\frac{A}{R^6} + \frac{B}{R^2}\right) \tag{112}$$

The Faraday rotation through the solar corona was calculated using the *Explorer* 33 magnetometer magnetic field data and Eq. (112) with various values for B (Fig. 43a) and A (Fig. 43b). The *Explorer* 33 magnetometer data were used, rather than the Mount Wilson magnetograph data, because of the slightly better correlation with the measured data.

It appears from these results that the value of B assumed for a quiet sun is too high for this region of interest. Values of 6.0 and 0.002 for A and B, respectively, fit the data considerably better than the values of 1.55 and 0.01 originally assumed (Figs. 43a and 43b). When the power of R in the first term is varied, further trials give an even better fit (Fig. 43c) using

$$N = 10^{14}\left(\frac{6000}{R^{10}} + \frac{0.002}{R^2}\right) \tag{113}$$

The magnetic field data are apparently more reliable upon entry than exit as shown by the better agreement between the Mount Wilson magnetograph and *Explorer* 33 magnetometer data. For this reason, the electron density was selected to give the best fit in the entry region. The higher order power for R in Eq. (113) was required to displace the curve (for $A = 10$, Fig. 43b) on entry toward the sun.

Computed values for Eq. (113) are tabulated in Table 5 for comparison with published (see Ref. 2) results of electron density in the solar corona. These values are between the limits of the other results at 10 solar radii but are higher than any of the others at 4 solar radii. However, these data were taken near a solar maximum while the Pottasch data (11.09 at 4 solar radii) were taken during a solar minimum. The Van DeHulst data (10.95 at 4 solar radii) at a maximum are seemingly inconsistent with the Pottasch result since a greater density near a maximum is expected. This indicates the difficulty of obtaining accurate electron density data in the solar corona. Therefore, it is concluded that the electron density obtained from the *Pioneer VI* Faraday rotation experiment is reasonably consistent with the published data.

Other fits could be obtained using least squares or similar curve-fitting techniques for this or other forms involving higher order terms. However, the scatter of the present data does not seem to warrant these refined techniques. The three parts of Fig. 43 all indicate a better correlation between measured and computed polarizations if the upper values for the measured points at ray offsets of −4.2 and 4.0 are used. There is no obvious way to "prove" which of these ambiguous data points are valid. It is apparent, however, that the polarization is changing exceedingly rapid at 4 solar radii from the sun. It is as if the sun appeared to have a diameter of about 8 solar radii at 2.3 GHz.

VII. Conclusions and Suggestions for Future Work

A. Summary of Conclusions

The primary goal of this experiment, which was to perform the first measurement of Faraday rotation of a linearly polarized CW signal passing through the solar corona, has been achieved. A comparison with modest theoretical model studies has been made. The computer program developed to determine ray bending in the solar corona indicates that this effect is not important in the solar corona at S-band frequencies. The pointing error caused by a signal traversing the solar corona with an offset greater than 3 radii to the sun center is less than 0.0004 deg. This pointing error is below the present instrumental resolution of the Goldstone 210-ft antenna.

A detailed "exact" solution of the Faraday rotation through a stratified layer with the magnetic field at an

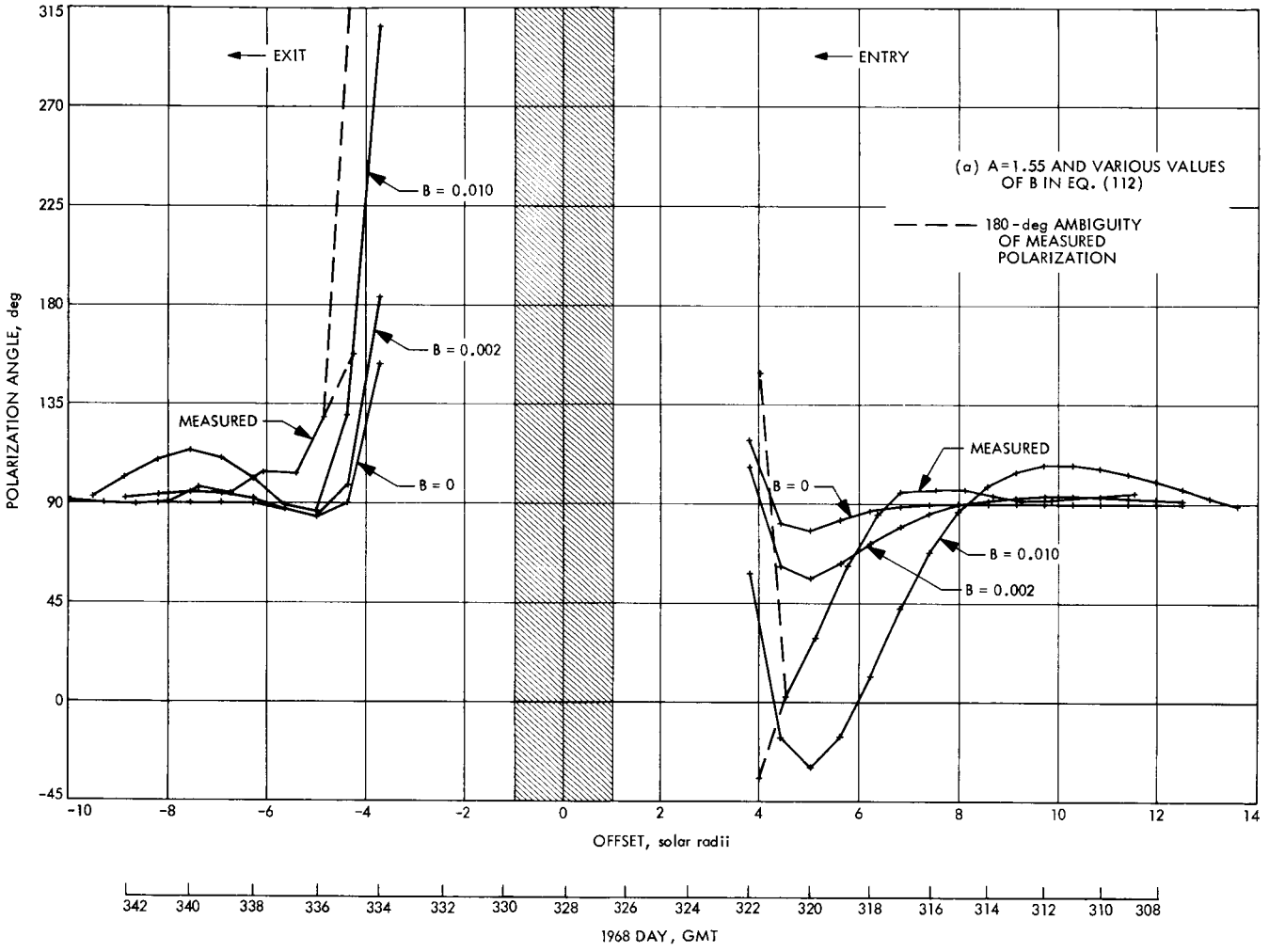

Fig. 43. Comparison of measured signal polarization and that calculated using *Explorer 33* magnetic field data with various values of *A* and *B*

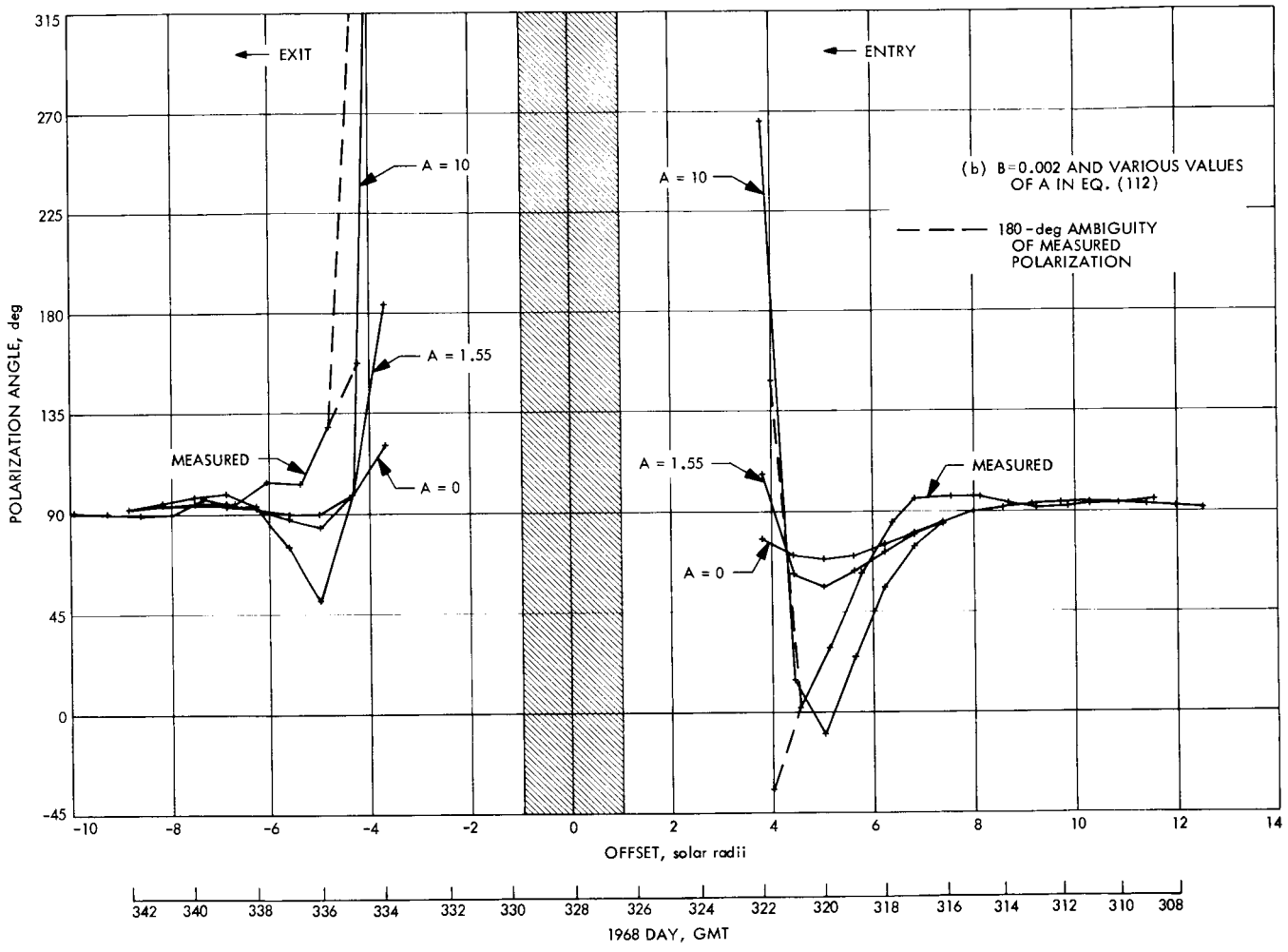
EXIT
ENTRY
A = 10
A = 10
(b) B=0.002 AND VARIOUS VALUES OF A IN EQ. (112)
180-deg AMBIGUITY OF MEASURED POLARIZATION
A = 1.55
MEASURED
A = 0
A = 1.55
MEASURED
A = 0
POLARIZATION ANGLE, deg
315
270
225
180
135
90
45
0
-45
-10
-8
-6
-4
-2
0
2
4
6
8
10
12
14
OFFSET, solar radii
342
340
338
336
334
332
330
328
326
324
322
320
318
316
314
312
310
308
1968 DAY, GMT

Fig. 43 (contd)

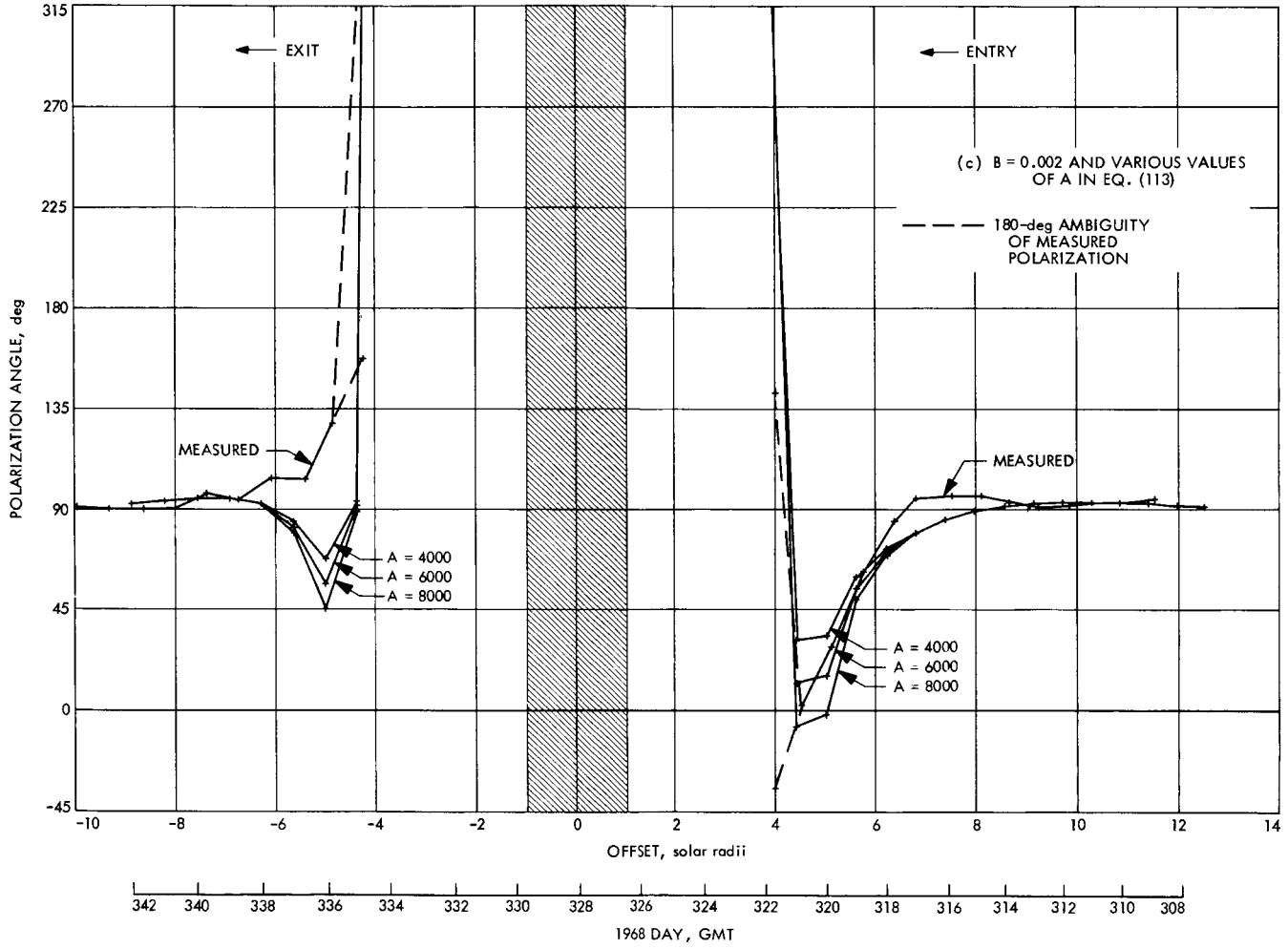
EXIT
ENTRY
(c) B = 0.002 AND VARIOUS VALUES OF A IN EQ. (113)
180-deg AMBIGUITY OF MEASURED POLARIZATION
MEASURED
MEASURED
A = 4000
A = 6000
A = 8000
A = 4000
A = 6000
A = 8000
POLARIZATION ANGLE, deg
315
270
225
180
135
90
45
0
-45
-10
-8
-6
-4
-2
0
2
4
6
8
10
12
14
OFFSET, solar radii
342
340
338
336
334
332
330
328
326
324
322
320
318
316
314
312
310
308
1968 DAY, GMT

Fig. 43 (contd)

Table 5. Comparison tabulation of electron densities in the solar corona

Distance from center of sun, units of solar radii	Log electron density, m^{-3}				
	Pottasch minimum (1960)	Van DeHulst maximum (1953)	Allen–Baumbach (Ref. 4)	Modified Allen–Baumbach [Eq. (3)]	From *Pioneer VI* Faraday rotation experiment [Eq. (113)]
1.0043	16.54	—	—	—	—
1.0144	15.40	—	—	—	—
1.043	14.56	14.45	14.44	—	—
1.072	14.21	14.32	14.30	—	—
1.1	14.00	14.20	14.18	—	—
1.2	13.59	13.85	13.83	—	—
1.3	13.33	13.58	13.56	—	—
1.4	13.14	13.36	13.34	—	—
1.5	12.97	13.17	13.15	—	—
1.6	12.79	13.00	12.97	—	—
1.7	12.63	12.84	12.81	—	—
1.8	12.48	12.70	12.66	—	—
1.9	12.36	12.57	12.52	—	—
2.0	12.25	12.45	12.38	—	—
2.5	11.81	11.92	11.80	11.90	—
3.0	11.52	11.50	11.33	11.51	—
4.0	11.09	10.95	10.58	11.00	11.77
5.0	10.80	10.65	9.99	10.70	10.84
6.0	10.58	10.46	9.52	10.49	10.19
10.0	10.10	—	8.19	10.00	9.31

arbitrary angle with respect to the propagation direction has been made and used in the Faraday rotation computer program. The difference between the Faraday rotation of a CW signal passing through the solar corona within 6 solar radii to the sun center is less than 10^{-6} deg which was computed using the "exact" solution or using the quasi-longitudinal approximation. The exact analysis may have other applications (e.g., in the earth's ionospheric studies or other planetary experiments).

A computer program was developed to compare the polarization of the CW signal as received and measured at the Goldstone Mars station with that transmitted perpendicular to the plane of the ecliptic.[9] The measured variation in the "apparent" polarization of the received signal as seen by the az–el antenna is on the order of 100 deg through an 8-h track because of the changing geometry between the station (horizon) and probe (plane of the ecliptic). This is an important effect, which is accounted for. This computer program has potential application to deep space communication systems using linearly polarized signals.

The receiving system polarimeter and associated instrumentation is described. The polarimeter is constructed integral to the RF "front-end" rather than at the "tail-end" to eliminate the effects of phase shift in the amplifiers. The system sensitivity is analyzed and excellent agreement with actual performance was obtained during operations. The 1σ standard deviation of the polarimeter angular measurement resolution (200-s data, away from the sun, −164 dBmW receiving signal strength) was about 0.4 deg. The performance is degraded when tracking near the sun, primarily because of the increased system temperature caused by the antenna sidelobes "seeing" the sun.

Polarization data were taken with the final polarimeter configuration from October 26 to December 10, 1968. Three significant transient "events" were seen on Novem-

[9]Stelzried, C. T., et al., "Received Signal Polarization Tracking Using a HA-DEC Antenna," in *Deep Space Network*, Space Programs Summary 37-62, Vol. II. Jet Propulsion Laboratory, Pasadena, Calif., Mar. 31, 1970.

ber 8, 12, and 16; both polarization change and spectral broadening occurred during these events. Identification with dekametric noise bursts infer a solar plasma velocity on the order of 0.5–1.5 km/s. In addition to the transient phenomenon, a steady-state Faraday rotation greater than 125 deg was measured between about 4 and 10 solar radii. These data are corrected for the earth's ionosphere effect. Theoretical electron densities and a Parker magnetic field model are inadequate to predict this rotation.

The main difficulty is the inadequacy of the Parker model to predict the magnetic field polarity. Magnetic field data from the Mount Wilson magnetograph and the *Explorer* 33 earth satellite magnetometer are used to provide a comparison with the measurements. Reasonable correlation is obtained using a modified Allen–Baumbach "quiet" sun electron density. Assuming twice this density or an "active" sun) does not appear to be appropriate. Some effort was made to further modify the electron density to obtain a better fit to the data.

The magnetic field data are apparently more reliable upon entry, as shown by the agreement between the Mount Wilson magnetograph and *Explorer* 33 magnetometer data. For this reason, the electron density was chosen to give the best fit in this region. A higher power in R was required to displace the curve toward the sun. The resulting equatorial electron density is given (in m^{-3}) by

$$N \simeq 10^{14}\left(\frac{6000}{R^{10}} + \frac{0.002}{R^2}\right), \qquad (4 < R < 12)$$

with R in solar radii.

B. Suggestions for Future Work

The success of this first attempt to measure the Faraday rotation of a CW signal passing through the solar corona indicates the value of observing any physical phenomenon in a "new" fashion. The transient polarization phenomena were completely unexpected. A complete understanding of these events (including the "fine" structure) should lead to a better understanding of the solar corona. The electron density in the space surrounding the sun is a function of both position and time. Least-squares techniques applied to steady-state polarization measurement data could provide a valuable tool for probing and monitoring the solar corona. This implies much more data over longer periods of time. This could probably best be accomplished with a spacecraft at 1 AU placed stationary with respect to the earth–sun line.

The present overall measurement system performance can be improved by providing more transmitted power from the spacecraft and increasing the sensitivity of the receiving system in the proximity of the sun. (This implies redesign of the RF feed system.) Decreasing the receiving system bandwidth is not very effective because of the spectral broadening of the signal traversing the solar corona. Similarly, decreasing the system operating noise temperature is of limited usefulness because of the dominant noise contribution of the sun. The 180-deg ambiguity in the polarization determinations near the sun can be removed by continuous tracking. This can be accomplished with a world-wide tracking network.

Appendix A

Stratified Layer Ray Tracing Computer Program Listing

This program (see Section II-B) computes the ray path of a signal traversing the solar corona. The analysis assumes a solar corona model with radial symmetry composed of uniform stratified layers. This program is written for the Univac 1108 computer.

```
1*    C     SUNBEND2 PROGRAM, CTS/38   (JPL PROG. I.D. 5930000)
2*    C       FOR C.STELZRIED, BY L.BUSCH, 05/69
3*    C
4*    C       FORTRAN V FOR UNIVAC 1108 (EXEC 8)
5*    C
6*          DIMENSION RHO(1850), RHOP(1850), THETA(1850), THETR(1850)
7*          DIMENSION ALPHAP(1850), ALPHRP(1850)
8*          DOUBLE PRECISION  Y, ARGR, PI, PIH, EX10, NOX, N, THETR, THETA, YA
9*          DOUBLE PRECISION  FPQ, ANGC, ALPHRP, ALPHAP, ARG, SALP, DIFRO, ROA
10*         DOUBLE PRECISION  THETF, DARSIN, THESL, RHO, RHOP, DRHO, RI, RIP
11*   C
12*         DATA PI  /3.14159265358979300/
13*         DATA PIH /1.57079632679489700/
14*         DATA EX10/2.30258509299404600/
15*   C
16*   C                 ASSUME N IS A FUNCTION OF RHO
17*         DEFINE NOX(R)=1.0D+14 * (1.55D0/R**6 + 1.0D-02/R**2)
18*         DEFINE FPQ(R)=8.97837D0*8.97837D0 * NOX(R)
19*         DEFINE N(R,F)=DSQRT(1.0D0-FPQ(R)/(F*1.0D+6)**2)
20*         DEFINE DARSIN(T)=DATAN(1.0D0/(DSQRT(1.0D0/(T*T)-1.0D0)))
21*   C               READ INPUT CONSTANTS
22*      10 READ(5,40,ERR=36,END=38) F,A,RO1,RN,DTHETA
23*         ANGC=180.D0/PI
24*   C               CALCULATE INITIAL CONDITIONS
25*         I=1
26*         RHO(I)=RO1
27*         THETR(I)=DARSIN(A/RHO(I))
28*         THETA(I)=ANGC * THETR(I)
29*         ALPHRP(I)=THETR(I)
30*         ALPHAP(I)=THETA(I)
31*         WRITE(6,50)
32*         WRITE(6,51) F, A, DTHETA
33*         WRITE(6,52)
34*         WRITE(6,53) I,THETA(I),RHO(I),ALPHAP(I)
35*         I=I+1
36*         THETA(I)=THETA(I-1)+DTHETA
37*         THETR(I)=THETA(I)/ANGC
38*         RHO(I)=A/DSIN(THETR(I))
39*         RHOP(I)=RHO(I)
40*   C               INCREMENT THETA
41*         NPR=0
42*         XPR=0.0
43*      20 I=I+1
44*         THETA(I)=THETA(I-1)+DTHETA
45*         THETR(I)=THETA(I)/ANGC
46*         ARGR=ALPHRP(I-2)+THETR(I-1)-THETR(I-2)
47*         ARG=DSIN(ARGR)
48*         RODEN=ALPHRP(I-2)+THETR(I)-THETR(I-2)
49*         IF(RODEN.GE.PI) GO TO 35
50*         RHOP(I)=RHO(I-1)*ARG/DSIN(ALPHRP(I-2)+THETR(I)-THETR(I-2))
51*         RI=.5D0 * (RHO(I-1)+RHO(I-2))
52*         RIP=.5D0* (RHOP(I)+RHO(I-1))
53*         SALP=N(RI,F)*ARG/N(RIP,F)
54*         IF(SALP.LE.1.0D0) GO TO 22
```

```
55*           WRITE(6,60) SALP
56*           ALPHRP(I-1)= PI-ARGR
57*           GO TO 25
58*        22 ALPHRP(I-1)=DARSIN(SALP)
59*        25 IF(ARGR.GE.PIH) ALPHRP(I-1)=PI-ALPHRP(I-1)
60*           RHO(I)=RHO(I-1)*SALP/DSIN(ALPHRP(I-1)+THETR(I)-THETR(I-1))
61*        30 ALPHAP(I-1)=ANGC*ALPHRP(I-1)
62*           DRHO=RHO(I-1)-RHOP(I-1)
63*           I1=I-1
64*           Y=RHO(I-1)*DSIN(THETR(I-1))
65*           YA=Y-A
66*           ROA=RHO(I-1) - A
67*           IF((I-NPR).NE.3) GO TO 31
68*           WRITE(6,55) I1,THETA(I-1),RHO(I-1),RHOP(I-1),DRHO,ALPHAP(I-1),
69*          *  YA,ROA
70*           XPR=XPR+2.0
71*           NPR=XPR*5.0
72*        31 DIFRO=RHO(I-1)-RHO(1)
73*           IF(DIFRO) 32,10,35
74*        32 IF((ALPHAP(I-1)+DTHETA).GT.180.D0) GO TO 35
75*           GO TO 20
76*        35 THETF=THETR(I-2)-ALPHRP(I-2)+PI-DARSIN(DSIN(ALPHRP(I-2))*
77*          *  RHO(I-2)/RN)
78*           THETF=ANGC*THETF
79*           THESL=180.0D0-DARSIN(A/RN)*ANGC
80*           WRITE(6,54) RN,THETF,THESL
81*           GO TO 10
82*        36 I=INSTAT(X)
83*           WRITE(6,65) X
84*        38 WRITE(6,50)
85*           STOP
86*     C
87*        40 FORMAT(5F10.0)
88*        50 FORMAT(1H1)
89*        51 FORMAT(1H0,8X,'FREQUENCY (MHZ) =',F10.3//9X,22HRAY OFFSET (SOLAR R
90*          *) = F9.3,17X,'(Y-A)=RHO(I)*SIN(PHI(I))-RAY OFFSET'//9X,
91*          * 'PHI INCREMENT (DEG.) =',F9.5,15X,'RHO(I)-A = RHO(I)-RAY OFFSET',
92*          * ///)
93*        52 FORMAT(1H0,8X'POLAR COORDINATES OF RAY PATH'//5X,'I',4X'PHI(I)',5X
94*          *,'RHO(I)',4X,7HRHO'(I),3X14HRHO(I)-RHO'(I),2X9HALPHA'(I),7X
95*          *  5H(Y-A),8X8HRHO(I)-A/ 10X5H(DEG),4X9H(SOLAR R),2X9H(SOLAR R),4X
96*          *  9H(SOLAR R),6X5H(DEG),23X9H(SOLAR R)//)
97*        53 FORMAT(1X,I5,2F11.5,26X,F11.5)
98*        54 FORMAT(//,6X,'R(N) =',F11.5,//6X,'PHI(N) =',F11.5,//6X,
99*          * 'PHI(STRAIGHT LINE) =',F11.5)
100*       55 FORMAT(1X,I5,3F11.5,E15.5,F11.5,E18.8,F12.5)
101*       60 FORMAT(/,2X,19HSIN(ALPHA'(I-1)) = ,E12.5)
102*       65 FORMAT(' ERROR = ', O12)
103*    C
104*          END
```

Appendix B

Integral Solution Ray Tracing Computer Program Listing

This program (see Section II-B) computes the ray path of a signal traversing the solar corona. The technique, from Bracewell (see Ref. 32), consists of evaluating the closest point of approach or "turning point" and evaluating an integral. This program is written for the Univac 1108 computer and uses a standard integration subroutine available for this computer.

```
1*   C     SUNBEND 3  (JPL PROGRAM I.D. 5968000)
2*   C     DRIVER FOR DOUBLE PRECISION INTEGRATION ROUTINE, DVDQ
3*   C     FOR C. STELZRIED, 7/69, L. BUSCH
4*   C
5*         DIMENSION TSTEP(100), DT(20,1), PHI(100), ROT(100)
6*         INTEGER   NEQ,KD,IFLAG,MXSTEP,KSTEP,KEMAX,KQ,JN,J,N,I
7*         REAL  EP,HMINA,HMAXA,EMAX
8*         DOUBLE PRECISION  R, Y, F, H, DELT, TFINAL, YN, FI, AI, PI, C, C1,
9*        *    TSTEP, ASQ, CTERM, DT, G, GT, FF, RN, DELTR, ROT, PHI, PHIMG
10*        DATA  PI,C,C1 /3.14159265358979300, 8.97837D0, 155.D0/
11*        DATA  NEQ,R,KD,EP,H,HMINA,HMAXA,DELT,TFINAL,MXSTEP / 1, 1.D8, 1,
12*       *    1.E-10, -1.D6, 1.E-10, 1.E6, -1.D8, 1.D8, 10000/
13*  C
14*        READ (5,104) FF,AI,RN,DELTR
15*        FI=FF*1.D6
16*        DELT=DELT+EP
17*        ASQ=AI*AI
18*        CTERM=((C*C)/(FI*FI))*1.D12
19*        I=1
20*        TSTEP(I)=0.D0
21*      5 I=I+1
22*        TSTEP(I)=TSTEP(I-1)+DELTR
23*        IF(TSTEP(I).LT.RN) GO TO 5
24*        TSTEP(I)=RN
25*        JN=I
26*        J=I+1
27*        N=J
28*        CALL DVDQ(NEQ,R,Y,F,KD,EP,IFLAG,H,HMINA,HMAXA,DELT,TFINAL,
29*       *    MXSTEP,KSTEP,KEMAX,EMAX,KQ,YN,DT)
30*        CALL DVDQG (1,1,G,GT)
31*     20 F= AI/(R*DSQRT(R*R-ASQ-CTERM*(C1/R**4+1.D0)))
32*     45 CALL DVDQ1
33*     50 GO TO (80,45,45,60,45,70,55,55,200,200,55,55), IFLAG
34*     55 HMINA=DABS(H)
35*     60 ROT(N)= R
36*        PHI(N)=(180.D0/PI) * Y
37*        J=J-1
38*        N=J
39*        IF(J.LT.1) N=1
40*        IF(IFLAG.GT.7) GO TO 210
41*        IF(IFLAG.NE.4) GO TO 45
42*        TFINAL=TSTEP(J)
43*        IF(J.EQ.0) TFINAL=0.D0
44*        GO TO 45
45*     70 EP=32.E0*EMAX*EP
46*        WRITE(6,103) R,EP
47*        GO TO 45
48*     80 F= AI/(R*DSQRT(G))
49*        GO TO 45
50*    200 G=R*R-ASQ-CTERM*(C1/R**4+1.D0)
51*        GO TO 45
52*  C
53*    210 PHI(1)= -1.D0 * PHI(1)
54*        WRITE(6,100) FF, PHI(1), AI, ROT(1), DELTR
55*        WRITE(6,101)
```

```
56*           DO 220 I=2,JN
57*           II = I-1
58*           PHI(I)= -1.D0 * PHI(I)
59*           PHIMG = 2.D0*PHI(1)-PHI(I)
60*       220 WRITE(6,102) II, ROT(I), PHI(I), PHIMG
61*           WRITE(6,105)
62*     C
63*       100 FORMAT(1H1,4X,'FREQUENCY (F),MHZ =',F11.5,10X,'PHI(A) =',F12.6//
64*      * 5X,'RAY OFFSET (A),SOLAR RADII =',F7.2,5X,'R(A) =',D20.12//5X,
65*      * 'R INCREMENT,SOLAR RADII =',F9.3//)
66*       101 FORMAT(1H0,4X,'I',8X,'R',10X,'PHI',8X,'IMAGE PHI'/9X'(SOLAR R)',6X
67*      *'(DEG)',9X,'(DEG)',/)
68*       102 FORMAT(1H ,I5,F11.2,2F14.5)
69*       103 FORMAT(1H ,5X,'R='1PD20.12,5X,'EP TOO SMALL, NEW VALUE OF EP =',
70*      * E13.6)
71*       104 FORMAT(4D20.5)
72*       105 FORMAT(1H1)
73*     C
74*           STOP
75*           END
```

Appendix C

Faraday Rotation Computer Program Listing

This program (see Sections II-C and VI) computes the Faraday rotation of a signal passing through a plasma in the presence of a static magnetic field. An "exact" solution (the usual quasi-longitudinal approximation for the magnetic field is not used) computes the Faraday rotation for uniform stratified sections. The signal polarization and ellipticity are computed for each step. The program is written for the Univac 1108 computer.

```
C     CTS/42 .. FARADAY ROTATION PREDICTION  (I.D. 5955000)
C         FOR C.STELZRIED, BY L.BUSCH, 04/69
C
C         FORTRAN V FOR UNIVAC 1108 (EXEC 8)
C
C          INPUT FORMAT ...
C     CARD
C       1  NDAYS,NEXACT,NSTEPS   (3I5)          NDAYS=NO.CARDS IN (DAY,A,
C                                                 RN,R1) INPUT TABLE
C                                               NEXACT (=1),COMPUTE EXACT1
C                                                      (=2),COMPUTE EXACT2
C                                               NSTEPS (BLANK),PRINT ALL
C                                                             STEPS
C                                                      (= 10),PRINT EVERY
C                                                             10TH STEP
C       2  DAY(J),A(J)           (2F10.0,20X,
C          RN(J),R1(J),            2F10.0)      DAY NO., RAY CLOSEST
C            J=1,NDAYS                          APPROACH, FINAL SUN-EARTH
C                                               DIST., INIT. SUN-PROBE DIST
C
C       3  NBP,NBM               (2I5)          SIZE OF T(0),B(0) TABLES
C
C             (IF ONLY THE THEORETICAL B CASE IS TO BE RUN,
C              USE BLANK CARD 3, AND OMIT CARDS 4 AND 5)
C
C       4  TUI(1,N),BUI(1,N),  (2F10.0)          T(0),B(0) TABLE FOR
C            N=1,NBP                              POSITIVE @A@ RUNS
C
C       5  TUI(1,N),BUI(1,N),  (2F10.0)          T(0),B(0) TABLE FOR
C            N=1,NBM                              NEGATIVE @A@ RUNS
C
C       6  NCASE                 (I5)            1, THEORETICAL B CASE
C           (1,2,3,OR 4)                         2, MEAS.B,RADIAL FIELD ONLY
C                                                3, MEAS.B,AZIM. FIELD ONLY
C                                                4, MEAS.B.RADIAL AND THEO.
C                                                     AZIMUTHAL FIELD
C
C       7  BOT                   (F10.0)         B(0) FOR THEOR. B CASE
C
C             (OMIT CARD 7 IF NCASE = 2, 3, OR 4)
C
C       8  TITLE                 (13A6)          DATA IDENTIFICATION
C                                                  (INDICATE THEOR. OR
C                                                   MEAS. B TYPE)
C
C       9  DTHETA,F,L            (F10.0,         THETA INCREMENT (DEG.),
C                                  2E15.7)         FREQUENCY (HERTZ),LENGTH
C                                                  SCALE FACTOR
C
C             (REPEAT INPUT FROM CARD 6 FOR MORE THAN 1 @NCASE@)
C
```

```
      DIMENSION DAY(200),A(200),RN(200),R1(200),TOI(2,1000),BOI(2,1000)
     *  ,R(2000),THETR(2000),THETA(2000),OMEGA(2000),OMEGAE(2000),
     *  TITLE(13),AI(2000),BI(2000),CI(2000),DI(2000)
      DOUBLE PRECISION OINC,PI,DARSIN,ANGC,BO,K,THETR,THETA,RB,TARG,
     *  SARG,COARG,BL,BT,S,R,N,DELS,DELO,OMEGA,  X,YT,YL,G,H,RPP,BRP,RP,
     *  AP,APP,BBP,BBPP,OMEGAE,SNP,SNPP,KMINUS,KPLUS,DR1,  SINKP,COSKP,
     *  SINKM,COSKM,AI,BI,CI,DI,EXTERM,EX,ETTERM,ETHE,NTERM,DTERM,ERROR
      DOUBLE PRECISION YLGQ,GYLQ,XCO1,XCO2,LOSS,EPLQ,EMIQ,RATIO,TER1,
     * TER2,DS,OMEGCK
      DOUBLE PRECISION  YLG4, GYL4
      COMMON    DTHETA, AABS, RB, ANGC, WV
      REAL  L
      DATA  WV /.00464/
      DATA  PI /3.141592653589793D0/
      DATA  QP,QT /135.4816, 1.896205E+08/
C                   DOUBLE PRECISION ARCSIN
      DEFINE DARSIN(T)=DATAN(1.D0/(DSQRT(1.0D0/(T*T)-1.0D0)))
C                   RADIAN/ANGLE CONVERSION FACTOR
      ANGC=180.0D0/PI
C           PUNCH LABEL FOR PUNCHED CARD OUTPUT
      PUNCH 121
C               INPUT FOR ALL CASES
    5 READ(5,109) NDAYS,NEXACT,NSTEPS
      READ(5,101) (DAY(J),A(J),RN(J),R1(J), J=1,NDAYS)
      READ(5,109) NBP, NBM
C               INPUT FOR MEASURED B CASES ONLY
      IF (NBP.LT.1) GO TO 6
C               READ TABLE FOR POSITIVE @A@
      READ(5,100)(TOI(1,M),BOI(1,M),M=1,NBP)
C               READ TABLE FOR NEGATIVE @A@
      READ(5,100)(TOI(2,M),BOI(2,M),M=1,NBM)
C               READ @NCASE@ AND PROCEED ACCORDINGLY
    6 READ(5,109,ERR=80,END=85) NCASE
      IF (NCASE.GT.1) GO TO 10
      READ(5,100) BOT
      BO=BOT
   10 READ(5,99) TITLE
      READ(5,110) DTHETA,F,L
      K=(2.D0*PI*F*L)/2.99793D+08
C
      DO 70 J=1,NDAYS
      AABS=ABS(A(J))
C                   ESTABLISH THETA LIMIT
      THETAN=180.0D0-DARSIN(AABS/RN(J))*ANGC
C                   CALCULATE INITIAL CONDITIONS
      I=1
      R(1)=R1(J)
      THETR(I)=DARSIN(AABS/R(1))
      THETA(I)=ANGC*THETR(I)
      RB=R(1)
      TARG=THETA(I)-DTHETA/2.0D0
      SARG=DSIN(TARG/ANGC)
      COARG=DCOS(TARG/ANGC)
      IF(NCASE.EQ.1) GO TO 25
      CALL BMEAS (TOI,BOI,NBP,NBM,THETA(I),DAY(J),A(J),NCASE,BL,BT,BO)
      GO TO 26
   25 BL=(BO/RB**2)*ABS(COARG)
      BT=(BO/RB**2)*SARG
   26 N=1.0D+14 * (1.00D+03/RB**8 +0.02D-01/RB**2)
   28 S=0.D0
      AI(I)=1.D0
      BI(I)=0.D0
      CI(I)=0.D0
      DI(I)=0.D0
      OMEGA(I)=90.0D0
      OMEGAE(I)=90.0D0
```

```
      WRITE(6,102) TITLE
      WRITE(6,103) DAY(J),A(J),R1(J),DTHETA,L,RN(J)
   29 WRITE(6,112)
   31 WRITE(6,113) I,THETA(I),R(I),N,BT,BL,OMEGA(I),OMEGAE(I)
C                    INCREMENT THETA
   32 LIMT=0
      NPR=0
      XPR=0.0
   30 I=I+1
      THETA(I)=THETA(I-1)+DTHETA
      IF(THETA(I).LT.THETAN) GO TO 40
      LIMT=1
      THETA(I)=THETAN
   40 THETR(I)=THETA(I)/ANGC
      R(I)=AABS/DSIN(THETR(I))
      TARG=THETA(I)-DTHETA/2.0D0
      SARG=DSIN(TARG/ANGC)
      COARG=DCOS(TARG/ANGC)
      RB=0.5D0*(R(I)+R(I-1))
      IF(NCASE.EQ.1) GO TO 43
      CALL BMEAS (TOI,BOI,NBP,NBM,THETA(I),DAY(J),A(J),NCASE,BL,BT,BO)
      GO TO 44
   43 BL=(BO/RB**2)*ABS(COARG)
      BT=(BO/RB**2)*SARG
   44 N=1.0D+14 * (1.00D+03/RB**8 +0.02D-01/RB**2)
      DELS=AABS*DSIN(DTHETA/ANGC)/(DSIN(THETR(I))*DSIN(THETR(I-1)))
      DELO=L*QP*DELS*BL*N/F**2
      S=S+DELS
      OMEGA(I)=OMEGA(I-1)+DELO
      X=(8.97837D0*8.97837D0*N)/F**2
      YL=(2.799202D+6*BL)/F
      YT=(2.799202D+6*BT)/F
C
C
      G=YT**2/(2.D0*(1.D0-X))
      YLGQ=YL/G*YL/G
      GYLQ=G/YL*G/YL
      YLG4=YLGQ*YLGQ
      GYL4=GYLQ*GYLQ
      IF(ABS(G/YL).LT.1.0D-3) GO TO 34
      IF(ABS(YL/G).LT.1.0D-3) GO TO 35
      GO TO 38
   34 H=YL*(1.D0+0.5D0*GYLQ-GYL4/8.D0)
      BRP=G/YL-1.D0-0.5D0*GYLQ+GYL4/8.D0
      NCYL=1
      GO TO 36
   35 H=G*(1.D0+0.5D0*YLGQ-YLG4/8.D0)
      BRP=-0.5D0*YLGQ + YLG4/8.D0
      NCYL=3
      GO TO 36
   38 H=DSQRT(YL**2+G**2)
      BRP=(G-H)/YL
      NCYL=2
   36 RP=G-H
      RPP=G+H
      XC01=X/(1.D0-RP)
      SNP=DSQRT(1.D0-XC01)
      IF(XC01.LT.1.D-6) SNP=1.D0-0.5D0*XC01-XC01*XC01/8.D0-XC01*XC01*
     *  XC01/16.D0
   37 XC02=X/(1.D0-RPP)
      SNPP=DSQRT(1.D0-XC02)
      IF(XC02.LT.1.D-6) SNPP=1.D0-0.5D0*XC02-XC02*XC02/8.D0-XC02*XC02*
     *  XC02/16.D0
      KMINUS=(-K*DELS*H*X)/((1.D0-YL*YL-2.D0*G)*(SNP+SNPP))
      KPLUS= K*DELS*(SNP+SNPP)/ 2.0D0
```

```
C                    GO TO 41 FOR EXACT 1, TO 42 FOR EXACT 2
      GO TO (41,42), NEXACT
   41 DR1=BRP*BRP + 1.D0
      AP = (BRP*AI(I-1)+DI(I-1))/DR1
      BBP = (BRP*BI(I-1)-CI(I-1))/DR1
      APP = (-BRP*DI(I-1)+AI(I-1))/DR1
      BBPP = (BRP*CI(I-1)+BI(I-1))/DR1
      SINKP=DSIN(KPLUS)
      COSKP=DCOS(KPLUS)
      SINKM=DSIN(KMINUS)
      COSKM=DCOS(KMINUS)
      AI(I)=COSKM*(-(BRP*BBP+BBPP)*SINKP + (BRP*AP+APP)*COSKP) + SINKM*
     * ((BRP*BBP-BBPP)*COSKP + (BRP*AP-APP)*SINKP)
      BI(I)=COSKM*( (BRP* AP+ APP)*SINKP + (BRP*BBP+BBPP)*COSKP)+ SINKM*
     * (-(BRP*AP-APP) *COSKP + (BRP*BBP-BBPP)*SINKP)
      CI(I)=COSKM*((BRP*APP-AP)*SINKP + (BRP*BBPP-BBP)*COSKP) + SINKM*
     * ((BRP*APP+AP) *COSKP - (BRP*BBPP+BBP)*SINKP)
      DI(I)=COSKM*((BRP*BBPP-BBP)*SINKP - (BRP*APP-AP)*COSKP) + SINKM*
     * ((BRP*BBPP+BBP)*COSKP + (BRP*APP+AP)*SINKP)
   42 CONTINUE
      EXTERM=AI(I)*AI(I)+BI(I)*BI(I)
      EX=0.D0
      IF(EXTERM.GT.0.D0) EX=DSQRT(EXTERM)
      ETTERM=CI(I)*CI(I)+DI(I)*DI(I)
      ETHE=0.D0
      IF(ETTERM.GT.0.D0) ETHE=DSQRT(ETTERM)
      NTERM=2.D0*(BI(I)*DI(I)+AI(I)*CI(I))
      DTERM=AI(I)*AI(I)+BI(I)*BI(I)-CI(I)*CI(I)-DI(I)*DI(I)
      OMEGAE(I)=0.D0
      IF(NTERM.NE.0.D0.AND.DTERM.NE.0.D0) OMEGAE(I)=90.D0+0.5*DATAN2(NTE
     *RM,DTERM)*ANGC
      DO 444 IC=1,3601,90
      DINC=IC-1
      DS= -1.D0
      DO 444 JC=1,2
      DINC=DINC*DS*-1.D0
      DS=DABS(DS)
      OMEGCK=OMEGAE(I)+DINC
      IF(DABS(OMEGCK-OMEGAE(I-1)).LT.4.4D1)GO TO 445
  444 CONTINUE
      WRITE(6,116) OMEGCK
      WRITE(6,117) NTERM,DTERM,OMEGAE(I)
  117 FORMAT(1H0,2X,@NTERM = @,E13.6,2X,@DTERM = @,E13.6,2X,@ OMEGAE(I)
     *= @,E13.6)
      OMEGAE(I)=0.D0
  445 OMEGAE(I)=OMEGCK
      ERROR=OMEGAE(I)-OMEGA(I)
      TER1=AI(I)*AI(I)+BI(I)*BI(I)+CI(I)*CI(I)+DI(I)*DI(I)
      TER2=DSQRT(ABS((AI(I)*AI(I)+CI(I)*CI(I)-BI(I)*BI(I)-DI(I)*DI(I))
     **2+4.D0*(AI(I)*BI(I)+CI(I)*DI(I))**2))
      EPLQ=0.5D0*(TER1+TER2)
      EMIQ=0.5D0*(TER1-TER2)
      LOSS=-20.D0*DLOG10(EPLQ)
      RATIO=EMIQ/EPLQ
      IF(NSTEPS.NE.10) GO TO 50
   47 IF(LIMT.EQ.1) GO TO 50
      IF((I-NPR).NE.2) GO TO 60
   50 WRITE(6,114) I,THETA(I),R(I),N,BT,BL,    DELO,OMEGA(I),EX,ETHE,
     *    OMEGAE(I),ERROR,LOSS,RATIO,NCYL
   55 XPR=XPR+2.0
      NPR=XPR*5.0
   60 IF(LIMT.LT.1) GO TO 30
      WRITE(6,115) OMEGA(I),OMEGAE(I),ERROR,LOSS,AI(I),BI(I),CI(I),
     * DI(I),EX,ETHE
      PUNCH 120, A(J),OMEGAE(I),DAY(J)
   70 CONTINUE
      GO TO 6
```

```
   80 I=INSTAT(X)
      WRITE(6,82) X
   82 FORMAT(@ ERROR =@,012)
   85 WRITE(6,86)
   86 FORMAT(1H1)
      STOP
C
   99 FORMAT(13A6)
  100 FORMAT(2F10.0)
  101 FORMAT(2F10.0,20X,2F10.0)
  102 FORMAT(1H1,8X,13A6,// )
  103 FORMAT(9X,5HDAY =,F11.6,4X,3HA =,F11.6,4X,6HR(L) =,F11.6,//9X,
     *@DPHI =@,F10.5,4X,3HL =,E12.5,3X,4HRN =,F13.6,//)
  109 FORMAT(3I5)
  110 FORMAT(F10.0,2E15.7)
  112 FORMAT(5X@I  PHI(I)   R(I)       N(I)      BT(I)      BL(I)     DO(I)
     *   O(I)    EX(I)   ET(I)     OE(I)   ERR(I)  LOSS(I) RATIO     YL@
     * /)
  113 FORMAT(1H ,I5,2F8.3,1P3E10.3,8X,1PE9.2,16X,1PEl1.4)
  114 FORMAT(1H ,I5,2F8.3,1P3E10.3,1PE8.1,1PE9.2,1P2E8.1,1PE11.4,1P3E8.1
     *,I5)
  115 FORMAT(//9X,@OMEGA =@,1PE13.6,@ DEG.@,4X,@OMEGA(E) =@,1PE13.6,@ DE
     *G.@,4X,@ERROR =@,1PE13.6,@ DEG.@,4X,@LOSS =@,1PE13.6,@ DB@,
     *         //9X@A =@,1PE14.6,4X,@B =@,E18.6,4X@C =@,E16.6,4X,@D =@,
     * E16.6//9X@EX =@,1PE13.6,4X,@ETHETA =@,E13.6)
  116 FORMAT(1HO,5X,@AFTER ALL INCREMENTS OMEGAE(I) =@,1PE8.1)
  120 FORMAT(3F10.4)
  121 FORMAT(@RETURN CARDS TO  LBB   BLDG 125, BOX 43@)
C
      END
      SUBROUTINE BMEAS(TOI,BOI,NBP,NBM,THET,DAY,A,NCASE,BL,BT,BO)
C         CALCULATE BL(I) AND BT(I) FOR MEASURED B CASES
      DIMENSION TOI(2,2), BOI(2,2)
      DOUBLE PRECISION  BO, BLR, BTR, BLA, BTA
      DOUBLE PRECISION  THET, BL, BT, TERM,RB,ANGC
      COMMON    DTHETA, AABS, RB, ANGC, WV
C
      DT=(-A/AABS)*13.6265*(1.0-(THET-DTHETA/2.0)/180.)
      T= DAY+DT
      IF(A) 6,8,8
    6 I=2
      NN=NBM
      GO TO 10
    8 I=1
      NN=NBP
   10 DO 15 N=2,NN
      IF(T.GT.TOI(I,N-1) .AND. T.LT.TOI(I,N)) GO TO 12
      GO TO 15
   12 B1=BOI(I,N-1)
      B2=BOI(I,N)
      T1=TOI(I,N-1)
      T2=TOI(I,N)
      GO TO 20
   15 CONTINUE
C         IF T(I) NOT IN INPUT TABLE RANGE, SET B1,B2,T1,T2 =0.0
      B1=0.0
      B2=0.0
      T1=0.0
      T2=0.0
   20 BO=B1+(T-T1)*(B2-B1)/(T2-T1)
      TERM=THET/ANGC - (DTHETA/2.0)/ANGC
      BLR=(-BO/RB**2)*DCOS(TERM)
      BTR=(BO/RB**2)*DSIN(TERM)
      BLA=(A/AABS)*(BO/RB)*WV*DSIN(TERM)
      BTA=(A/AABS)*(BO/RB)*WV*DCOS(TERM)
      GO TO (55,30,35,40), NCASE
```

```
30 BL=BLR
   BT=BTR
   GO TO 50
35 BL=BLA
   BT=BTA
   GO TO 50
40 BL=BLR+BLA
   BT=BTR+BTA
50 RETURN
55 WRITE(6,60)
60 FORMAT(1HO,5X,@NCASE=1, SHOULD NOT HAVE ENTERED BMEAS SUBROUTINE@)
   STOP
   END
```

Appendix D

Signal Polarization Coordinate Transformation Computer Program Listing

This program (see Sections III-D and V) performs a coordinate transformation of the received signal polarization as measured at the local station to the plane of the ecliptic. This is accomplished through a sequence of matrix manipulations. This program is written for the IBM 7094 computer.

```
$IBFTC POLEAS
      COMMON /DRDATA/ DECS(105,4),RAS(105,4)
      DOUBLE PRECISION CX,CY,CZ,U,AZ,EL,LAT,LONG,ZER,D2R,R2D,C1,C2,C3,
     *    C4,C5,EPS,DUM,FAT,FONG,CP,CT,SP,ST,PH,THET,S1,S2,S3,DOT1,DOT2,
     *    FDAYS,TAUT,OBLQ,ONE,BAT,BONG,SNEL,RA,DEC,FLHA,PIO2,PRED,P2,
     *    DNSEC
      DIMENSION B1(100),B2(100)
      DIMENSION U(3),DR1(2),DR2(2),FT(2),POL(5000),DAYNO(5000),
     *    TITLE(14),XNAME(14),YNAM1(10),RW11(2,8),YNAM2(10),
     *    RW12(2,8),ROW2(8),MDAYS(12)
      DIMENSION BUF(250),FMT(12),FMS(12)
      DIMENSION TMP(250)
      DIMENSION XY(5000,2),JX(3),JY(3),NP(3),INTRP(3),SYMBL(3)
      DIMENSION NPASS(3),IPASS(3),KTMP(4)
      DIMENSION PTIT(14,4)
      EQUIVALENCE(DAYNO(1),XY(1,1)),(POL(1),XY(1,2)),(CAL(1),XY(1,3))
      EQUIVALENCE (TMP(1),IT),(TMP(2),ITIME),(TMP(3),P)
      EQUIVALENCE (DEC1,DR1(1)),(DEC2,DR1(2)),(RA1,DR2(1)),(RA2,DR2(2)),
     *           (FNS1,FT(1)),(FNS2,FT(2))
      DATA SYMBL(1)/6H*     /
      DATA (MDAYS(I),I=1,12),I100 /0,31,60,91,121,152,182,213,244,274,
     * 305,335,100/
      DATA ZER,D2R,R2D,BAT,BONG,EPS,ONE,C1,C2,C3,C4,C5,PIO2,NR
     *    /0.0D0,1.7453292519943D-2,57.2957795131,35.426D0,243.111D0,
     *    23.45D0,1.0D0,100.07554260D0,9.85647346D-1,2.9015D-13,
     *    4.17807417D-3,5.21D-13,3.141592653589793,2/
      DATA COMP,FINPT     /6HCOMPTD,6HINPUT /
      DATA BLNK/6H      /,KSTOP/4HSTOP/,KEOF/4HEOF /
      DATA XNAME(1) /42H                                          DAY NU/
      DATA XNAME(8) /42HMBER                                           /
      DATA YNAM1(1) /30H                        MEAS SC /
      DATA YNAM1(6) /30HPOL                             /
      DATA RW11(1,1)/12HAVE DAY NO. /
      DATA RW11(1,2)/12HAVE SC POL. /
      DATA PTIT(1,1)/80H          PN-06 SIGNAL POLARIZATION - LEAST SQUA
     *RES DATA                          /
      DATA PTIT(1,2)/80H          PN-07 SIGNAL POLARIZATION - LEAST SQUA
     *RES DATA                          /
      DATA PTIT(1,3)/80H          PN-08 SIGNAL POLARIZATION - LEAST SQUA
     *RES DATA                          /
      DATA PTIT(1,4)/80H          PN-09 SIGNAL POLARIZATION - LEAST SQUA
     *RES DATA                          /
      MAXREC=5000
      NSIZ=7
      REWIND 12
      IFLAG=0
      PRED=90.0
      IYEAR=68
      FAT =D2R*BAT
      FONG=D2R*BONG
      IT1=0
      IT2=2400
      ASG=3.
      NNP=100
      FNS1  =     0.0
```

```
      FNS2  =    86400.0
      READ(5,1042) IPLOT,IPUNCH,NPAV
 1042 FORMAT(10I5)
      IF(NPAV.GT.NNP)GO TO 106
      NSC=0
      TIMLST=-1.
      JKL=0
  444 CONTINUE
      NNSC=NSC
      READ(12)NPASS,IDAYNO,KYR,KPNTS,NSC
      IF(NPASS(1).EQ.KSTOP.OR.NPASS(1).EQ.KEOF) GO TO 90
      NSC=NSC-5
      IF(NNSC.EQ.0)GO TO 445
      IF(NSC.NE.NNSC)GO TO 943
  445 CONTINUE
      J1=JKL+1
      J2=JKL+KPNTS
      IF(J2.GT.MAXREC)GO TO 52
      READ(12) (DAYNO(J),POL(J),J=J1,J2)
      KPNT=0
      IF(NNSC.NE.0)GO TO 333
      DO 443 I=1,14
  443 TITLE(I)=PTIT(I,NSC)
      PUNCH 1040, TITLE
 1040 FORMAT(13A6,A2)
      AV1 = 0.0
      AV2 = 0.0
      AV3=0.0
       DUM = ZER
      LINES=0
      W = FINPT
      ITMP  = (IYEAR-  50)
      IDAYS = 365 * ITMP + (ITMP+1)/4
      IDAYS=IDAYS+IDAYNO-1
       FDDAYS = FLOAT(IDAYS)
       FDAYS  = FDDAYS
      KDY=IDAYNO-262
      DEC1=DECS(KDY,NSC)
      DEC2=DECS(KDY+1,NSC)
      RA1=RAS(KDY,NSC)
      RA2=RAS(KDY+1,NSC)
      IDT=IDAYNO
      WRITE(6,1000) TITLE,IDT,DEC1,RA1,IT1,DEC2,RA2,IT2
 1000 FORMAT(1H1,26X,13A6,A2 ///
     *       54X,10HDAY NUMBER I4//
     *        39X,5HDEC1 F8.3,4X,4HRA1 F8.3,4X,5HTIME  I6/
     *        39X,5HDEC2 F8.3,4X,4HRA2 F8.3,4X,5HTIME  I6//)
       IF(IFLAG .EQ. 0) W=COMP
       WRITE(6,1001)W
 1001 FORMAT(4X,4HDATE,5X,4HTIME,7X,2HAZ,8X,2HEL,8X,3HDEC,7X,2HRA,
     *        5X,8HPOL READ,2X,8HPOL READ,2X,9HPRED-READ,2X,6HHE POL,
     *        3X,7HMEAS SC,3X,11H90-MEAS POL   /
     *        2X,7HDAY NO.,5X,3HGMT,7X,3HDEG,7X,3HDEG,7X,3HDEG,7X,3HDEG,
     *        7X,3HDEG,6X,4HPRED,7X,3HDEG,7X,3HDEG,7X,3HPOL,9X,3HDEG    /
     *        32X,A6,3X,A6,24X,3HDEG,28X,3HDEG/10X,A6                  /)
       IAV=0
       PAV1=0.0
       PAV2=0.0
       IDS=1
  333 CONTINUE
C
C      INPUT POLARIZATION DATA
C
      TSYM=BLNK
   14 CONTINUE
      KPNT=KPNT+1
      IF(KPNT.GT.KPNTS) GO TO 17
```

```
      TIME=DAYNO(JKL+1)
      P=POL(JKL+1)
   62 IF(TIME .GE. TIMLST) GO TO 19
      IF((TIMLST-TIME) .LT. 23.0) GO TO 66
      IDAYNO=IDAYNO+1
      DO 1022 IJ=1,2
      KDYIIJ=KDY+IJ
      DR1(IJ)=DECS(KDYIIJ,NSC)
 1022 DR2(IJ)=RAS(KDYIIJ,NSC)
   19 TIMLST=TIME
      GO TO 18
   66 TSYM=SYMBL(1)
      GO TO 18
   17 CONTINUE
      TIME=-1.0
   18 CONTINUE
      P2=P
      IF( TIME)444,20,20
   20 CONTINUE
C
C
C     COMPUTE GAMMA(T)
C
      FNSEC=3600.0 * TIME
      JKL=JKL+1
      DAYNO(JKL)=FLOAT(IDAYNO)+FNSEC/86400.0
      AV2 = AV2 + DAYNO(JKL)
      DNSEC=FNSEC
      TAUT=D2R*(C1+C2*FDAYS+C3*FDAYS*FDAYS+DNSEC*C4/(ONE+C5*FDAYS))
      P1 =FINTRP(FNSEC,FT,DR1)
      DEC=P1
      DEC= D2R*DEC
      P1=FINTRP(FNSEC,FT,DR2)
      RA=P1
      RA=D2R*RA
      IF(IFLAG.NE. 0) GO TO 25
C
C     COMPUTE AZ,EL
C
      S1 = D2R * (360.0D0 -BONG)
      FLHA=(TAUT-RA-S1) *R2D
      FLHA=FMOD(FLHA)
      FLHA=D2R*FLHA
      S3 = DSIN(FLHA)
      S2 = DSIN(DEC)
      DUM = DCOS(DEC)
      SP = DSIN(FAT)
      CP = DCOS(FAT)
      SNEL = SP*S2 + CP*DUM*DCOS(FLHA)
      P1 = SNEL
      P1 = ARSIN(P1)
      EL = P1
      DUM = DCOS(EL)
      AZ =(S2-SP*SNEL)/(CP*DUM)
      P1=AZ
      P1=ARCOS(P1)
      AZ=P1
      AZ = R2D*AZ
      AZ=FMOD(AZ)
      EL = R2D*EL
      IF(EL .GE. -90.0D0 .OR. EL      .LE. 90.0D0) GO TO 24
      EL=FMOD(EL)
      IF(EL .GT. 270.0D0) GO TO 23
      EL=180.0D0-EL
      GO TO 24
   23 EL=EL-360.0D0
   24 CONTINUE
```

```
      IF(FLHA .GE. PID2) GO TO 25
      AZ = 360.0D0 - AZ
C
C     COMPUTE POLARIZATION
C
   25 CONTINUE
      OBLQ  =  D2R * EPS
      CALL TRIG(OBLQ,TAUT,S1,S2,S3,DUM)
      CALL TRIG(FAT,FONG,CP,CT,SP,ST)
      CX = -( SP*CT*DUM*S3 + SP*ST*S2*S3 + CP*S1 )
      CY = ST*DUM*S3 - CT*S2*S3
      CZ = -CP*CT*DUM*S3 -CP*ST*S2*S3 + SP*S1
      PH=D2R*EL
      THET=D2R*AZ
      CALL TRIG(PH,THET,CP,CT,SP,ST)
      U(1) = CY * SP - CZ * CP * ST
      U(2) = -CZ * CP * CT - CX * SP
      U(3) =  CX * CP * ST + CY * CP * CT
      CALL DOT(U,U,DOT1)
      DUM = DCOS(PH) * DSQRT(DOT1)
      DOT2 = -U(3) / DUM
      P1 = DOT2
      P1 = ARSIN(P1)
      DUM  = P1
      DUM  = R2D * DUM
      S2 =FMOD(DUM)
      POL(JKL)=FMOD(P2-S2)
      AV1 = AV1 + POL(JKL)
      S1=PRED+S2
      S1=FMOD(S1)
      AV3=AV3+S1
      DEC = R2D*DEC
      RA=R2D*RA
      DUM=S1-P2
      S3=DUM
      IF(ABS(S3) .LT. 180.0D0) GO TO 40
      IF(S3 .GE. ZER) GO TO 30
      S3=S3+360.0D0
      GO TO 40
   30 CONTINUE
      S3=S3-360.0D0
   40 CONTINUE
      DUM=S3
      P1=90.0D0-POL(JKL)
      WRITE(6,1005)DAYNO(JKL),TSYM,TIME,AZ,EL,DEC,RA,P,S1,DUM,S2,
     *             POL(JKL),P1
 1005 FORMAT(1X,F9.5,A1,F8.4,10F10.3/)
      LINES=LINES+1
      IF(LINES .LT. 47) GO TO 332
      LINES=0
      WRITE(6,1000)TITLE,IDT,DEC1,RA1,IT1,DEC2,RA2,IT2
      WRITE(6,1001)
  332 CONTINUE
      IF(NPAV.EQ.0)GO TO 335
      IAV=IAV+1
      PAV1=PAV1+DAYNO(JKL)
      PAV2=PAV2+POL(JKL)
      IF(IAV.LT.NPAV) GO TO 333
      CALL STAT(IAV,DAYNO(IDS),PAV1,PSG1)
      CALL STAT(IAV,POL(IDS),PAV2,PSG2)
      KAV=0
      PAV3=0.0
      PAV4=0.0
      DO 1070 I=1,IAV
      IDP=IDS+I-1
      IF(ABS( POL( IDP)-PAV2)    .GT. ASG*PSG2) GO TO 1070
      KAV=KAV+1
```

```
      B1(KAV)=DAYNO(IDP)
      B2(KAV)=POL(IDP)
      PAV3=PAV3+B1(KAV)
      PAV4=PAV4+B2(KAV)
 1070 CONTINUE
      IF(KAV.EQ.IAV) GO TO 1113
      CALL STAT(KAV,B1,PAV3,PSG3)
      CALL STAT(KAV,B2,PAV4,PSG4)
      GO TO 1114
 1113 CONTINUE
      PAV3=PAV1
      PAV4=PAV2
      PSG3=PSG1
      PSG4=PSG2
 1114 CONTINUE
      WRITE(6,1111)KAV,PAV3,PAV4,PSG4,PAV1,PAV2,PSG2
 1111 FORMAT(I5,8F12.5)
      PUNCH 1117, PAV3,PAV4,PSG4,PAV1,PAV2,PSG2,KAV
 1117 FORMAT(6F10.5,I10)
      IAV=0
      PAV1=0.0
      PAV2=0.0
      IDS=JKL+1
      GO TO 333
  335 CONTINUE
      IF(IPUNCH .EQ. 1 .OR. IPUNCH .EQ. 3) GO TO 333
      PUNCH 1006,DAYNO(JKL),POL(JKL)
 1006 FORMAT(2F10.5)
   99 GO TO 333
C
C     COMPUTE AVE DAY NO , AVE POLARIZATION
C
   90 CONTINUE
      IF(JKL .LT. 2) GO TO 447
      CALL STAT(JKL,DAYNO,AV2,SIG1)
      CALL STAT(JKL,POL,AV1,SIG2)
      WRITE(6,1010)AV2,SIG1,AV1,SIG2
 1010 FORMAT(1HO,   19HAVE DAY NO,STD DEV 73X,
     * 20HAVE MEAS POL,STD DEV/
     *F11.3,1H,F9.5,76X,              F12.3,1H,F9.5)
      IF(IPUNCH .EQ. 2 .OR. IPUNCH .EQ. 3) GO TO 82
      PUNCH 1030,AV2,AV1,AV3
 1030 FORMAT(3F10.3)
   82 IF(IPLOT .EQ. 0) GO TO 447
      IF(JKL .LT. 4) GO TO 447
      ROW2(1) = AV2
      ROW2(2) = AV1
      NP(1)=JKL
      INTRP(1)=0
      JX(1)=1
      JY(1)=2
      KC=1
      CALL KCPL(XY,MAXREC,KC,JX,JY,NP,INTRP,SYMBL,TITLE,XNAME,YNAM1,
     *    RW11,ROW2,NR)
  447 WRITE(6,525)
  525 FORMAT(18H1JOB COMPLETE          )
      STOP
  943 CONTINUE
      WRITE(6,448)
  448 FORMAT(30HO SPACECRAFT NOT THE SAME       )
      GO TO 90
   52 WRITE(6,520)
```

```
  520 FORMAT( 66HOTHE MAXIMUM ALLOWABLE NUMBER OF DATA POINTS HAS BEEN E
     *XCEEDED        )
       STOP
  106 WRITE(6,1060)NNP
 1060 FORMAT(44H1NUMBER OF POINTS IN RUNNING AVERAGE EXCEEDS  I5)
       STOP
       END
$IBFTC DCRA
       BLOCK DATA
C    TRAJECTORY DATA STARTS WITH SEPT. 19,1969
       COMMON /DRDATA/ DECS(105,4),RAS(105,4)
       DATA (DECS(I,1),RAS(I,1),I=001,012)/
      *  4.7127,168.8401, 4.3011,169.8113, 3.8875,170.7835,
      *  3.4718,171.7568, 3.0543,172.7312, 2.6351,173.7069,
      *  2.2142,174.6840, 1.7918,175.6625, 1.3681,176.6427,
      *  0.9430,177.6245, 0.5168,178.6081, 0.0896,179.5937/
       DATA (DECS(I,1),RAS(I,1),I=013,060)/
      *      -0.3386, 180.5812,  -0.7675, 181.5709,  -1.1970, 182.5629,
      *      -1.6271, 183.5572,  -2.0576, 184.5540,  -2.4884, 185.5535,
      *      -2.9193, 186.5557,  -3.3502, 187.5609,  -3.7810, 188.5690,
      *      -4.2115, 189.5803,  -4.6417, 190.5949,  -5.0713, 191.6129,
      *      -5.5002, 192.6343,  -5.9282, 193.6594,  -6.3553, 194.6882,
      *      -6.7811, 195.7209,  -7.2057, 196.7575,  -7.6288, 197.7982,
      *      -8.0502, 198.8430,  -8.4699, 199.8921,  -8.8875, 200.9456,
      *      -9.3030, 202.0036,  -9.7161, 203.0661, -10.1268, 204.1333,
      *     -10.5347, 205.2053, -10.9398, 206.2821, -11.3418, 207.3639,
      *     -11.7406, 208.4506, -12.1359, 209.5423, -12.5276, 210.6392,
      *     -12.9155, 211.7414, -13.2995, 212.8488, -13.6792, 213.9616,
      *     -14.0546, 215.0798, -14.4254, 216.2036, -14.7914, 217.3329,
      *     -15.1525, 218.4678, -15.5085, 219.6084, -15.8592, 220.7547,
      *     -16.2043, 221.9067, -16.5437, 223.0645, -16.8772, 224.2280,
      *     -17.2046, 225.3973, -17.5256, 226.5723, -17.8402, 227.7530,
      *     -18.1480, 228.9394, -18.4488, 230.1315, -18.7426, 231.3293/
       DATA (DECS(I,1),RAS(I,1),I=061,104)/
      *     -19.0291, 232.5326, -19.3080, 233.7415, -19.5793, 234.9557,
      *     -19.8426, 236.1754, -20.0980, 237.4003, -20.3450, 238.6303,
      *     -20.5837, 239.8653, -20.8137, 241.1052, -21.0350, 242.3497,
      *     -21.2473, 243.5988, -21.4506, 244.8524, -21.6446, 246.1102,
      *     -21.8292, 247.3721, -22.0043, 248.6379, -22.1698, 249.9075,
      *     -22.3254, 251.1806, -22.4720, 252.4571, -22.6070, 253.7368,
      *     -22.7326, 255.0194, -22.8481, 256.3047, -22.9533, 257.5924,
      *     -23.0480, 258.8824, -23.1324, 260.1743, -23.2062, 261.4680,
      *     -23.2694, 262.7632, -23.3220, 264.0596, -23.3639, 265.3569,
      *     -23.3951, 266.6550, -23.4156, 267.9535, -23.4254, 269.2521,
      *     -23.4244, 270.5505, -23.4127, 271.8488, -23.3903, 273.1463,
      *     -23.3571, 274.4427, -23.3134, 275.7379, -23.2590, 277.0315,
      *     -23.1941, 278.3233, -23.1187, 279.6130, -23.0329, 280.9004,
      *     -22.9367, 282.1852, -22.8303, 283.4671, -22.7138, 284.7461,
      *     -22.5872, 286.0217, -22.4507, 287.2939/
       DATA (DECS(I,2),RAS(I,2),I=001,012)/
      *  -17.6787,227.0486, -17.9432,228.0480, -18.2030,229.0520,
      *  -18.4581,230.0605, -18.7082,231.0735, -18.9531,232.0910,
      *  -19.1928,233.1128, -19.4271,234.1387, -19.6558,235.1686,
      *  -19.8787,236.2023, -20.0957,237.2395, -20.3067,238.2801/
       DATA (DECS(I,2),RAS(I,2),I=013,060)/
      *     -23.5767, 272.5982, -23.5583, 273.5585, -23.5340, 274.5201,
      *     -23.5037, 275.4830, -23.4674, 276.4470, -23.4250, 277.4120,
      *     -23.3767, 278.3780, -23.3223, 279.3449, -23.2619, 280.3126,
      *     -23.1955, 281.2811, -23.1230, 282.2503, -23.0445, 283.2202,
      *     -22.9599, 284.1908, -22.8693, 285.1619, -22.7726, 286.1336,
      *     -22.7933, 255.3171, -22.8901, 256.4048, -22.9795, 257.4951,
      *     -23.0616, 258.5879, -23.1363, 259.6831, -23.2034, 260.7807,
      *     -23.2630, 261.8803, -23.3149, 262.9819, -23.3592, 264.0851,
      *     -23.3956, 265.1896, -23.4243, 266.2952, -23.4451, 267.4014,
      *     -23.4580, 268.5080, -23.4631, 269.6146, -23.4603, 270.7209,
      *     -23.4497, 271.8267, -23.4313, 272.9319, -23.4051, 274.0362,
      *     -23.3711, 275.1394, -23.3294, 276.2415, -23.2801, 277.3424,
```

```
*     -23.2231, 278.4420, -23.1586, 279.5401, -23.0865, 280.6368,
*     -23.0070, 281.7320, -22.9200, 282.8256, -22.8256, 283.9176,
*     -22.7239, 285.0080, -22.6148, 286.0968, -22.4984, 287.1839,
*     -22.3748, 288.2692, -22.2439, 289.3529, -22.1059, 290.4347/
 DATA (DECS(I,2),RAS(I,2),I=061,104)/
*     -21.9606, 291.5148, -21.8083, 292.5930, -21.6489, 293.6691,
*     -21.4825, 294.7431, -21.3092, 295.8146, -21.1290, 296.8835,
*     -20.9422, 297.9494, -20.7488, 299.0121, -20.5490, 300.0714,
*     -20.3429, 301.1270, -20.1306, 302.1789, -19.9122, 303.2268,
*     -19.6880, 304.2706, -19.4580, 305.3104, -19.2225, 306.3459,
*     -18.9814, 307.3773, -18.7349, 308.4045, -18.4832, 309.4276,
*     -18.2264, 310.4465, -17.9645, 311.4612, -17.6977, 312.4720,
*     -17.4261, 313.4788, -17.1497, 314.4817, -16.8687, 315.4808,
*     -16.5830, 316.4762, -16.2929, 317.4680, -15.9984, 318.4564,
*     -15.6994, 319.4413, -15.3962, 320.0432, -15.0887, 321.4016,
*     -14.7771, 322.3771, -14.4615, 323.3493, -14.1419, 324.3185,
*     -13.8186, 325.2844, -13.4916, 326.2471, -13.1613, 327.2062,
*     -12.8276, 328.1619, -12.4908, 329.1139, -12.1512, 330.0622,
*     -11.8087, 331.0068, -11.4637, 331.9476, -11.1162, 332.8848,
*     -10.7664, 333.8182, -10.4144, 334.7480/
 DATA (DECS(I,3),RAS(I,3),I=001,012)/
*  -23.3442,261.2262, -23.3946,262.1608, -23.4395,263.0980,
*  -23.4789,264.0377, -23.5127,264.9800, -23.5409,265.9248,
*  -23.5634,266.8719, -23.5801,267.8214, -23.5911,268.7730,
*  -23.5963,269.7266, -23.5957,270.6821, -23.5892,271.6394/
 DATA (DECS(I,3),RAS(I,3),I=013,060)/
*      -0.0000,  -0.0000,  -0.0000,  -0.0000,  -0.0000,  -0.0000,
*      -0.0000,  -0.0000,  -0.0000,  -0.0000,  -0.0000,  -0.0000,
*      -0.0000,  -0.0000,  -0.0000,  -0.0000,  -0.0000,  -0.0000,
*      -0.0000,  -0.0000,  -0.0000,  -0.0000,  -0.0000,  -0.0000,
*      -0.0000,  -0.0000,  -0.0000,  -0.0000,  -0.0000,  -0.0000,
*     -22.6699, 287.1058, -22.5611, 288.0784, -22.4463, 289.0515,
*     -22.3254, 290.0249, -22.1984, 290.9987, -22.0653, 291.9729,
*     -21.9262, 292.9473, -21.7810, 293.9219, -21.6297, 294.8966,
*     -21.4724, 295.8714, -21.3091, 296.8461, -21.1398, 297.8206,
*     -20.9646, 298.7947, -20.7836, 299.7684, -20.5966, 300.7415,
*     -20.4039, 301.7139, -20.2054, 302.6856, -20.0013, 303.6566,
*     -19.7915, 304.6266, -19.5760, 305.5957, -19.3551, 306.5639,
*     -19.1286, 307.5311, -18.8968, 308.4974, -18.6595, 309.4626,
*     -18.4170, 310.4268, -18.1691, 311.3900, -17.9160, 312.3522,
*     -17.6578, 313.3133, -17.3944, 314.2735, -17.1260, 315.2327,
*     -16.8526, 316.1910, -16.5741, 317.1484, -16.2908, 318.1050/
 DATA (DECS(I,3),RAS(I,3),I=061,104)/
*     -16.0025, 319.0607, -15.7094, 320.0156, -15.4115, 320.9698,
*     -15.1090, 321.9233, -14.8017, 322.8760, -14.4899, 323.8279,
*     -14.1737, 324.7790, -13.8531, 325.7293, -13.5282, 326.6786,
*     -13.1991, 327.6271, -12.8660, 328.5746, -12.5289, 329.5211,
*     -12.1879, 330.4668, -11.8432, 331.4115, -11.4948, 332.3554,
*     -11.1428, 333.2983, -10.7874, 334.2405, -10.4286, 335.1818,
*     -10.0665, 336.1224,  -9.7012, 337.0623,  -9.3328, 338.0016,
*      -8.9615, 338.9403,  -8.5872, 339.8785,  -8.2101, 340.8163,
*      -7.8302, 341.7538,  -7.4478, 342.6910,  -7.0627, 343.6281,
*      -6.6751, 344.5651,  -6.2851, 345.5023,  -5.8928, 346.4396,
*      -5.4982, 347.3771,  -5.1014, 348.3151,  -4.7026, 349.2535,
*      -4.3019, 350.1923,  -3.8993, 351.1317,  -3.4951, 352.0716,
*      -3.0893, 353.0121,  -2.6821, 353.9532,  -2.2736, 354.8949,
*      -1.8640, 355.8373,  -1.4533, 356.7805,  -1.0418, 357.7244,
*      -0.6296, 358.6691,  -0.2167, 359.6147/
 DATA (DECS(I,4),RAS(I,4),I=49,60)/
*    21.0328,132.1434,-15.0012,325.7994,-13.7574,327.8777,
*   -13.2614,328.6914,-12.9250,329.2401,-12.8180,329.4149,
*   -12.6981,329.6124,-12.6088,329.7615,-12.5388,329.8808,
*   -12.4816,329.9811,-12.4329,330.0690,-12.3901,330.1485/
 END
```

```
$IBFTC INTRP
      FUNCTION FINTRP(X,XA,YA)
      DIMENSION XA(2),YA(2)
      X1 = XA(1)
      X2 = XA(2)
      Y1 = YA(1)
      Y2 = YA(2)
      IF(X1 .EQ. X2) GO TO 90
      IF((X.LT.X1).OR.(X.GT.X2)) GO TO 90
      IF(X .EQ. X1) GO TO 70
      IF(X .EQ. X2) GO TO 80
      Y=Y2-Y1
      IF(ABS(Y) .LE. 180.0) GO TO 10
      IF(Y) 5,5,7
    5 Y2=Y2+360.0
      GO TO 10
    7 Y1=Y1+360.0
   10 CONTINUE
      FINTRP = ((X-X1)*Y2+(X2-X)*Y1) / (X2-X1)
      IF(FINTRP .GT. 360.0) FINTRP=FINTRP-360.0
      RETURN
   70 FINTRP = Y1
      RETURN
   80 FINTRP = Y2
      RETURN
   90 WRITE(6,100) X,XA,YA
  100 FORMAT(21HOINTERPOLATION ERROR        5E16.8)
      STOP
      END
$IBFTC STATIS
      SUBROUTINE STAT(N,A,AVE,SIG)
      DIMENSION A(2)
      FN=FLOAT(N)
      AVE = AVE / FN
      S=0.0
      DO 10 I=1,N
      SIG = AVE - A(I)
   10 S=S+SIG*SIG
      SIG = SQRT(S/FN)
      RETURN
      END
$IBFTC FMODD
      DOUBLE PRECISION FUNCTION FMOD(FLHA)
      DOUBLE PRECISION FLHA,ZER,S1
      DATA ZER,S1/0.0D0,360.0D0/
   21 CONTINUE
      IF(FLHA .LE.S1) GO TO 22
      FLHA=FLHA-S1
      GO TO 21
   22 CONTINUE
      IF(FLHA .GE. ZER) GO TO 23
      FLHA=FLHA+S1
      GO TO 22
   23 CONTINUE
      FMOD=FLHA
      RETURN
      END
$IBFTC ROTM
      SUBROUTINE TRIG(PHI,THETA,COSPHI,COSTH,SINPHI,SINTH)
      DOUBLE PRECISION PHI,THETA,COSPHI,COSTH,SINPHI,SINTH
      COSPHI = DCOS(PHI)
      COSTH  = DCOS(THETA)
      SINPHI = DSIN(PHI)
      SINTH  = DSIN(THETA)
      RETURN
      END
```

```
$IBFTC DOTP
      SUBROUTINE DOT(S,E,DOTP)
       DOUBLE PRECISION S,E,DOTP
      DIMENSION S(3),E(3)
      DOTP=S(1)*E(1)+S(2)*E(2)+S(3)*E(3)
      RETURN
      END
```

Appendix E

Special Data Manipulating Computer Programs Listings

These programs were written for the IBM 1620 computer and used to manipulate the data required for various phases of the experiment. The programs are summarized as follows:

(1) Program CTS 40 (see Section III-C) corrects right ascension and declination antenna pointing data as obtained from the JPL SPACE computer program. The corrections are obtained from antenna boresight data.

(2) Program CTS 41 (see Section III-C) is used to manipulate the updated data from program CTS 40 to compute the position of the probe relative to the sun in the plane of the ecliptic. Punched card output is available for plotting and for use with the Faraday rotation program CTS 42.

(3) Program CTS 43 (see Section V-B) is used to correct the measured signal polarization for the Faraday rotation due to the earth's ionosphere. A linear interpolation of the data obtained from the ATS-1 satellite is subtracted from the original measured data. Punched card output is provided.

(4) Program CTS 44 (see Section VI-B) transforms the magnetic field as measured in the vicinity of the earth (using *Explorer* 33 data) to the central meridian of the sun. Punched card output is available for use with the Faraday rotation program CTS 42.

(5) Program CTS 46 (see Sections IV-C and V-B) is used to simultaneously average data for specified sequence lengths in two parameters. Typically, one of the parameters is time. Standard deviations of the two parameters are provided.

CTS 40

```
C       ORBIT DATA PROGRAM CTS40,2/1969
        DIMENSION X(200),Y(200),X1(200),Y1(200),X2(200),Y2(200),DOY(200),
      1 X3(200),Y3(200)
     50 READ 1,N
      1 FORMAT (I5)
        PRINT 10
     10 FORMAT (1H1, 3X3HDOY 8X2HX1 8X2HY1 8X2HX2 8X2HY2 9X1HX 9X1HY)
        READ 2,(DOY(I),X1(I),Y1(I),X2(I),Y2(I),I=1,N)
      2 FORMAT (5F10.0)
        DO 100 I=1,N
        C1D=.0917
        C1RA=.0983
        C2D=-.0002222
        C2RA=-.0004444
        X(I)=X1(I)+C1D+C2D*DOY(I)
        Y(I)=Y1(I)+C1RA+C2RA*DOY(I)
        X3(I)=X(I)-X2(I)
        Y3(I)=Y(I)-Y2(I)
        PRINT20,DOY(I),X(I),Y(I),X2(I),Y2(I),X3(I),Y3(I)
        PUNCH 20,Y(I),X(I)
     20 FORMAT (7F10.3)
    100 CONTINUE
        PUNCH30, (Y3(I),X3(I),I=1,N)
     30 FORMAT (2F10.4)
        GO TO 50
        END
```

```
C      C.STELZRIED  CTS 41   3/22/69
       DIMENSION DAY(100),DP(100),AP(100),RP(100),DS(100),AS(100),RS(100)
      1 ,R(100),Z(100),X(100),XP(100),YP(100),ZP(100),XS(100),YS(100),
      1 ZS(100),ACOS(100),RP1(100),SIGN(100),RSP(100)
   50 READ1,N
    1 FORMAT (I5)
       PRINT 2
    2 FORMAT (1H1,48H                          C.STELZRIED,CTS 41   3/22/69)
       PRINT 3
    3 FORMAT ( 1H,47H EQUATORIAL TO PLANE OF ECLIPTIC TRANSFORMATION)
       PRINT 10
   10 FORMAT (1HO,3HDAY6X4HDECP6X3HRAP8X3HRP 8X4HDECS5X3HRAS7X3HRS 7X
      1 1HR 8X1HX 8X1HZ 8X4HRSP )
       READ 11,(DAY(I),DP(I),AP(I),DS(I),AS(I),I=1,N)
   11 FORMAT (5F10.0)
       READ 12,(RS(I),RP(I),I=1,N)
   12 FORMAT (45X,2E15.5)
       RSUN=.69598*10.**6
       C =57.29577951
       E =23.440/C
       C1A=.0643
       C2A=-.0003543
       DO 100 I=1,N
       DP(I)=DP(I)/C
       AP(I)=(AP(I)+C1A+C2A*DAY(I))/C
       RP(I)= RP(I)/RSUN
       RS(I)= RS(I)/RSUN
       DS(I)= DS(I)/C
       AS(I)= AS(I)/C
       XP(I)= RP(I)*COS(DP(I))*COS(AP(I))
       XS(I)= RS(I)*COS(DS(I))*COS(AS(I))
       YP(I)=RP(I)*(COS(DP(I))*SIN(AP(I))*COS(E)+SIN(DP(I))*SIN(E))
       YS(I)=RS(I)*(COS(DS(I))*SIN(AS(I))*COS(E)+SIN(DS(I))*SIN(E))
       ZP(I)=RP(I)*(-COS(DP(I))*SIN(AP(I))*SIN(E)+SIN(DP(I))*COS(E))
       ZS(I)=RS(I)*(-COS(DS(I))*SIN(AS(I))*SIN(E)+SIN(DS(I))*COS(E))
       ACOS(I)=(XP(I)*XS(I)+YP(I)*YS(I)+ZP(I)*ZS(I))/(RS(I)*RP(I))
       RP1(I)=RS(I)*ACOS(I)
       R(I)=SQRT(ABS(RS(I)**2-RP1(I)**2))
       Z(I)=ZP(I)*RP1(I)/RP(I)
       SIGN(I)=(AS(I)-AP(I))/ABS(AS(I)-AP(I))
       X(I)=SIGN(I)*SQRT(ABS(R(I)**2-Z(I)**2))
       RSP(I)=SQRT(ABS(RS(I)**2+RP(I)**2-2.*RS(I)*RP(I)*ACOS(I)))
       PRINT 20,DAY(I),DP(I),AP(I),RP(I),DS(I),AS(I),RS(I),R(I),X(I),Z(I)
      1 ,RSP(I)
   20 FORMAT (F7.1,2F10.5,F11.3,2F10.5,5F9.3)
       PUNCH 25,DAY(I),X(I),Z(I),RP(I),RS(I),RSP(I)
   25 FORMAT (6F10.4)
  100 CONTINUE
       PUNCH 30,(X(I),Z(I),I=1,N)
   30 FORMAT (2F10.4)
       GO TO 50
       END
```

CTS 43

```
C       DATA CORRECTION  CTS 43  5/6/69
        DIMENSION  T2(800),Y2(800)
        PRINT 110
  200   N=1
  100   READ 107,T2(N),Y2(N)
        IF (T2(N)-99999.)5,8,5
    5   N=N+1
        GO TO 100
    8   CONTINUE
        N=N-1
        PRINT 107,(T2(I),Y2(I),I=1,N )
        PRINT 109
  150   READ 107,T1,Y1
        DO 300 J=1,N
        IF(T1-T2(J))250,300,300
  300   CONTINUE
  250   C=Y2(J-1)+(Y2(J)-Y2(J-1))*((T1-T2(J-1))/(T2(J)-T2(J-1)))
        Y=Y1-C
        PRINT 108, T1,Y,Y1,T2(J),Y2(J),C
        PUNCH 107,T1,Y
        GO TO 150
  107   FORMAT (2F10.5)
  108   FORMAT (6F10.5)
  109   FORMAT (1H ,2HT1,9X1HY,9X2HY1,7X5HT2(J),7X5HY2(J),5X1HC)
  110   FORMAT (1H1, 30HDATA CORRECTION PROGRAM,CTS 43)
        END
```

CTS 44

```
C       EXPLORER 33 DATA MODIFICATION,CTS 44
        PRINT 100
  100   FORMAT (1H1,  35H EXPLORER 33 DATA CORRECTION,CTS 44)
        PRINT 120
  120   FORMAT ( 8X,4HDAYC,8X2HBC)
  101   READ 110 ,DAY,EH,EM,ES,B,T,P
  110   FORMAT (4F5.0,3F10.0)
        DAY=DAY+EH/24.+EM/(24.*60.)+ES/(24.*60.*60.)
         DAYC= DAY-4.-1.5/24.
        C=3.14159 /180.
        T=T*C
        P=P*C
        BC=-(B*COS(T)*COS(P)*215.*215./100000.)
        PRINT 130, DAYC,BC
  130   FORMAT (2F10.5)
        PUNCH 130, DAYC,BC
        GO TO 101
        END
```

CTS 46

```
C     AVERAGES CTS 46
      DIMENSION X(200),Y(200)
  200 N=1
  100 READ 107,X(N),Y(N)
      IF(X(N)-99999.)5,8,5
    5 IF(N-4 )6,9,6
    6 N=N+1
    7 GO TO 100
    8 CONTINUE
      N=N-1
      IF(N-0)9,200,9
    9 CONTINUE
      EN=N
      SX=0.
      SY=0.
      SSX=0.
      SSY=0.
      DO110 I=1,N
  102 SX=SX+X(I)
      SY=SY+Y(I)
      SSX=SSX+X(I)*X(I)
      SSY=SSY+Y(I)*Y(I)
  110 CONTINUE
      PRINT 107, (X(I),Y(I),I=1,N)
      X1=SX/EN
      Y1=SY/EN
      SX1=SQRT((SSX/EN)-X1*X1)
      SY1=SQRT((SSY/EN)-Y1*Y1)
      PRINT 108,X1,Y1,SX1,SY1
      PUNCH 108,X1,Y1,SX1,SY1
  107 FORMAT (2F10.5)
  108 FORMAT (4F10.5)
      GO TO 200
      END
```

References

1. Smith, A. G., *Radio Exploration of the Sun.* D. Van Nostrand, Princeton, N. J., 1969.

2. Evans, J. W., *The Solar Corona.* Academic Press, New York, 1963.

3. Alfven, H., "Granulation, Magneto-Hydrodynamic Waves, and the Heating of the Solar Corona," *Mon. Not. Roy. Astron. Soc.*, Vol. 107, pp. 211–219, 1947.

4. Allen, C. W., "Interpretation of the Electron Densities from Corona Brightness," *Mon. Not. Roy. Astron. Soc.*, Vol. 107, pp. 426–432, 1947.

5. Baumbach, S., "Strahlung, Ergiebigkeit und Elekronendichte der Sonnen Corona," *Astron. Nachr.*, Vol. 263, p. 263, 1937.

6. Hollweg, J. V., "A Statistical Ray Analysis of the Scattering of Radio Waves by an Aniostropically Turbulent, Non-Homogeneous Solor Corona," Ph.D. dissertation, Massachusetts Institute of Technology, Cambridge, Mass., 1967.

7. Parker, E. N., "Dynamics of the Interplanetary Gas and Magnetic Fields," *Astrophys. J.*, Vol. 128, pp. 664–676, 1958.

8. Newkirk, G. A., "Structure of the Solar Corona," *Annu. Rev. Astron. and Astrophys.*, Vol. 5, p. 213, 1967.

9. Levine, M. A., "Plasmas in Space," *IEEE Spectrum*, Vol. 3, pp. 43–47, Nov. 1966.

10. Hata, S., and Saito, K., "The Flattening, Total Light, Brightness Distribution and Polarization of the Solar Corona," *Anna. Tokyo Astron. Abs.*, Vol. 10, pp. 16–52, 1966.

11. Hansen, R. T., et al., "Brightness Variations of the White Light Corona During the Years 1964–67," article submitted to *Solar Physics*, High Altitude Observatory, Kamuela, Hawaii, 1969.

12. Hewish, A., "The Irregular Structure of the Outer Regions of the Solar Corona," *Proc. Roy. Soc. London*, Vol. 228A, pp. 238–251, 1955.

13. Ramaty, R., and Lingenfelter, R. E., "Determination of the Coronal Magnetic Field and the Radio-Emitting Electron Energy from a Type IV Solar Radio Burst," *Solar Phys.*, Vol. 5, pp. 531–545, Dec. 1968.

14. Schatten, K. H., "Large Scale Configuration of the Coronal and Interplanetary Magnetic Field," Ph.D. dissertation, University of California, Berkeley, 1968.

15. Howard, R., "Observations of Solar Magnetic Fields," *Astrophys. J.*, Vol. 130, pp. 193–201, 1959.

16. Schatten, K. H., "Prediction of the Coronal Structure for the Solar Eclipse of September 22, 1968," *Nature*, Vol. 22, p. 1211, Dec. 1968.

17. Ness, N. F., and Wilcox, J. M., "Solar Origin of the Interplanetary Magnetic Field," Phys. Rev. *Lett.*, Vol. 13, p. 461, 1964.

18. Kaufmann, P., et al., "Polarization Bursts in the Sun Observed at Microwave Frequencies," *Nature*, Vol. 220, pp. 1298–1300, Dec. 1968.

19. Evans, J. V., and Hagfors, T., *Radar Astronomy.* McGraw–Hill, New York 1968.

References (contd)

20. Ohlson, J. E., *A Radar Investigation of the Solar Corona,* Technical Report 21. Stanford Electronics Laboratories, Stanford, Calif., 1967.

21. Goldstein, R. M., et al., *The Superior Conjunction of Mariner IV,* Technical Report 32-1092. Jet Propulsion Laboratory, Pasadena, Calif. 1967.

22. Olbert, S., "Interplanetary Magnetic Fields," paper presented at the meeting on Solar Magnetic Fields and High-Resolution Spectroscopy, Rome, Italy, Sept. 14, 1964.

23. Papas, C. H., *Theory of Electromagnetic Wave Propagation.* McGraw–Hill, New York, 1965.

24. Ginzburg, V. L., *The Propagation of Electromagnetic Waves in Plasmas.* Pergamon Press, New York, 1964.

25. Whitmer, R. F., "Principles of Microwave Interactions with Ionized Media," *Micro. J.,* Vol. 2, pp. 17–50, Feb. 1959.

26. Stix, T. H., *The Theory of Plasma Waves.* McGraw–Hill, New York 1962.

27. Kraus, J. D., *Radio Astronomy.* McGraw–Hill, New York, 1966.

28. Daniels, F. B., and Bauer, S. J., "The Ionospheric Faraday Effect and its Applications," *J. Franklin Inst.,* Vol. 267, pp. 187–200, Mar. 1959.

29. Smerd, S. F., and Westfold, K. C., "The Characteristics of Radio-Frequency Radiation in an Ionized Gas, with Applications to the Transfer of Radiation in the Solar Atmosphere," *Phil. Mag.,* Vol. 40, pp. 831–848, 1949.

30. Haselgrove, J., *Ray Theory and a New Method for Ray Tracing,* report of Physical Society Conference on Physics of Ionosphere, held in Cambridge, England, Sept. 1955. Physical Society of London, 1955.

31. Shmoys, J., "Ray Tracing in the Ionosphere," *Electron. Lett.,* Vol. 4, pp. 302–304, July 1968.

32. Bracewell, R. N., and Preston, G. W., "Radio Reflection and Refraction Phenomena in the High Solar Corona," *Astrophys. J.,* Vol. 123, pp. 14–29, Jan. 1956.

33. Kline, M., and Kay, I. W., *Electromagnetic Theory and Geometrical Optics.* Interscience Publishers, New York, 1965.

34. Watts, R. N., "Pioneer 6 Orbits the Sun, *Sky and Telescope,* Vol. 31, pp. 152–153, Mar. 1966.

35. Massey, W. A., *Pioneer VI Orientation Control System Design Survey,* TRW Systems, Inc., Redondo Beach, Calif., Mar. 1968.

36. *Pioneer VI Mission.* Ames Research Center, Palo Alto, Calif., May 1967.

37. Seigmeth, A. J., "Pioneer VI Mission Support," in *The Deep Space Network,* Space Programs Summary 37-50, Vol. II. Jet Propulsion Laboratory, Pasadena, Calif., Mar. 31, 1968.

38. Levy, G. S., and Seidel, B., "Rotating Linear Polarization Modification of the DSS 14 Receiver," in *The Deep Space Network,* Space Programs Summary 37-49, Vol. II. Jet Propulsion Laboratory, Pasadena, Calif., Jan. 1968.

References (contd)

39. White, R. J., *SPACE—Single Precision Cowell Trajectory Program,* Technical Memorandum 33-198. Jet Propulsion Laboratory, Pasadena, Calif., Jan. 1965.

40. Holdridge, D. B., *Space Trajectories Program for the IBM 7090 Computer,* Technical Report 32-223. Rev. 1. Jet Propulsion Laboratory, Pasadena, Calif., Sept. 1962.

41. Levy, G. S., Stelzried, C. T., and Seidel, B., "Pioneer VI Faraday Rotation Solar Occultation Experiment," in *The Deep Space Network,* Space Programs Summary 37-53, Vol. II. Jet Propulsion Laboratory, Pasadena, Calif., Sept. 1968.

42. Stelzried, C. T., Otsohi, T. Y., and Wallace, K. B., "JPL System Checkout of S-Band Multifrequency Cone (SMF SNI Mod 1)," in *The Deep Space Network,* Space Programs Summary 37-54, Vol. II. Jet Propulsion Laboratory, Pasadena, Calif., Nov. 1968.

43. Balakrishnan, A. V., *Space Communications.* McGraw-Hill, New York, 1963.

44. Bathker, D. A., and Brown, D. W., "Large Ground Antenna Performance with Solar Noise Jamming," *Proc. IEEE,* Vol. 54, pp. 1949–1951, Dec. 1966.

45. Levy, G. S., et al., "Pioneer 6: Measurement of Transient Faraday Rotation Phenomena Observed During Solar Occultation," *Science,* Vol. 166, No. 3905, pp. 596–598, Oct. 31, 1967.

46. Goldstein, R. M., "Superior Conjunction of Pioneer 6," *Science,* Vol. 166, No. 3905, pp. 598–601, Oct. 31, 1967.

47. *Solar Geophysical Data No. 293,* U. S. Department of Commerce, Boulder, Colo., Jan. 1969.

48. *Solar Geophysical Data No. 292,* U. S. Department of Commerce, Boulder, Colo., Dec. 1968.

49. Mulhall, B. D., and Thuleen, K. L., "Conversion of Faraday Rotation Data to Ionospheric Measurements," in *The Deep Space Network,* Space Programs Summary 37-55, Vol. II. Jet Propulsion Laboratory, Pasadena, Calif., Jan. 1969.

50. Wilcox, J. M., and Colburn, D. S., "Interplanetary Sector Structure in the Rising Portion of the Sunspot Cycle," *J. Geophys. Res.,* Vol. 74, pp. 2388–2392, 1969.

NASA — JPL — Coml., L.A., Calif.